CLOSED-LOOP REAL-TIME CONTROL OF A NOVEL LINEAR MAGNETOSTRICTIVE ACTUATOR

A Thesis

by

CHIEN-FAN CHEN

Submitted to the Office of Graduate Studies of
Texas A&M University
in partial fulfillment of the requirements for the degree of

MASTER OF SCIENCE

August 2010

Major Subject: Mechanical Engineering

CLOSED-LOOP REAL-TIME CONTROL OF A NOVEL LINEAR MAGNETOSTRICTIVE ACTUATOR

A Thesis

by

CHIEN-FAN CHEN

Submitted to the Office of Graduate Studies of
Texas A&M University
in partial fulfillment of the requirements for the degree of

MASTER OF SCIENCE

Approved by:

Chair of Committee,	Won-jong Kim
Committee Members,	Shankar P. Bhattacharyya
	Bryan Rasmussen
Head of Department,	Dennis O'Neal

August 2010

Major Subject: Mechanical Engineering

ABSTRACT

Closed-Loop Real-Time Control of A Novel Linear Magnetostrictive Actuator.

(August 2010)

Chien-Fan Chen

B.S., National Taiwan University, Taiwan

Chair of Advisory Committee: Dr. Won-jong Kim

This thesis presents the design of various closed-loop real-time control of a novel linear magnetostrictive actuator. The novel linear magnetostrictive actuator which uses Terfenol-D as the magnetostrictive material was developed by Sadighi. It solves the problem of power consumption in a conventional magnetostrictive actuator. However, the control system of this magnetostrictive actuator cannot control the current in the coils, which limits the performances of the real-time position control. In the closed-loop real-time control system proposed in this thesis, the controller is designed depending on the change of current.

The closed-loop real-time control design focused on the position control of the active element in the novel linear magnetostrictive actuator. The closed-loop position-control system of the linear magnetostrictive actuator was successfully designed by implementing a closed-loop current-control system as an inner loop of the entire control system. This design offers the flexibility to design various position controllers in the closed-loop position-control system.

The closed-loop current-control design uses pulse-width modulation (PWM) signal to change the current in the coils of the novel linear magnetostrictive actuator. By changing the duty ratio of the PWM signal, the current in the coils can be changed from zero to its maximum value. With a current controller using an integrator with a gain of 10, the current can be controlled with high response time and an error of ±0.01 A.

The position-controller design was successfully conducted by using four different approaches. First, a proportional-integral-derivative (PID) controller which was designed by relay-auto tuning method with experiments exhibited a position error of ±1 μm with a 5 μm peak-to-peak position noise. Second, a PID controller which was designed by root-locus can control the position with a position error of ± 3~4 μm with a 5 μm peak-to-peak position noise. Third, a linear variable velocity controller exhibited a position error of ±5 μm with a 5 μm peak-to-peak position noise. Then, the sliding mode control (SMC) exhibited a position error of ±5 μm with a 5 μm peak-to-peak position noise.

ACKNOWLEDGMENTS

First and foremost, I would like to express my sincere gratitude towards my advisor, Professor Won-jong Kim, for his support, encouragement, and patience in my master's research. Whenever I had problems in my research he was always there to help. He was a constant source of inspiration and motivation to me. During my association with him, I have learned a lot from his vast knowledge about the design and development of control systems.

I would like to thank Prof. Bryan Rasmussen for serving on my thesis committee. I am highly privileged to have him on my thesis committee. I would also like to thank Prof. Shankar P. Bhattacharyya for serving on my thesis committee. I am grateful to him for giving me a lot of knowledge in the Control System Design class in the fall of 2009.

My special thanks go to Ali Sadighi for his help in this research of the novel linear magnetostrictive actuator. His knowledge has helped me to learn a lot about the working principle of the magnetostrictive actuator. His advice helped me overcome many obstacles and problems.

I would like to thank all my past and present lab mates. They have helped me whenever I had a problem, and helped me set up the experiments. I share a special friendship with each one of them.

To my parents Ming-Huei Chen and Fung-Ling Yang, I have the utmost respect and appreciation. They have been always there for me at all times. During the times when I was sad and depressed, they motivated me and made me feel good. They have

always supported me to learn and stressed achievement of knowledge. Throughout my life I will always be highly indebted to them. I would also like to thank my younger sister Yu-Sing. By looking at her smiling face and seeing her excitement, I will never forget my childhood. I love her a lot.

TABLE OF CONTENTS

Page

CHAPTER Page

CHAPTER Page

LIST OF TABLES

LIST OF FIGURES

FIGURE Page

FIGURE Page

FIGURE Page

FIGURE Page

CHAPTER I

INTRODUCTION

Linear motors have found many industrial applications and are extensively used in machine tools, sliding tables, pen recorders, textile sewing machines, free piston pumps and compressors, etc. [1]. However, there are some disadvantages for linear motors in these kinds of applications, such as space requirements and large power consumption. These disadvantages make us to develop new actuators with new technology [2]. Linear actuators that have large force generation, such as hydraulic actuators, cannot be used except where there is spacious space because there must be enough space to accommodate the auxiliary parts of the hydraulic system. On the other hand, direct-drive linear actuators with smaller space requirements cannot generate as large a force as the hydraulic ones. A rotary motor with a gear reducer and ball or lead screws can increase the force generation and overcome the disadvantage of direct-drive linear actuators that cannot compete with hydraulic actuators, but this requires adding a complex speed reducer and introduces backlash [3].

In order to overcome the limitations, new materials were applied to develop a novel actuator with less space requirement and high force generation. Giant magnetostrictive materials and piezo ceramics are two types of new materials that have been used [4].

This thesis follows the style of *IEEE/ASME Transactions on Mechatronics*.

Piezoceramics actuators are used because of their low power consumption and high output energy per mass, and the magnetostrictive materials have the advantages of low-voltage, high-force, high-power, low-frequency transducers, and space cryogenic positioning [5].

1.1 History of Magnetostrictive Actuators

Magnetic actuators transform electrical energy into mechanical energy by means of a magnetic field. A magnetostrictive actuator is a kind of magnetic motor that is different from the conventional electromagnetic ones based on Lorentz's law of electromagnetic forces and Faraday's law of magnetic induction. Magnetostrictive actuators incorporate a smart material that changes shape when it is exposed to an external stimulus in the structure of the actuator, and their working principle is based on the properties of the smart materials [3].

1.1.1 Invention of Magnetostrictive Actuators

Magnetostriction

The primary working principle of most magnetostrictive actuators is magnetostriction, first discovered by Joule in the nineteenth century [6]. Magnetostriction refers to the expansion of a ferromagnetic material from one shape to another in the presence of a magnetic field (Fig.1.1). This expansion keeps increasing with the magnetic field until magnetic saturation is achieved and the direction of the expansion depends on the direction of the magnetic field [7].

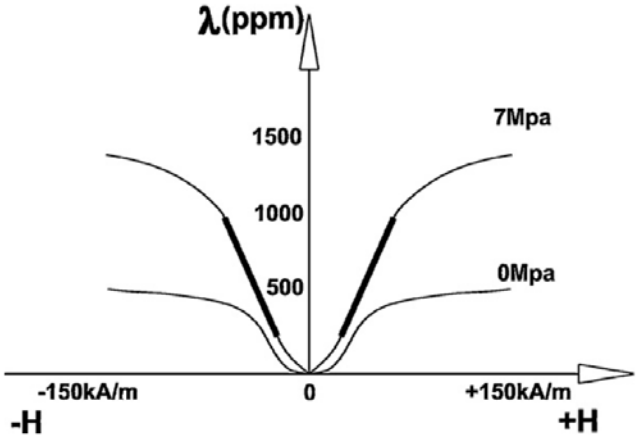

Fig. 1.1. Magnetostriction [7].

Terfenol-D

Terfenol-D is an alloy of formula $Tb_{0.3}Dy_{0.7}Fe_{1.92}$ developed in the 1950s at the Naval Ordnance Laboratory. Terfenol-D has high magnetostriction, up to 2,000 ppm, that can be used in a magnetostrictive motor [6], [8]. This property enables most of the available magnetostrictive actuators to generate high force within a very small range of actuation.

Terfenol-D has the highest energy density compare to other similar materials. The continuous cycling of Terfenol-D through a wide temperature range has no residual effect on its magnetostrictive performance, even if its Curie temperature is exceeded. Typical strain amounts from Terfenol-D rods are 0.001 inch per inch of exposed length in a magnetic field of 500 Oe. The properties of Terfenol-D are listed in Table 1. Because of the high energy density, Terfenol-D actuators can produce higher forces than other kinds of actuators [7].

Table 1.1 Properties of Terfenol-D [7]

Sl. No.	Terfenol-D property	Value range
1	Nominal composition	$Tb_{0.3}D_{0.7}Fe_{1.92}$
2	Density ρ	9250 kg/m^3
3	Mechanical properties	
	Compressive strength	305–880 MPa
	Tensile strength	28–40 MPa
	Young's modulus E^H	10–75 GPa
	Young's modulus E^B	30–80 GPa
	Sound speed	1640–1940 m/s
4	Thermal properties	
	Coefficient of thermal expansion	12 ppm/°C
	Specific heat coefficient	0.35 kJ/kg K @ 25 °C
	Thermal conductivity	13.5 W/m K @ 25 °C
5	Electrical properties	
	Resistivity	58×10^{-8} Ωm
6	Magneto mechanical properties	
	Relative permeability μ^T/μ_0	9–12
	Relative permeability μ^S/μ_0	3.0–5.0
	Saturation magnetization	1.0 T
	MS coupling coefficient K_{33}	0.75
	MS strain coefficient d_{33}	8–20 nm/A
	MS quality factor Q^H	3.0–20.0

1.1.2 Magnetostrictive Actuators with Direct and Indirect Motion Control

According to the mechanism of force generation and movements, magnetostrictive actuators are often classified into two different designs, direct motion control and indirect motion control.

Magnetostrictive Actuators with Direct Motion Control

In direct motion control, one end of the active material is fixed so that when the magnetic field is applied, the material will elongate through the other end. The mechanism has a relatively simple structure for achieving the required actuator

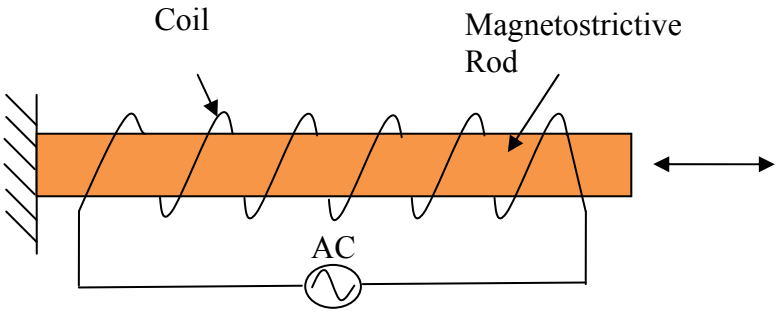

Fig. 1.2. Schematic diagram of magnetostrictive actuator with direct motion control [9].

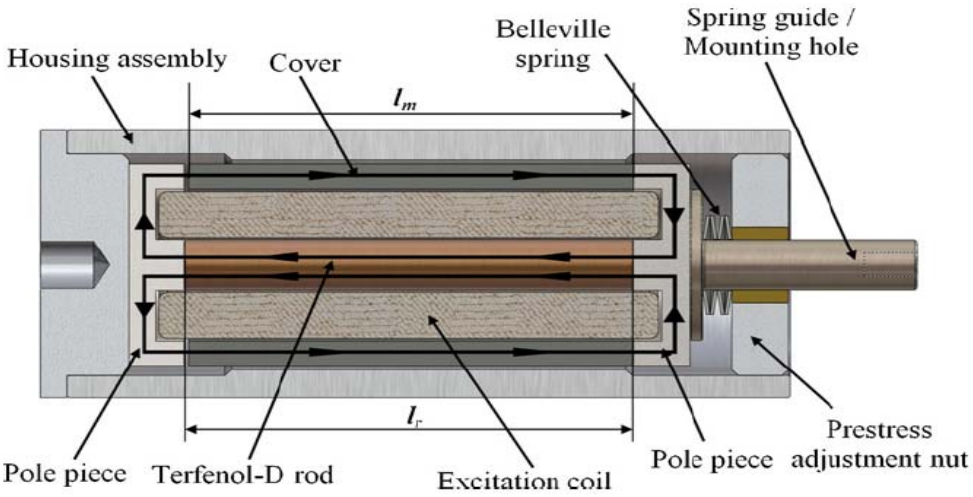

Fig. 1.3. Actuator configuration with direction control [7].

performance compare to the other actuators. However, these kinds of actuators have a very limited operational range that narrows their area of applications [9]. The schematic diagram of a magnetostrictive actuator with direct motion control is shown in Fig. 1.2 and the configuration of actuator with direction control is shown in Fig. 1.3.

Magnetostrictive Actuators with Indirect Motion Control

Unlike actuators with direct motion control, the magnetostrictive material of actuators with indirect motion control is not fixed at one end so it can move to generate a larger force and wider range of motion. The construction of the magnetostrictive actuator with indirect motion control is as shown in Fig. 1.4. The switch will turn on when the left clamp is active and causes the rod to move to the right, and the switch will turn off when the right clamp is active. When the process is repeated, the actuator can move further than one with direct motion control so that the operational range of the actuator is extended [10].

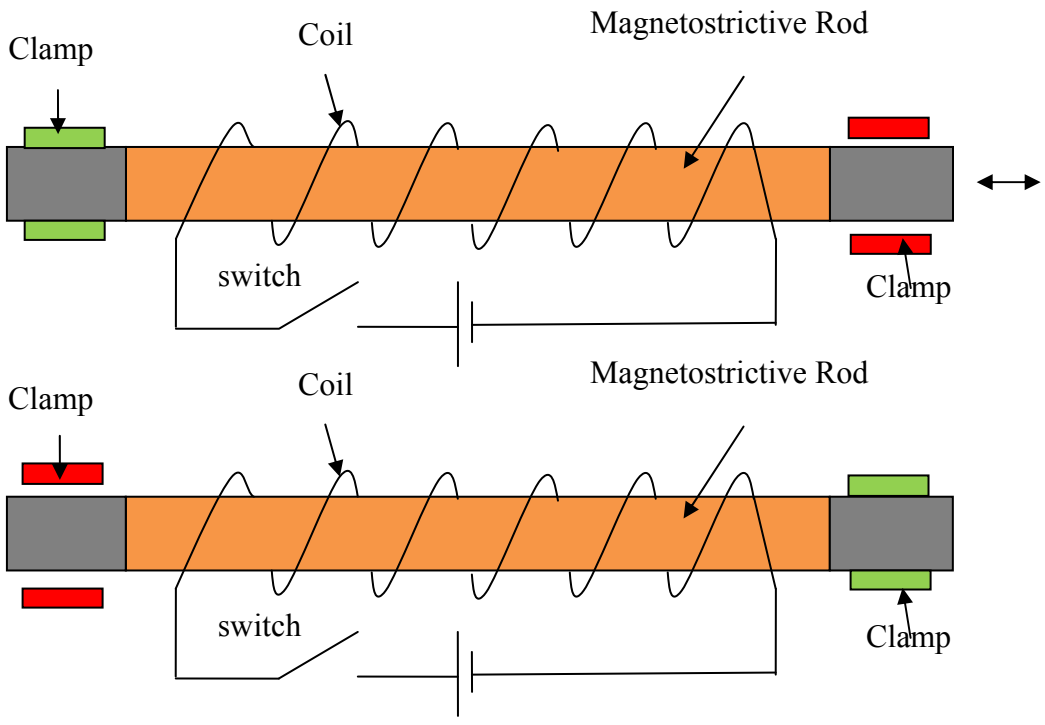

Fig 1.4. Schematic diagram of actuator with indirect motion control [10].

1.1.3 Kiesewetter Motor

Kiesewetter motor is a special type of extended-range magnetostrictive motor with indirect motion control. Kiesewetter took advantage of the properties of Terfenol-D to create a peristaltic motion by putting a Terfenol-D rod in a fitting tube. However, the disadvantage of this design is that the contact between the Terfenol-D rod and the fitting tube produces a wear problem and may weak the force-generating capability [10]. The schematic diagram of the Kiesewetter motor is shown in Fig.1.5.

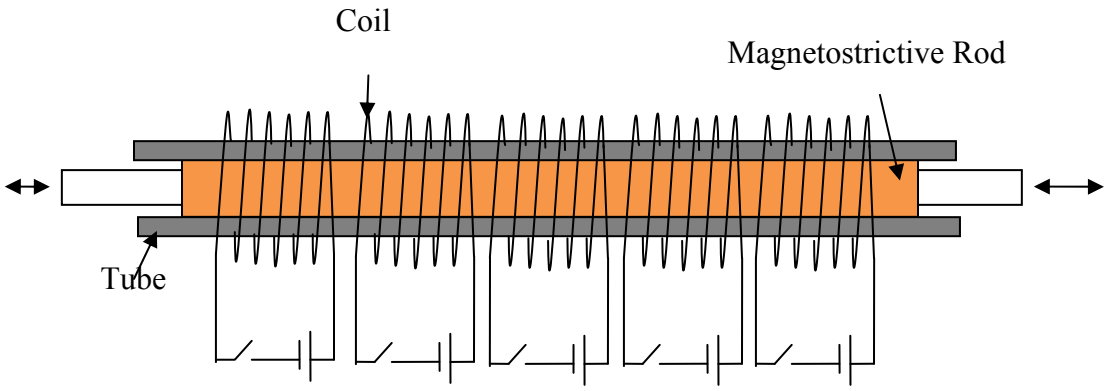

Fig. 1.5. Schematic diagram of Kiesewetter motor [10].

1.1.4 Extended-Range Linear Magnetostrictive Motor

Kim, et al. created an extended-range linear magnetostrictive motor by changing the stators to double-sided three-phase ones. Unlike Kiesewetter's motor, the Terfenol-D is placed between two tight-fitting spring-loaded plates [11]. This motor design can generate a force of up to 140 N and a traveling range of 25 mm. However, this design resulted in high power consumption due to eddy-current loss when applying

conventional three-phase excitation in high frequency [12]. Fig. 1.6 shows a photograph of the extended-range linear magnetostrictive actuator with double-side stator.

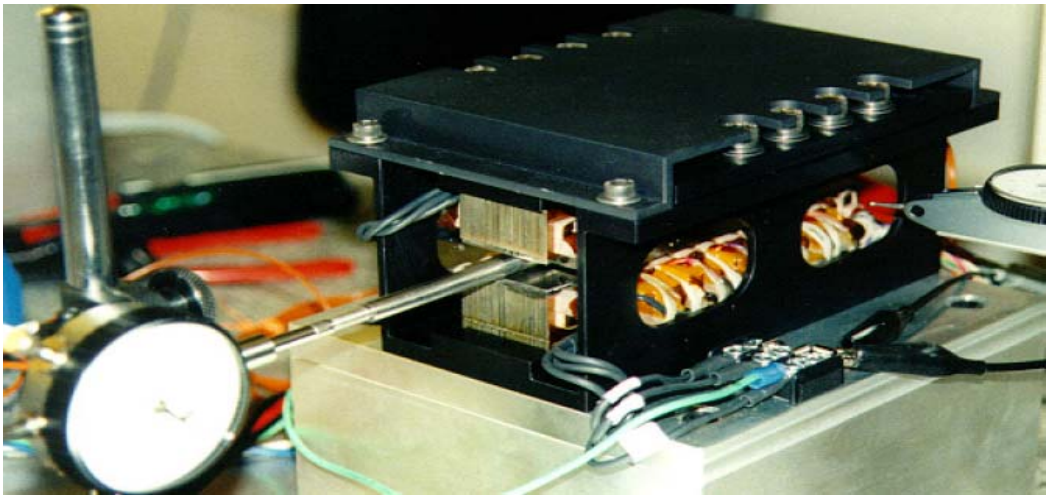

Fig. 1.6. Photograph of the magnetostrictive actuator with double-side stator [11].

1.1.5 Novel Low-Power Linear Magnetostrictive Actuator

To overcome the problem of high power consumption, Sadighi designed a new type of linear magnetostrictive motor that has a rectangular slab of Terfenol-D as the active element [9]. The configuration of the coils is changed so that the magnetic axis of the coils coincides with the active material's magnetic axis that aligns the direction of the magnetic field inside the Terfenol-D. Moreover, it allows the implementation of conventional multi-phase excitation or local multi-phase excitation [3].

However, the relay controller used in previous research of the novel actuator exhibited a 20 μm dead-zone threshold value [3]. This means that the system turns on

when the position error is more than 20 μm and turns off when the position error is less than 20 μm. Due to the characteristics of the relay controller, there will be an inevitable error close to the dead-zone threshold value and become the limitation of previous research [9]. The objective of this thesis is to design a closed-loop control system that enhances the performance of the previous research which used a closed-loop relay control system.

1.2 Application of Magnetostrictive Actuators

Magnetostrictive actuators are often applied in many ways because of their set point accuracy and high bandwidth capabilities [13]. Moreover, their characteristics of high force, high displacement motion, and high accuracy can also be used in various industrial applications.

1.2.1 Active Vibration Control

Research of active vibration control for micro-amplitude, low-frequency applications has focused on magnetostrictive actuators for years because of their stringent accuracy and performance. Besides the accuracy requirement, the vibration-control actuators also should be simple, reliable, and have a large displacement of motion and force. Magnetostrictive actuators have more displacement and force than the other actuators with common transducer materials, such as piezoceramics or nickel alloys. Moreover, the magnetostriction of Terfenol-D does not change with time or number of cycles of stress, which is proved to be very suitable for vibration control in a

damping field [14].

1.2.2 Manufacture Devices

High-accuracy, high-speed milling devices and torque sensing for steering systems have recently used magnetostrictive actuators to improve control authority and performance, reduce weight, and minimize power requirements [15]. Furthermore, magnetostrictive actuators also offer both actuator and sensor capabilities as well as broadband transduction and large output forces. For example, the application for milling out-of-round automotive parts at speeds of 3,000 rpm and tracking of 1–2 μm as detail uses a magnetostrictive actuator to drive the cutting head [15].

1.2.3 Damage Detection

Research done on damage detection has applied magnetostrictive actuators to transfer a certain amount of vibration energy to the structure, and the actuators are connected to the structure together with a force sensor. When damage occurs to a structure, it leads to variations in stiffness, damping, and the change of dynamic response of the system. The energy transmission path from the magnetostrictive actuator to the sensors that are closer to the fault will change [16], [17].

1.3 Contribution of the Thesis

The main contribution of the thesis is the design of a system for current control and its application on position control. After an effective closed-loop current-control system has been built, the velocity of the active element in the novel linear

magnetostrictive actuator is controllable. This increases the flexibility of designing a position-control system which is based on changing the velocity or current.

The performances, such as steady-state error and step response, of different closed-loop position-control systems with different controllers, including the results of previous research which used the relay controller [9], are tested and discussed in terms of the characteristics of the controllers used.

1.4 Objective and Proposed Approach

The objective of the thesis is to design a closed-loop control system that improves the performance of the previous research which used a closed-loop relay control system. Because of the dead-zone value threshold of the relay controller, the system would have self-oscillations in the system response or result in a steady-state error equal to the threshold value of the dead-zone [3], [9].

The primary goal of this thesis is to design controllers that are different from the relay controller and compare their performance with the results of the previous research. This thesis has achieved this goal by performing the following tasks:

1. Build a closed-loop current-control system to control the current in the coils by changing the voltage across the coil.
2. Change the velocity of the active element by implementing the closed-loop current-control system to all the coils in the magnetostrictive actuator.
3. Develop an effective closed-loop position-control system by designing different

controllers.

1.5 Overview of the Thesis

This thesis contains five chapters. Chapter I presents a review of the history and application of the magnetostrictive actuator.

Chapter II presents the working principle and theory of the magnetostrictive actuator. The various components of the power electronics and instrumentation structure are also presented.

Chapter III first describes the feedback closed-loop current-control system which depends on the PWM signal and then presents the design of the closed-loop position-control system.

Chapter IV presents the closed-loop control experiment results. The resolution of the position is improved and presented.

Chapter V concludes this thesis with a summary of the achievements in the work and suggestions for possible future work. Appendices include the Simulink block diagrams used to control the actuator.

CHAPTER II

WORKING PRINCIPLE AND ELECTROMAGNETIC DESIGN

This chapter describes the electromagnetic design for the magnetostrictive actuator, including the underlying theory of the working principle, the choice of the active element, and the digital circuit, software, electronic control method, and sensor that are applied to control the whole system.

2.1 Working Principle of the Linear Magnetostrictive Motor

As shown in Fig. 2.1, the working principle of the linear magnetostrictive motor is that by generating a traveling magnetic field through the active element and keeping it under pressure, a peristaltic motion can be generated with the result that the displacement of the active element will be in the opposite direction of the traveling field.

The active element is placed in a tight fit under pressure initially. The magnetic field is generated by a series of coils which surround the active element. Two stators are also used to enhance the magnetic flux density inside the active element. As long as the magnetic field travels through the active element, the magnetic field will interact with the active element. The active element which the magnetic field interacts with will change shape along the magnetic field lines. Because the volume of the active material does not change, the area of the cross section will decrease with the elongation of length and release the active material from its tight fit with the stator. When the magnetic field moves to the neighboring part of the active element, that part of the element will expand

and the last part will return to its original shape and self-lock against the channel. As the magnetic field completely travels through the entire active element, the element will move to the opposite side of the magnetic field's traveling direction. By repeating this process, a peristaltic motion is generated, resulting in overall displacement of the active material [7].

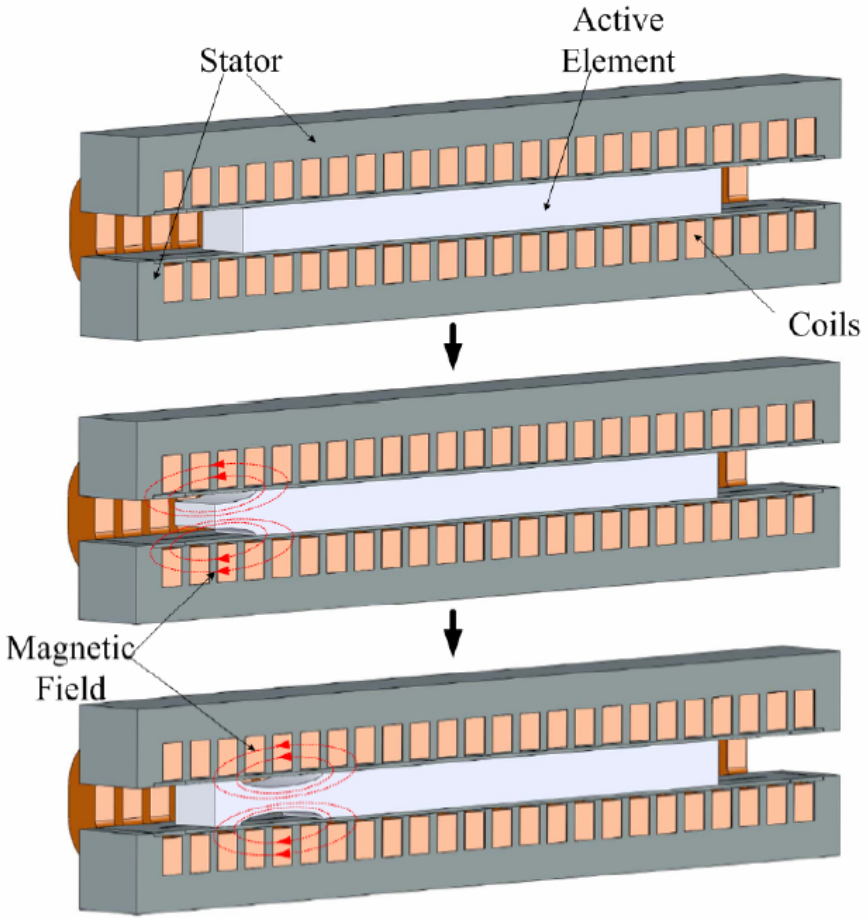

Fig. 2.1. Working principle of the linear magnetostrictive actuator. By generating a travelling magnetic field through the active element, peristaltic motion is generated which results in overall displacement of the active element in the opposite direction of the traveling magnetic field [3].

2.2 Underlying Theory

This section shows that the speed of a linear magnetostrictive motor is a function of the peak magnetostrictive strain, mechanical stress, and operation frequency [18]. In regard to the speed capability of the device, if the effect of the finite contact area between the Terfenol-D and the channel is neglected, the equation shows that the output speed of the magnetostrictive motor is [11]

$$v = \frac{\omega}{k} \left(\varepsilon_{\max} - \frac{F}{EA_T}\right) \tag{2.1}$$

where ω = temporal frequency (rad/s) of stress, strain, and displacement in the Terfenol-D (= 2 × electrical excitation frequency)

k = wave number (2π/ pole pitch), where the pole pitch is 28.8 mm

ε_{max}= peak magnetostrictive strain under no-load condition

E = Young's modulus of Terfenol-D

F = external load (N)

A_T = cross-sectional area of the Terfenol-D.

For the linear magnetostrictive motor under local multi-phase operation, the equation could be modified as [3]

$$v = N f p \left(\varepsilon_{\max} - \frac{F}{EA_T}\right) \tag{2.2}$$

where N = number of phases (3)

f = local multi-phase operation frequency (Hz)

p = slot pitch.

Therefore, the speed is proportional to $\varepsilon_{max} - F/EA_T$, where ε_{max} is the magnetostrictive strain and F/EA_T is the mechanical strain resulting from the external load applied on the active material [3], [9].

2.3 Magnetic Design

From (2.2), it is clear that the speed has a direct relation with the magnetostrictive and force capacity of the linear magnetostrictive motor. Therefore, one of the purposes in the previous research is to make the magnetic circuit direct the magnetic flux through the active element as much as possible. As long as the magnetic circuit directs more magnetic flux, the power requirement will be lower and the force capacity will be larger [3].

The finite element analysis (FEA) approach has been applied to design and optimize the magnetic circuit in previous research [19], [20]. The FEA results for different thicknesses of active material show that when the material is thinner, the magnetic flux will be higher, as shown in Fig. 2.2. However, the thickness of the active element is limited by the space between the two stators of the magnetostrictive actuator. Therefore, the thickness of the active element is chosen to be the minimum required space for the force transmission assembly. Due to this consideration, Terfenol-D of 12.7 mm × 31.5 mm × 200 mm was chosen as the size of the active element for the magnetostrictive actuator in previous research. The dimensions of the slab are shown in Fig. 2.3 [3].

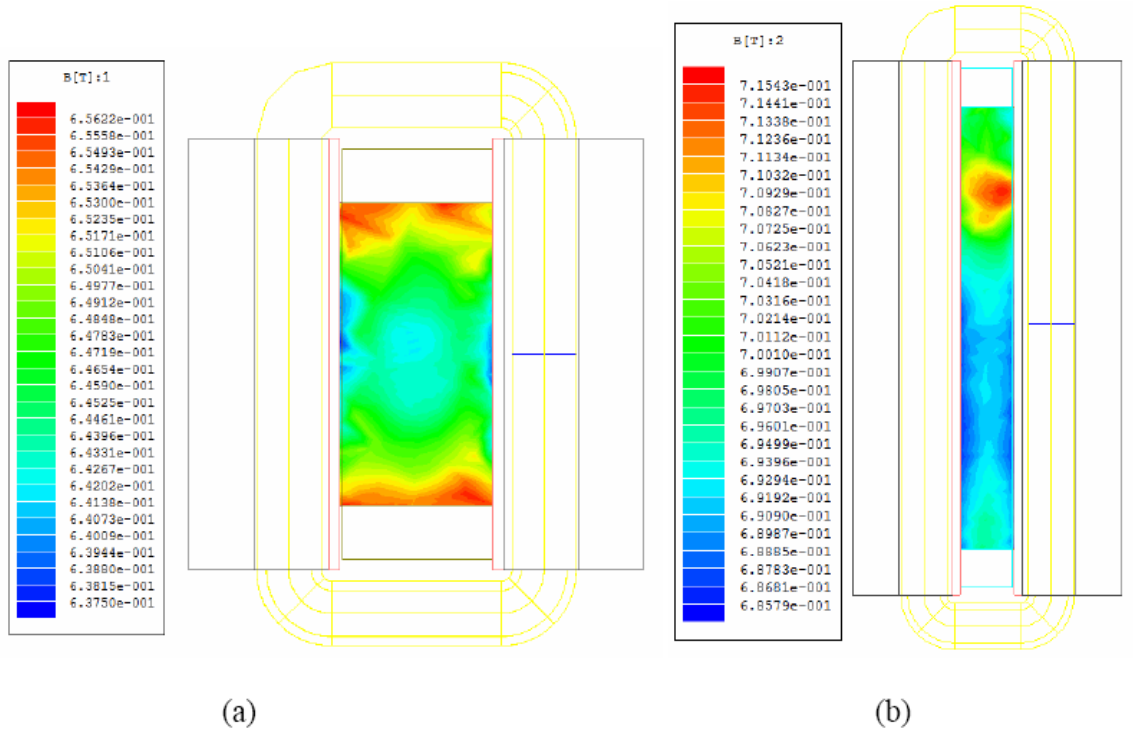

Fig. 2.2. Magnetic flux density in Terfenol-D slab with (a) Terfenol-D cross-section of 28 mm × 14.3 mm and (b) Terfenol-D cross section of 57 mm × 7 mm under the same excitation conditions [3].

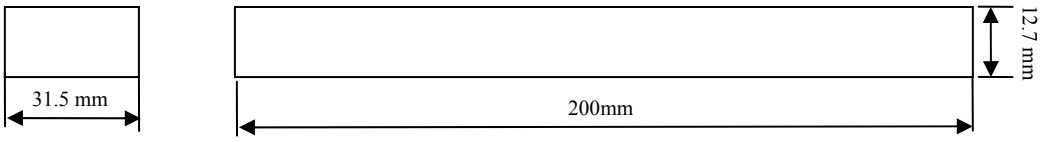

Fig. 2.3. Dimensions of Terfenol-D slab.

2.4 Winding Structure

In order to generate 0.6-T magnetic flux density inside the Terfenol slab, the actuator incorporated 24 coils, each consisting of 273 turns of AWG ＃24 wire. The

required tools were manufactured and the coils were wound by Wire Winders. The size arrangement in the coil is shown in Fig. 2.4 [9].

According to the American wire gauge (AWG) standard, the total length of wire in each coil, approximately 47.5 m, will result in a resistance of 4 Ω, and the exact resistance and inductance of each wire shown by the RCL meter is 4.28 Ω and 9.7 mH, respectively.

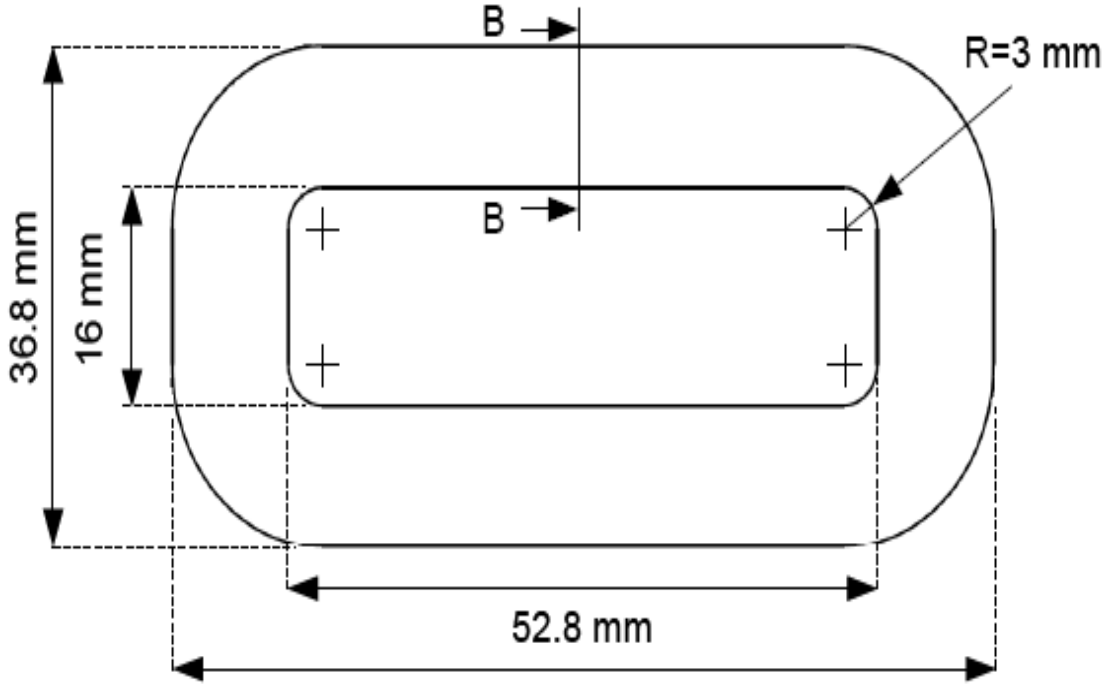

Fig. 2.4. Wire arrangement in the coils [9].

2.5 Power Electronics

In the magnetostrictive actuator, previous research focus on the local three-phase conventional operation, and according to the working principle, the actuator works by

generating a traveling magnetic field through the active element. Therefore, the arrangement and the local three-phase excitation sequence are as shown in Fig. 2.5.

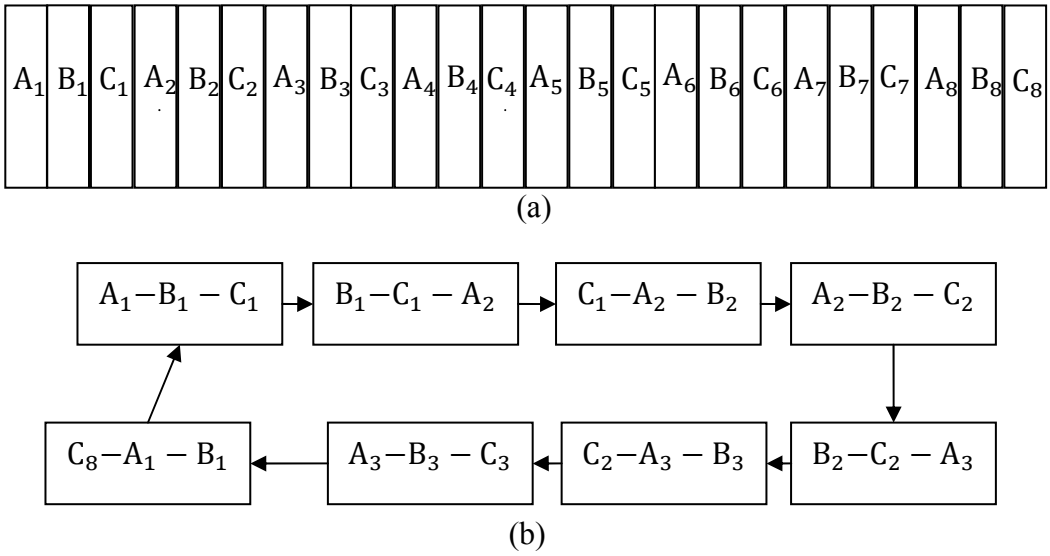

Fig. 2.5. (a) The arrangement of the coils in the magnetostrictive actuator; (b) the excitation sequence of the coils in the magnetostrictive actuator.

2.5.1 Power MOSFET

A metal-oxide-semiconductor field-effect transistor **(**MOSFET) is a type of field-effect transistor (FET) with three terminals, a drain (*D*), a source (*S*), and a gate (*G*) which is controlled by gate voltage. The cross section and schematic symbol for an n-channel enhancement-mode MOSFET are illustrated in Fig. 2.6. This MOSFET has a p-type substrate and an n-type source and drain that form PN junctions with the substrate. There is a thin silicon dioxide layer insulating the gate from the substrate. When a positive DC voltage is applied to the gate, an electric field formed in the substrate below the gate repels holes in the p-type substrate, leaving a narrow channel in the substrate in

which electrons predominate. This is referred to as an n-channel in the p-type substrate. The substrate is usually connected to the source internally so that the substrate-source PN junction is not forward biased.

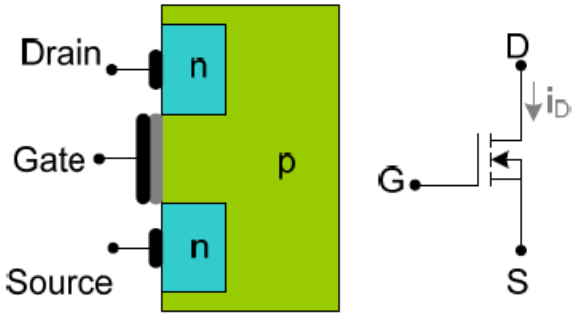

Fig. 2.6. N-channel MOSFET [21].

If the gate is grounded (V_g = 0), no drain-to-source current I_d flows for a positive drain voltage V_{dd} because the drain pn junction is reverse biased and no conducting channel has formed, the MOSFET is said to be in cutoff. As V_{gs} is gradually increased beyond a gate-to-source threshold voltage V_t, the n-channel begins to form. Then as V_{ds} is increased from 0, conduction occurs in the n-channel due to a flow of electrons from source to drain. The drain current I_d, by convention, is shown in the direction opposite to electron flow. With a positive V_{gs} larger than V_t, as V_{ds} is increased from 0, we enter the active region, also called the ohmic region, of the MOSFET. The characteristic curves are shown in Fig. 2.7 [21].

Due to their characteristics, MOSFETs are very useful for excellent high-current voltage-controlled switches, as shown in Fig. 2.8. Because the gate draws no current, the

MOSFET switch is very easy to design. If the control signal V_g is zero, the MOSFET will be cut off, resulting in a huge drain to source impedance and essentially blocking the current to the load. When the control signal V_g is larger than the largest value of the V_{in}, the drain to source channel will conduct with a low resistance, enabling the current to pass through the load [21].

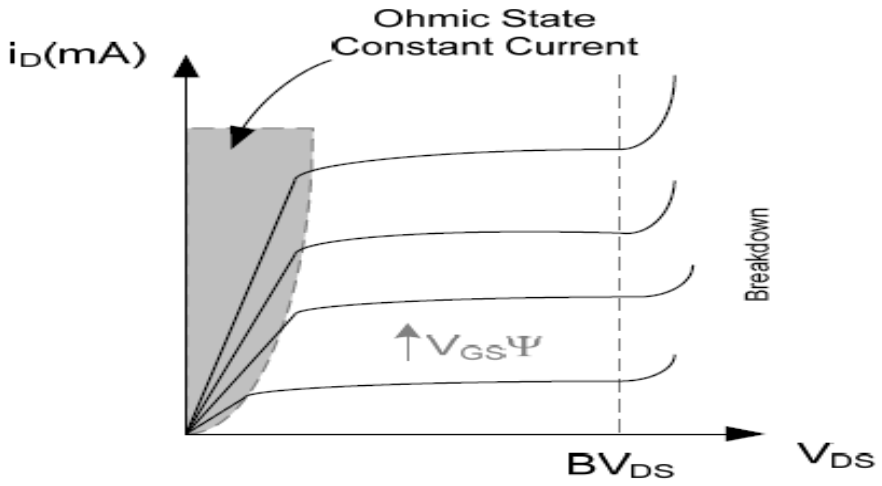

Fig. 2.7. N-channel MOSFET characteristic curves [21].

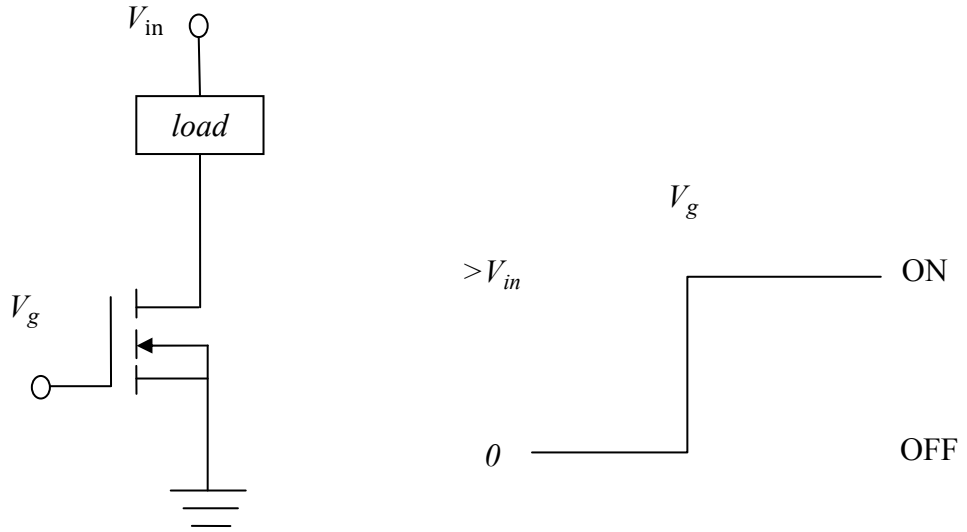

Fig. 2.8. MOSFET power switch circuit [21].

2.5.2 Switching Boards

The switching boards are used to reach the goal of directing the required current through three adjacent coils and then moving it to either side depending on the motor's motion direction. Each board includes eight power MOSFETs (model IRF3315Pbf by International Rectifier), eight MOSFET drivers (model TC4420 by Microchip), eight flyback diodes (model MUR405 by ON Semiconductor), three inverters, and one 3-line to 8-line decoder. Three power supplies (model E3644A by Agilent) are used to produce power for three different boards. The switching frequency of the power MOSFETs is controlled by using the digital inputs/outputs (I/Os) of a digital-signal-processing (DSP) board (model DS1104 by dSPACE). Fig. 2.9 shows the schematic diagram of the digital circuit and power electronics for a single phase [3].

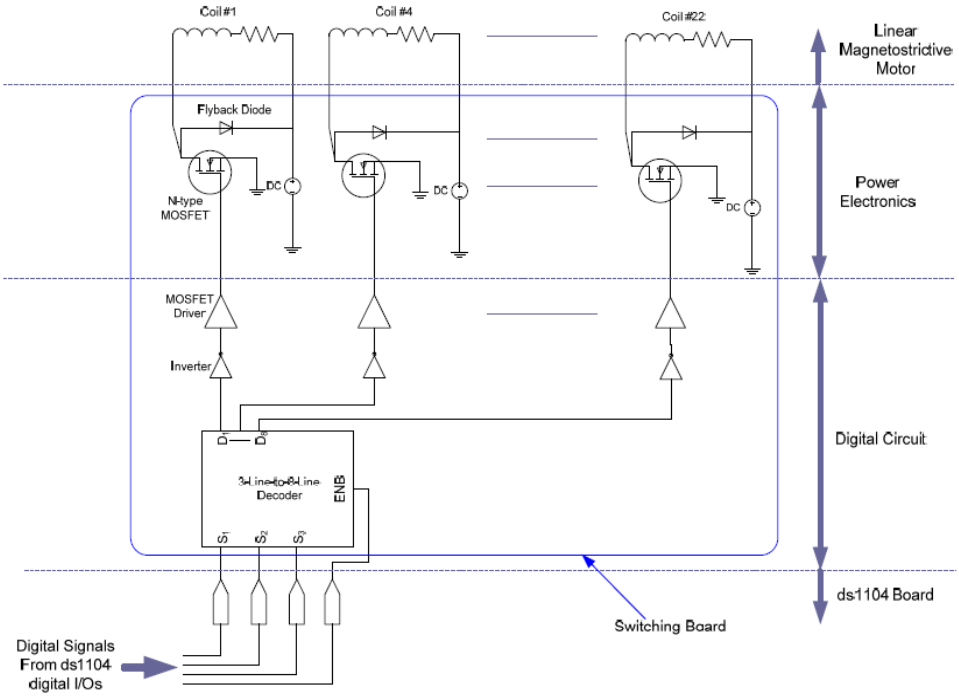

Fig. 2.9. Schematic diagram of digital circuit and power electronics for a single phase [3].

2.6 Electronic Control

As mentioned above, before design the closed-loop position-control system, it needs to control the current in every coil of the magnetostrictive actuator. After taking into consideration the lower power requirement and lower cost, pulse-width modulation (PWM) amplifiers are applied to control the current. Furthermore, the 3-to-8-line decoder can easily sent the PWM signal from one of its input. This advantage make it does need to redesign the switching board in previous research.

The principle of a PWM amplifier is shown in Fig. 2.10. A DC power supply voltage is rapidly switched at a fixed frequency f between two values (e.g., ON and OFF). The high value is held during a variable pulse width t within the fixed period T where

$$\mathrm{T} = \frac{1}{f} \tag{2.3}$$

The resulting asymmetric waveform has a duty cycle defined as the ratio between the ON time and the period of the waveform, usually specified as a percentage:

$$\text{Duty cycle} = \frac{t}{T} \times 100\% \tag{2.4}$$

As the duty cycle is changed (by the controller), the average current through the motor changes, causing changes in speed or torque at the output. It is primarily the duty cycle, and not the value of the power supply voltage, that determines the amount of average current. As shown in Fig. 2.11, as the duty cycle grows larger, the average current grows larger [21]. By passing the PWM signal through the MOSFET in the switching board, the current in the coils will change with the duty cycle. The design of

closed-loop current-control system mainly is mainly based on the relation between duty cycle and current.

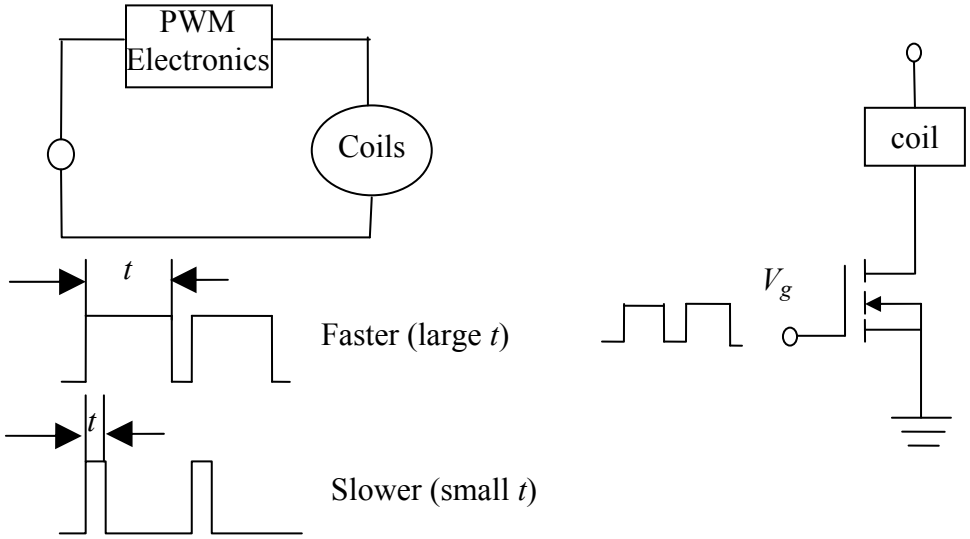

Fig. 2.10. Pulse-width modulation of actuator [21].

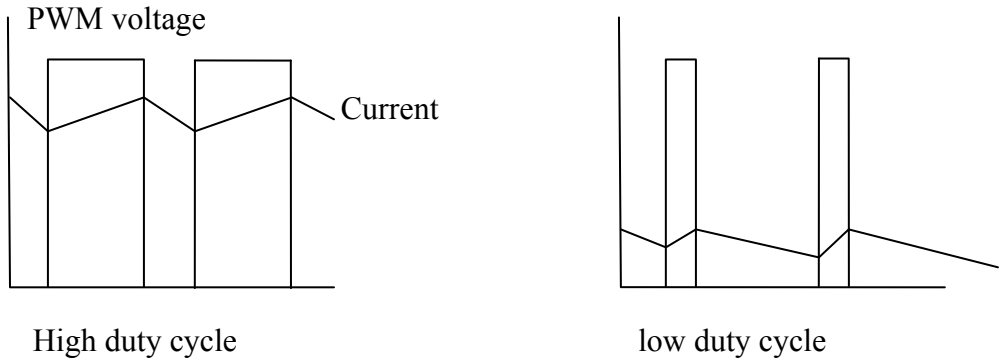

Fig. 2.11. PWM voltage and current [21].

2.7 Instrumentation Structure

The construction of the whole system is as shown in Fig. 2.12. The system is controlled by a PC which uses a digital signal processing board (DSP) as the interface. The switching frequency of the power MOSFETs is controlled by the I/Os of the DSP board which makes the actuator move in the required direction. The PWM signal is sent from the slave I/O PWM connector of the DSP board to the 3-to-8-line decoder, and the duty cycle is controlled by the software. The position of the active element is measured by the laser sensor and the current of the coils in the magnetostrictive actuator is measured by the current transducers. Both of the laser sensor and current transducer provide a signal to the A/D channels of the DSP board and be read by the software. Different parts of the system are presented below.

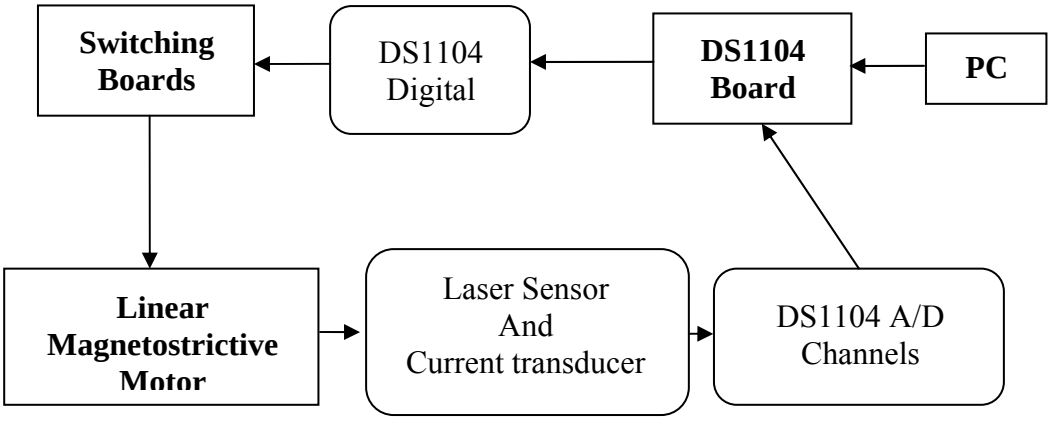

Fig. 2.12. Different components of the mechatronic system.

2.7.1 DS1104 Board

The DS1104 board (Fig. 2.13) contains a 32-bit 250-MHz floating point DSP. This board has eight analog to digital (A/D) channels, eight digital to analog (D/A) channels, twenty digital I/O channels.

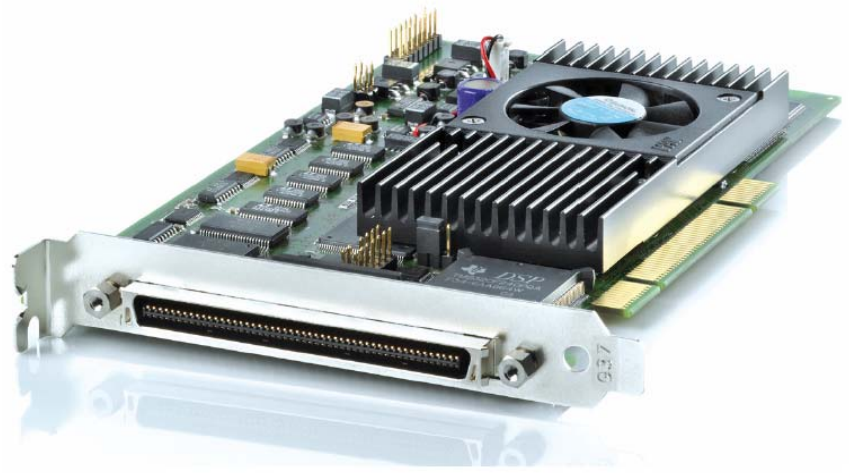

Fig. 2.13. DS1104 R&D board [6].

2.7.2 Software

All control systems in the magnetostrictive motor, such as monitoring of the position, current control, position control, switching frequency and sequences for the switching board, duty cycle of the PWM signal, and monitoring of the current, are designed by Simulink, and the code is generated using Real-Time Workshop. The real-time mode will be automatically compiled to C-code and then translated to the DSP board.

The ControlDesk was chosen to be the interface which provides the environment to monitor different signals, such as current or position, and to input the required control commands. The interface is shown in Fig. 2.14.

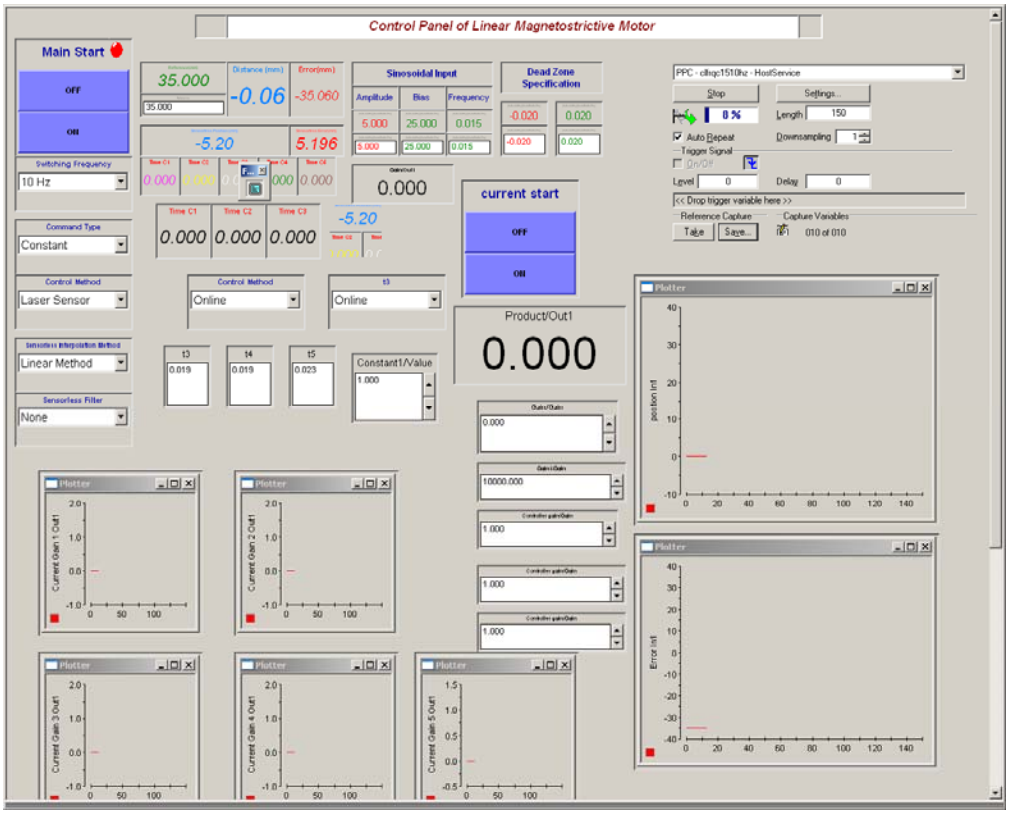

Fig. 2.14. User interface control panel.

2.7.3 Laser Sensors

The laser sensor (model OADM 20I6460/S14F by Baumer Electric shown in Fig. 2.15) has a measuring distance rage from 30 mm to 130 mm and a resolution of 5 µm to detect the position of the active element. The output signal of the sensor is a voltage that

varies between 0 and 10 VDC. The output voltage is sent to the DSP board to calculate the position. The connection diagram of the laser sensor is shown in Fig. 2.16.

Fig. 2.15. Laser distance sensor [22].

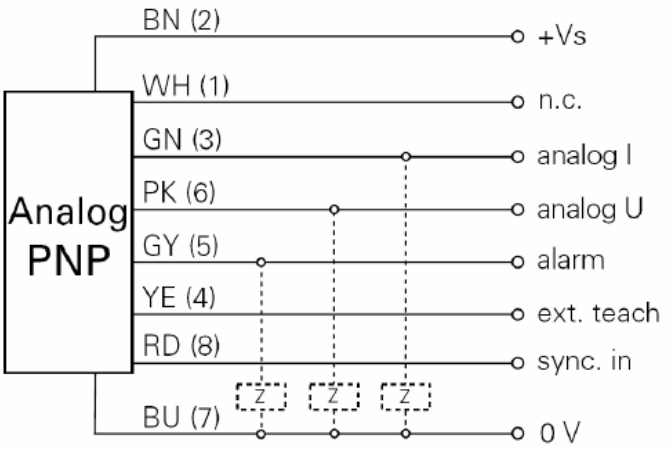

Fig. 2.16. Laser sensor connection diagram [22].

2.7.4 Current Transducer

In order to control the current, a current transducer (model LA 03-PB A47114) is used to detect the current in the coils. The transducer measures current within a range of

±4.5 A. The voltage supply is 15 V and the output voltage is between −4 V and +4 V. The output voltage is sent to the A/D channel of the DSP board and is displayed on the user interface control panel.

2.8 Mechanical Design and Fabrication

The magnetostrictive motor is subjected to the external load and the normal squeezing force. In order to stand these two loads, the components of the actuator need to be considered. Moreover, the construction should have tolerances that can stand the resulting strain of the magnetostrictive motor which are on the order of hundredths to tenths of millimeters. Not only the tolerance but also the surface condition needs to be considered, and the surface which transmits force and strain should be as flat and smooth as possible [23].

The suitable choices of housing, force transmission assembly, squeezing mechanism, stators, and load unit were designed in previous research of the novel linear magnetostrictive actuator by Sadighi and are presented in the following section.

2.8.1 Housing Assembly

The housing assembly has two functions. First, it provides the space that can accommodate the stators, coils, Terfenol-D slab, and force transmission assembly. Second, it should deliver enough normal force for squeezing the Terfenol-D slab. The housing assembly is shown in Fig. 2.17. The squeezing plate uses 16 sets of Belleville spring washers to provide the normal force against the upper stator. The upper block and

housing pin are used to fix the stator. The function of the base plate is to fix the housing assembly to the optical table [9].

Fig. 2.17. Housing assembly [9].

2.8.2 Stator

In designing the stator, two requirements should be considered. First, in order to decrease the reluctance of the magnetic circuit, the stator should have high relative permeability. Second, because the external load generates shear force and the squeezing force will place pressure on the stator, the stator should be strong enough to stand the force and pressure. To achieve these two requirements, Nickel-Iron Alloy 49 (EFI 50 by Ed Fagan Inc.) with high relative permeability up to 100,000 and mechanical properties

that the yield stress of 154 MPa was chosen. Moreover, because the normal squeezing pressure would damage the coils, a clearance of 0.5 mm between the bottom of the stator slots and the coil was designed. The stators are shown in Fig. 2.18 [9].

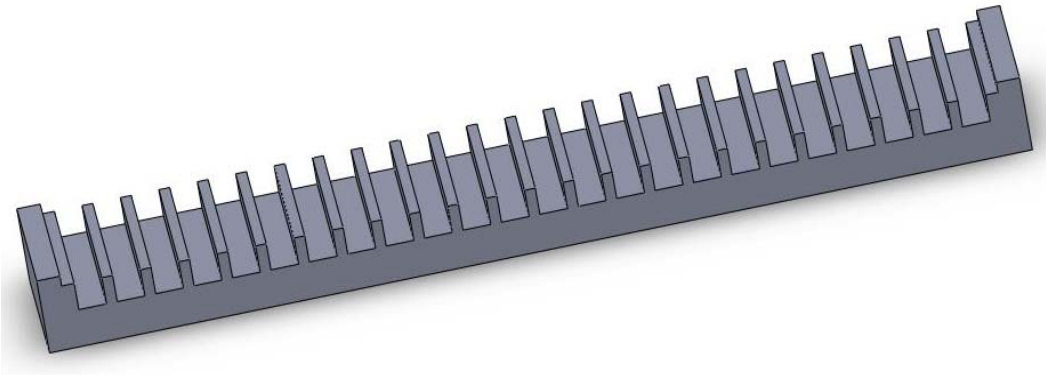

Fig. 2.18. Stator core [9].

CHAPTER III

CONTROL SYSTEM DESIGN

The control system design aims to design a controller to control the current in the coils of the actuator and a controller to control the position by changing the current. The process of designing a current-control system will be presented in Section 3.1. The closed-loop position-control system will be presented in Section 3.2. The process of designing the position controller will be discussed in Section 3.3.

3.1 The Current-Control System Design

In the current-control system, the duty ratio of the PWM signal was applied to control the current in the coils, as mentioned in Section 2.5. In order to reach the goal, the relationship between the duty ratio of the PWM signal and the current should be modeled, and then a controller can be designed so that the desired current in the coils can be controlled.

3.1.1 The Electronic Model for Experiment

All the experiment in the design of the closed-loop current-control system is done using an electronic model of one of the coils in the novel linear magnetostrictive actuator. The model is used to prevent the risk of damaging the magnetostrictive actuator itself due to any error of the experiment of designing a closed-loop system. The schematic diagram is as shown in Fig. 3.1.

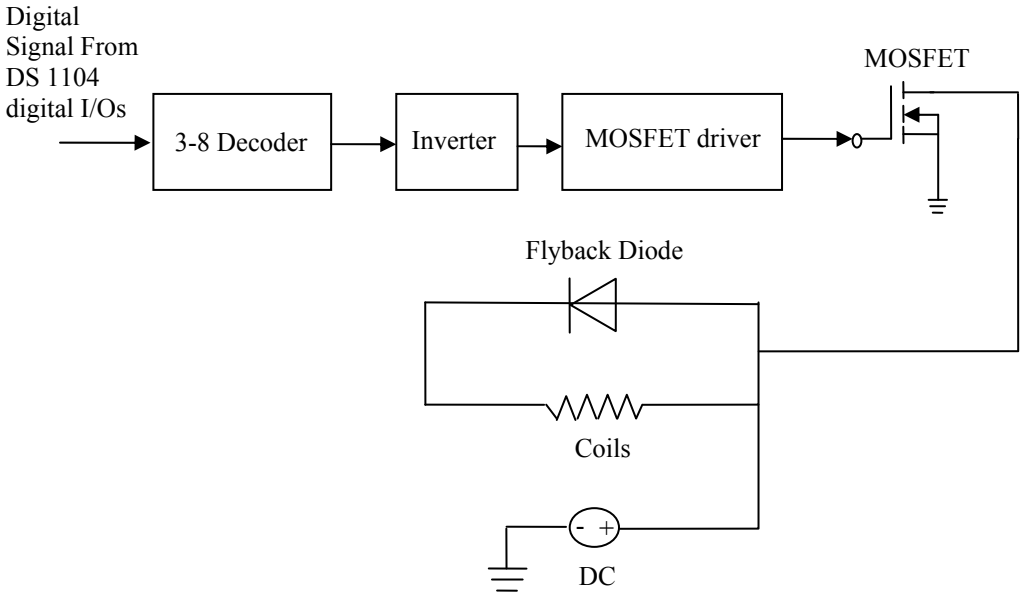

Fig. 3.1 Schematic diagram of the power electronic model and digital circuit of one coil.

The model can represent the digital circuit of one coil in the novel linear magnetostrictive actuator, including one 3-to-8-line decoder, one inverter, one MOSFET driver, and the power electronics of the coil. Therefore, if the current in the coil of the model can be controlled, the closed-loop current-control system for the model can be implemented to the magnetostrictive actuator as well.

3.1.2 Peak-Value Calculator

As mentioned above, the working principle of the linear magnetostrictive motor relies on generating a traveling magnetic field through the active element. Therefore, as shown in Fig. 2.5, the current of each coil in the motor is not constant but keeps turning on and off with a certain frequency. In other words, the value of the current will

change between zero and the value which generates the magnetic field. However, only the value that generates the magnetic field in the motor is of concern during the design process. For this reason, we need to design a peak value calculator which sends out only the current value that generates the magnetic field.

The Matlab Simulink is applied to design the calculator. The flowchart of the calculator is as shown in Fig. 3.2. If the value of the current is zero, the output of the calculator will be the value sampled at 10 ms before. If the value of the current is not zero, the output of the calculator will be equal to the input. If the process is repeated enough times, the output can send out only the current that generates the magnetic field. The flow chart shown in Fig. 3.3 illustrates this process.

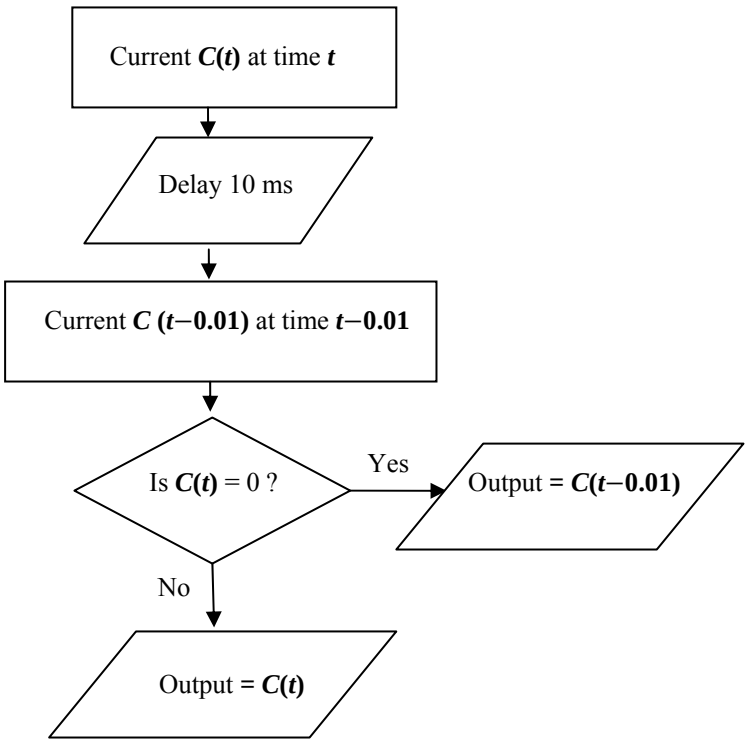

Fig. 3.2 Flow chart of the peak-value calculator.

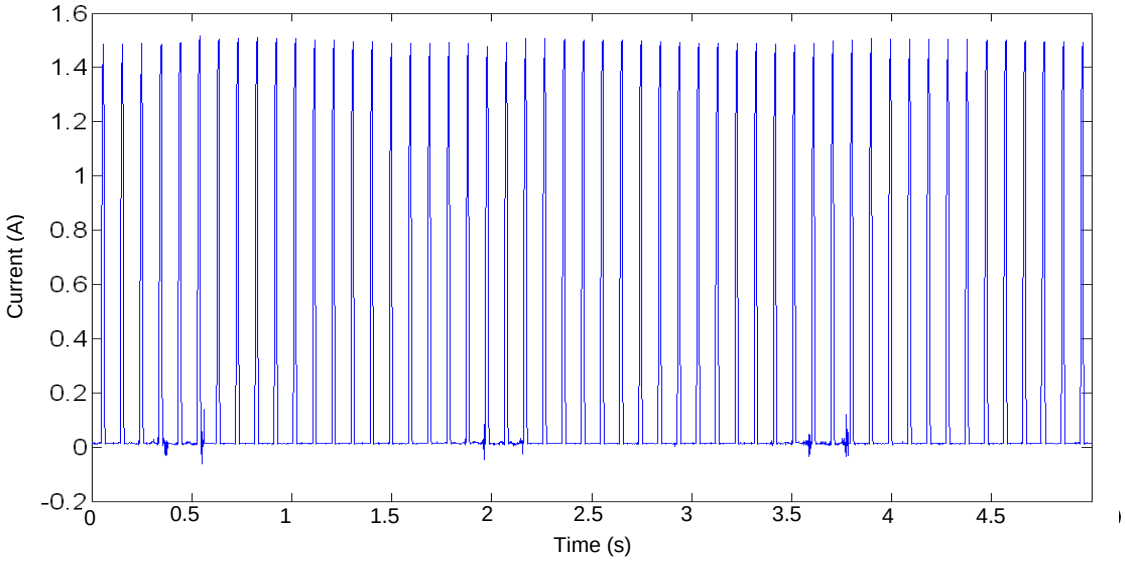

(a)

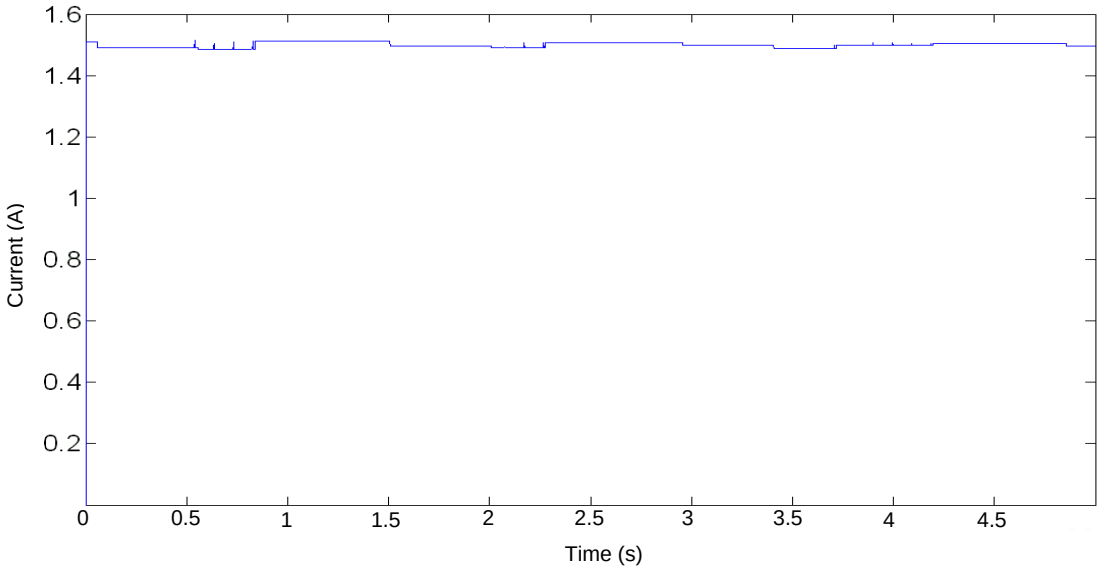

(b)

Fig. 3.3 (a) Original current signal with the peak value of 1.5 A. (b) Output current signal of the peak-value calculator.

3.1.3 Modeling the Relation Between PWM Duty Ratio and Current

To find the relationship between the duty ratio of the PWM signal and the current, an experiment was performed by using the first coil in the actuator with a DC 8 V voltage and the current at different duty ratios was recorded. The experimental result is as shown in Fig. 3.4, and the function between duty ratio and current can be approximate as:

$$I = 1.7659 \times D \tag{3.1}$$

where I is the current and D is the duty ratio of the PWM signal. Next, we can get the ratio of the current and duty ratio as follows:

$$P = \frac{I}{D} = 1.7659 \tag{3.2}$$

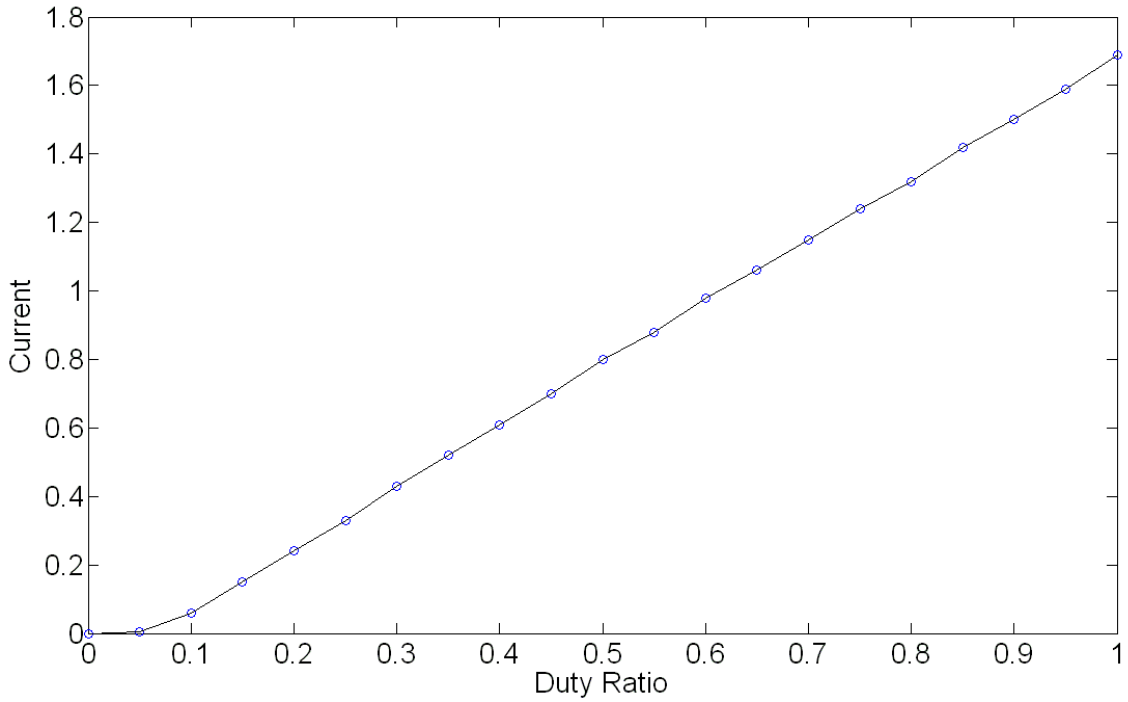

Fig. 3.4 The relationship between duty ratio and current.

3.1.4 Closed-Loop Current-Control System Design

With the peak-value calculator, a controller was successfully designed and implemented to control the current by changing the duty ratio of the PWM signal. The schematic diagram of the current-control system is shown in Fig. 3.5. The current is measured by the current transducer and sent to the current calculator to get the peak current value. Then, the current value will be fed back to the controller. The duty ratio which is based on the error will be sent to the PWM amplifier and generate the PWM signal out from the slave I/O PWM connector of the DSP board. The PWM signal will pass through the MOSFET which was connected to the coils in the power electronics of the magnetostrictive actuator. When different duty ratios of the PWM signal pass through the MOSFET, the voltage across the coils will be different according to the relation with the duty ratio. Because the resistance of the coils does not change, the current will change with the voltage and the relationship between current and PWM duty ratio as mentioned in Section 3.1.2. Due to this characteristic, the current in the coils can be controlled.

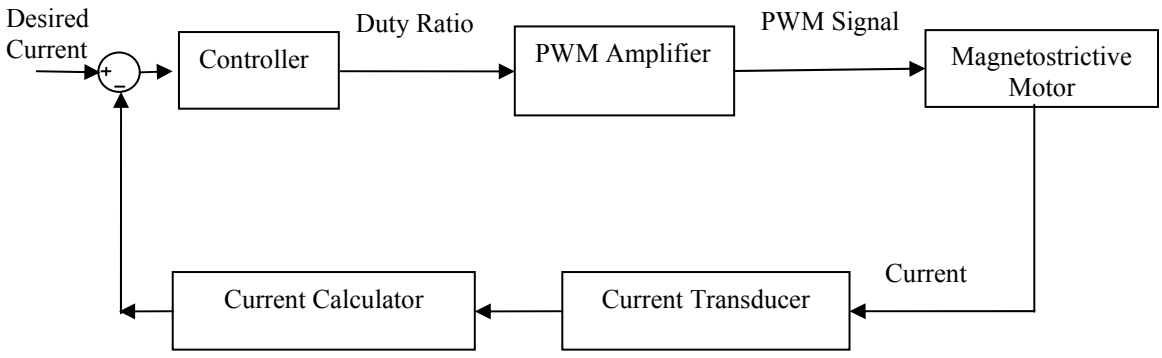

Fig. 3.5 Schematic diagram of the current-control system.

3.1.5 Controller Design

An integrator is chosen as the controller of the current-control system, and the transfer function is:

$$D(s) = \frac{K}{s} \tag{3.3}$$

K is the gain of the controller in order to shorten the rise time. Therefore, the closed-loop current-control system can be plot as Fig. 3.6. Where *u* is the current input, *o* is the current output and the ratio *P* is the ratio between duty ratio *D* and current *I*.

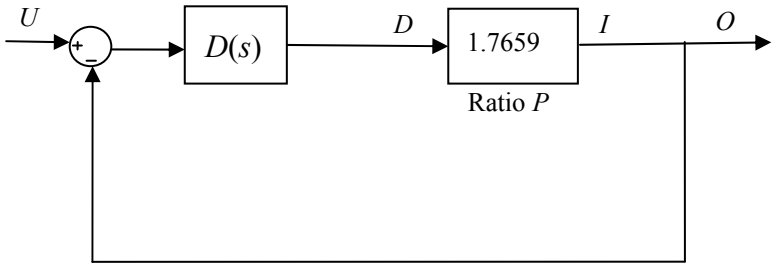

Fig. 3.6 The closed-loop current-control system with an integrator.

Then, the transfer function of the current-control system can be found from Fig. 3.6 and can be described as:

$$G(s) = \frac{O(s)}{U(s)} = \frac{1.7659D(s)}{1+1.7659D(s)} = \frac{1.7659K}{s+1.7659K} \tag{3.4}$$

The position-control of the active element is based on changing the current in the coils. In order to get high responding time of position-control, the responding time of the closed-loop current control system should as fast as possible. The step response with different gain (*K*) is shown in Fig. 3.7. When the gain is larger, the rise time is shorter and change slower with different gain.

The experimental results of the closed-loop current response are shown in Fig. 3.8. There is no overshoot and oscillation in the step response, so this shows that using an integrator can work for the current control.

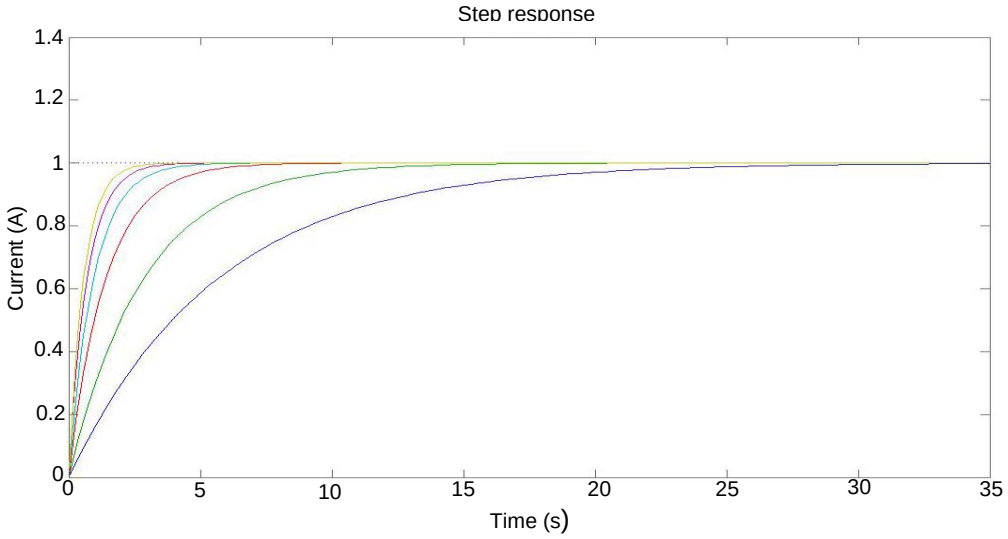

Fig. 3.7. Time response with different gain K = 10, 8, 6, 4, 2, and 1 from the top.

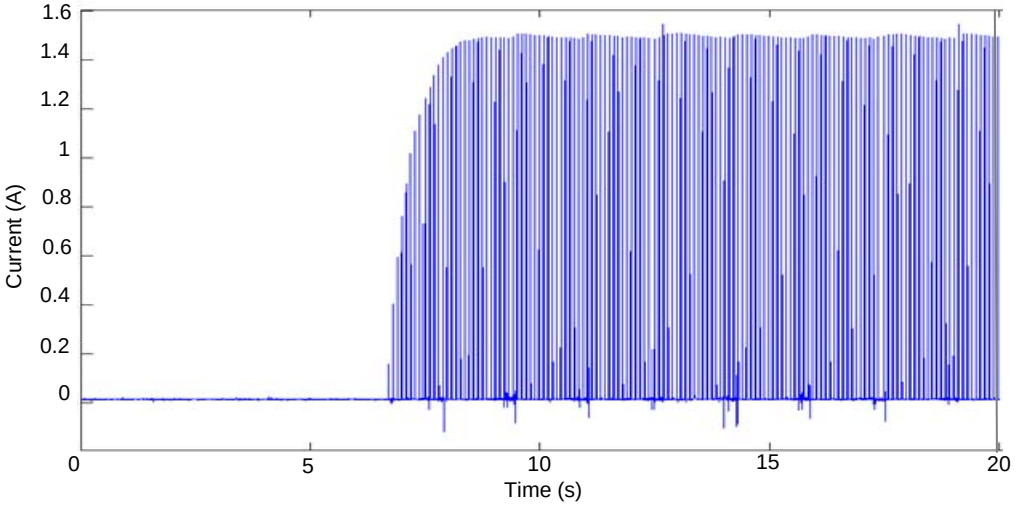

Fig. 3.8. Experiment result of the closed-loop current response from 0 A to 1.5 A.

As mentioned before, the closed-loop current-current control system is been used as an inner-loop of the closed-loop position control system so the responding time is important. The responding time should be as faster as possible and it would has less influence to the closed-loop position-control system.

Fig. 3.9 shows the bode-plot for the transfer function (3.4). As shown in Fig. 3.9, the bandwidth of the transfer function of the closed-loop current-control system is 17.659 rad/sec. The bandwidth is high enough to make the closed-loop current-control system has small influence to the closed-loop position-control system.

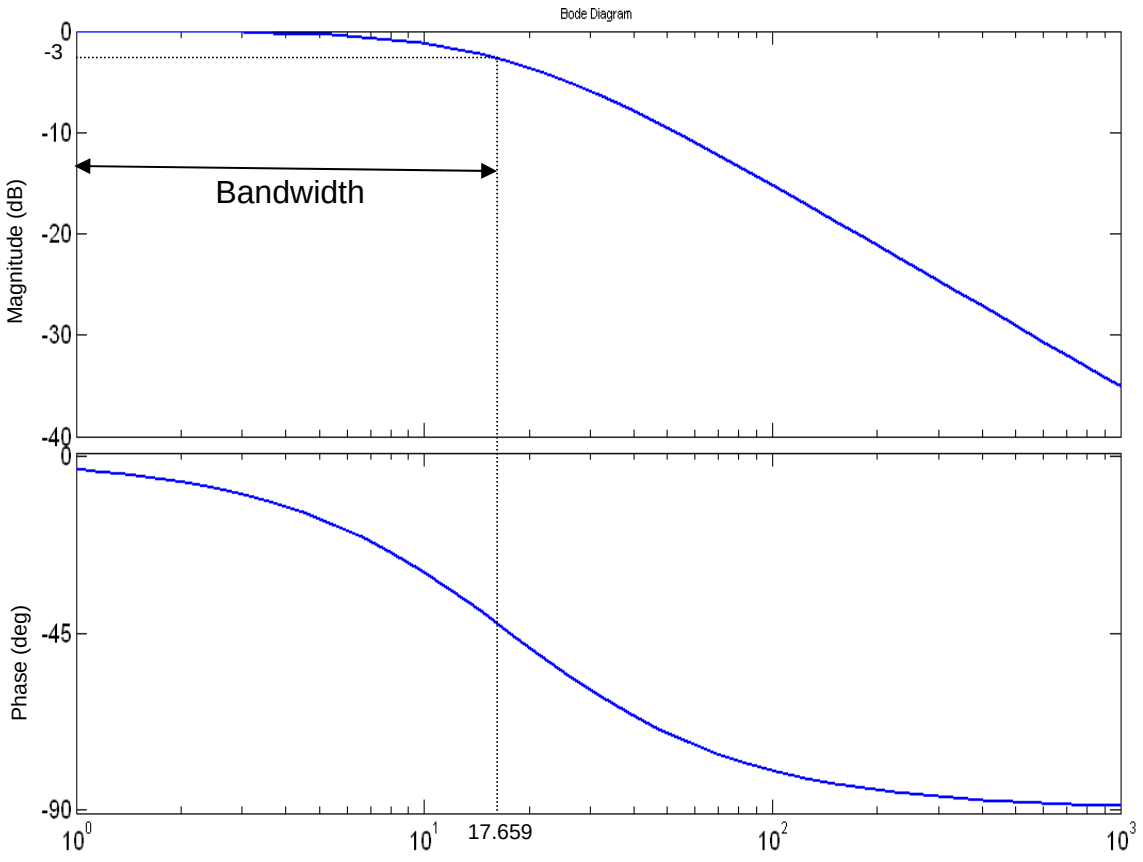

Fig. 3.9 Bode-plot for the transfer function (3.4).

3.2 Closed-Loop Position-Control System

After successfully implementing a current-control system, the active element position can be controlled by controlling the current. The schematic diagram that implements the current-control system in the position controller is shown in Fig. 3.10. *E*1 is the error of the position, *E*2 is the error of the current, and *C* is the output of the position controller. The closed-loop current-control system has been discussed in Section 3.1. The active material's position is monitored by using the laser distance sensor and fed back to the position controller. The required peak value of current is based on the error of the position. The design of the position controller will be presented in Section 3.3.

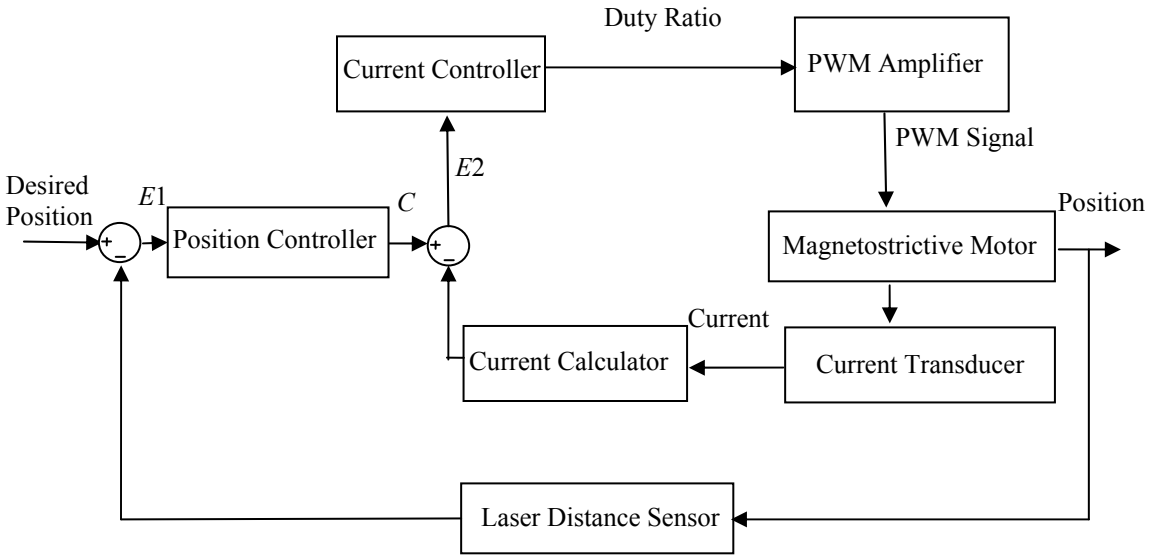

Fig. 3.10 Schematic diagram of the overall closed-loop system.

3.2.1 Direction of the Magnetostrictive Actuator

As mentioned in Chapter 2, the direction of the actuator is decided by the direction of the traveling magnetic field. In the closed-loop system the direction is based on the output of the position controller (*C*), and the control signal is generated, which makes the linear motor move in the desired direction by generating the required pulse signals which are sent via the digital I/O channels of the DSP board to the switching boards to generate the required direction of the traveling magnetic field. When the position controller output is positive, the magnetic field will travel to the positive direction of the displacement, and when the position controller output is negative, the magnetic field will travel to the negative direction of the displacement.

3.3 Position Controller Design with PID Controller

The design goals of the position control are to enhance performance of the previous research which used a closed-loop relay control system and increase the speed to reach the desired point as fast as possible. In order to achieve these goals, the controller is designed by using the maximum current to operate the actuator when the error is larger than 20 μm and uses the PID controller when the error is smaller than 20 μm. The flowchart is shown in Fig. 3.11. Using the maximum current can make the actuator operate at its fastest speed, and the PID controller can let the actuator move with desired accuracy. In order to retain the advantage of previous research, we chose 20 μm as the limit to switch between the PID controller and maximum current. The limit of 20 μm was chosen because the dead-zone value threshold for the relay controller in the

previous research is 20 μm, which has good performance in responding time and steady-state error [9]. If the threshold is less than 20 μm, the step response will exhibit oscillation [3]. Therefore, in order to avoid the oscillation and retain the advantage of the previous research, we chose 20 μm as the threshold.

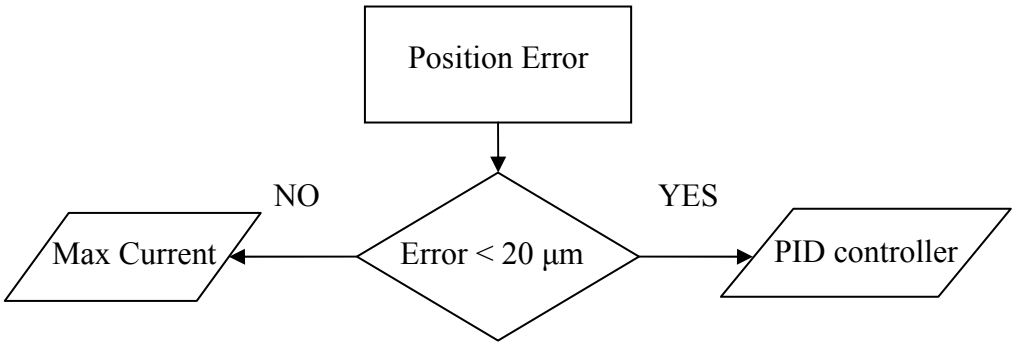

Fig. 3.11 The flowchart of controller selection.

3.3.1 Design of PID Controller by Relay-Auto Tuning Method

Sophisticated methods are available to design a PID controller that will meet steady-state and transient specification for tracking input references. However, these methods require the designer to have a dynamic model of the plant in the form of equations of motion or a detailed frequency response over a substantial range of frequencies [24]. The novel linear magnetostrictive actuator is an early development, so the data of a dynamic model can be quite difficult to obtain, and this difficulty has led to the development of sophisticated techniques of system model identification. Therefore, in the design of a PID controller for the linear novel magnetostrictive actuator, the

Ziegler-Nichols tuning method has been used for designing the parameter of the PID controller.

Ziegler-Nichols Tuning of PID Regulators

The Ziegler-Nichols tuning formula is a very useful empirical tuning methodology proposed in early 1942 by Ziegler and Nichols, who recognized that the step responses of a large number of process control systems with different plants exhibit a process reaction curve like that shown in Fig. 3.11 [24]. The process reaction curve can be obtained by a first-order plus dead time (FOPDT) plant and the transfer function is expressed by

$$G(s) = \frac{Ae^{-st_d}}{Ts+1} \tag{3.5}$$

which is a system with t_d seconds delay. The constants of $G(s)$ can be obtained from Fig. 3.12. The slope of the line is $R = A/T$, and the intersection of the tangent line with the time axis identifies the time delay $L = t_d$. In real-time process control systems, a large variety of plants can be approximately modeled by $G(s)$. $G(s)$ can be obtained from experiment, if the experimental step response of a plant exhibit like the process reaction curves shown in Fig. 3.12. From Fig. 3.12, the parameters of R and L which are obtained from the process reaction curve can be directly used to decide the optimum gains (proportional, integral and derivative gains) of the PID controller [24], [25]. The regulator parameters suggested by Ziegler and Nichols for the controller terms are given in Table 3.1.

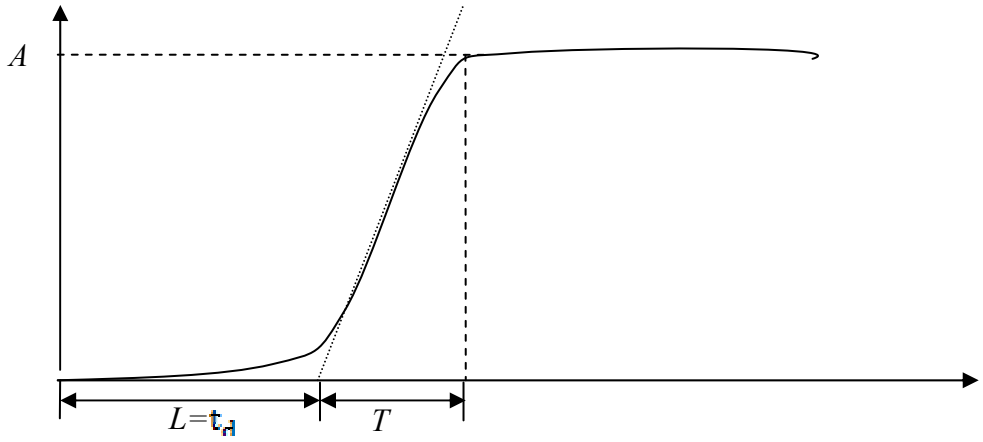

Fig. 3.12 Process reaction curve [24].

Table 3.1 Ziegler-Nichols Tuning for the Regulator $D(s) = k_P(1+\frac{1}{T_I s}+T_D s)$ [24]

Type of Controller	Optimum Gain
Proportional	$k_p = 1/RL$
PI	$k_p = 0.9/RL$ $T_I = L/0.3$
PID	$k_p = 1.2/RL$ $T_I = 2L$ $T_D = 0.5L$

Ultimate Sensitivity Method

If the step response is difficult or cannot be obtained, the ultimate sensitivity method is another way to tune the PID controllers. The ultimate sensitivity method is modified from the Ziegler-Nichols tuning method for tuning the PID controller of such a model and is based on evaluating the frequency response of the plant rather than on

taking a step response. The frequency response of the system used for tuning the PID controller will be an oscillation at the limit of stability. To use this method, a closed-loop system, as shown in Fig. 3.13, needs to be built. The proportional gain K_P is increased until the system becomes marginally stable and continuous oscillations just begin with amplitude limited by the saturation of the actuator. The corresponding gain that causes the oscillation is defined as K_u (called the ultimate gain) and the period of oscillation is P_u (called the ultimate period). These are determined as shown in Figs. 3.13 and 3.14. Similar to the way in which the step response can decide the optimum gain of the PID controller, the ultimate gain K_u and the ultimate period P_u can be used to tune the gains of the PID controller. The regulator parameters suggested by Ziegler and Nichols for the controller terms are given in Table 3.2 [24].

Table 3.2 Ziegler-Nichols Tuning for the Regulator $D(s) = k_P\left(1+\frac{1}{T_I s}+T_D s\right)$, based on the Ultimate Sensitivity Method [24]

Type of Controller	Optimum Gain
Proportional	$k_p = 0.5K_u$
PI	$k_p = 0.45K_u$ $T_I = P_u/1.2$
PID	$k_p = 0.6K_u$ $T_I = P_u/2$ $T_D = P_u/8$

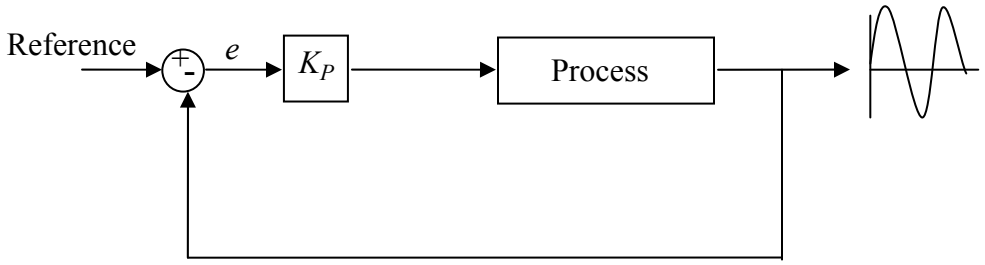

Fig. 3.13 Determination of the ultimate gain and period.

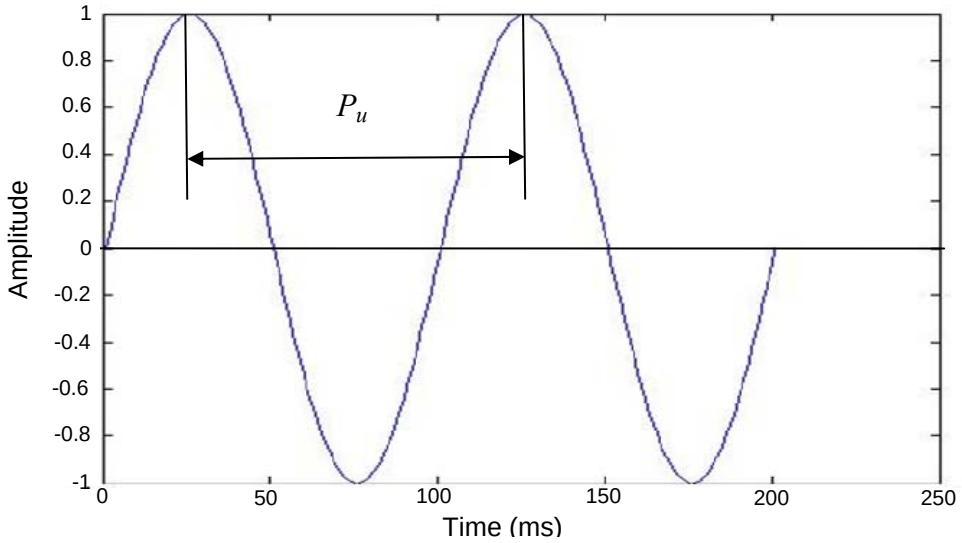

Fig. 3.14 Response of the closed-loop system in Fig. 3.13 [24].

Describing Function of a Relay Controller

A relay controller (also known as a bang-bang) has dynamic behavior resembling that shown in Fig. 3.15. Starting from its nominal bias value (denoted as 0 in the figure), the control action is increased by an amount denoted by *h* and later on decreased to a

value denoted by $-h$. Such controllers can be represented by describing function (K) [26].

Describing function K is the approach that one can use to approximately represent a static non-linear element, such as a relay controller, by an equivalent gain which is calculated by analyzing the so-called limit cycles or oscillation of the response of the closed-loop relay-control system. The describing function K that can represent the typical relay controller shown in Fig. 3.15 is:

$$K = 4h/A\pi, \tag{3.6}$$

where h is the relay amplitude of the relay controller, as shown in Fig. 3.15, and A is the amplitude of the oscillating response of the closed-loop relay-control system that used the relay controller in Fig. 3.16.

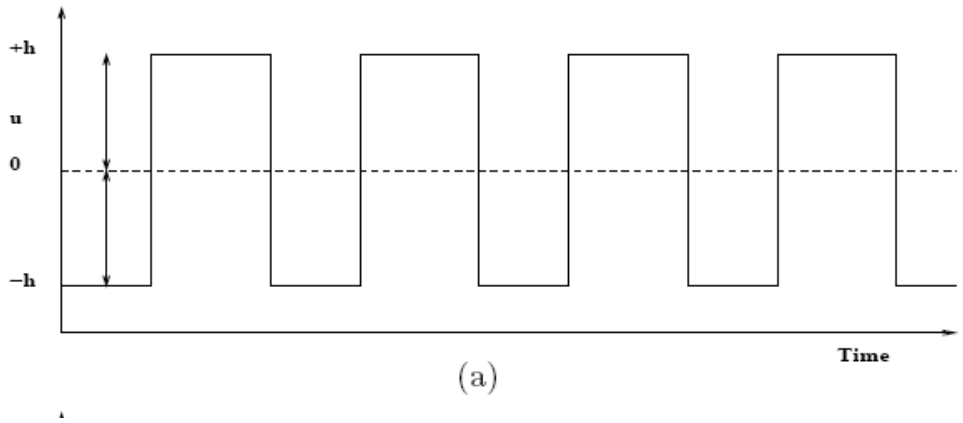

Fig. 3.15 Dynamic behavior of a relay controller [26].

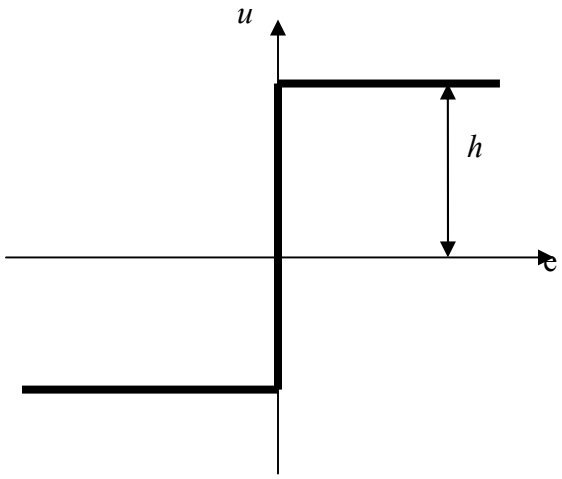

Fig. 3.16 Typical relay controller.

Relay Auto-Tuning PID Controller

Relay auto-tuning is a procedure based on the ultimate sensitivity method of Ziegler-Nichols tuning of the PID controller which uses a relay controller to get a frequency response similar to the response of ultimate sensitivity method. If we use a closed-loop relay-control system as shown in Fig. 3.17, due to the dynamic behavior of the relay controller, the output of the system will be a continuous oscillation and can be seen as the response of a closed-loop system with ultimate gain K_u, which is used for the ultimate sensitivity method.

From the ultimate sensitivity method of Ziegler-Nichols tuning methodology of the PID controller, the ultimate gain K_u that causes the system to become marginally stable and results in continuous oscillations and the ultimate period P_u of the oscillating response can be used to decide the parameters of the PID controller. Similarly, because the dynamic response of the closed-loop relay control system is similar, the describing

function K of the relay controller can be taken as the ultimate gain $K_u$because both the describing function K and the ultimate gain K_u can be described as the gain that causes the system to become marginally stable and continuous oscillations just begin with amplitude limited by the saturation of the actuator. The ultimate period P_u will be equal to the period of the response of the relay-control system because the describing function K is equal to the ultimate gain K_u. Therefore, relay auto-tuning can be used to decide the parameters of the PID controller as the ultimate sensitivity method [24], [26].

In this research, we used a typical relay-controller as the controller of the relay auto-tuning method. By inputting a constant reference to a closed-loop relay-control system, we can get the ultimate gain K_u and the ultimate period P_u to calculate the optimum parameters of the PID controller from Table 3.2.

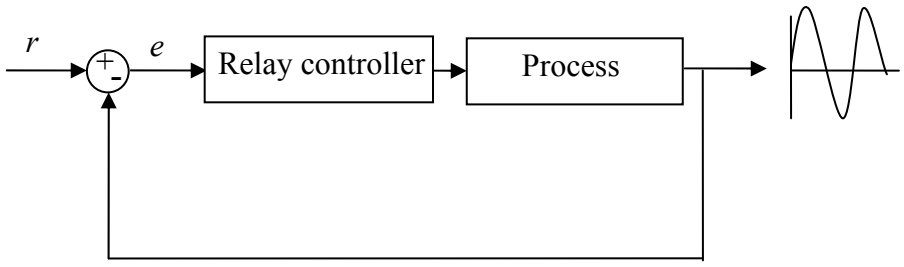

Fig. 3.17 Closed-loop system with a relay controller.

Tuning the PID Controller of the Closed-Loop Position-Control System

A closed-loop relay-control system, as shown in Fig. 3.18, needs to be built in order to get the ultimate gain and ultimate period. Parameters in function (3.6) and the

ultimate period P_u can be founded from the oscillating response of the system. The closed-loop relay-control system which was built to get the response of the novel linear magnetostrictive actuator is shown in Fig. 3.18, and the relay controller is defined as:

$$\text{Current} = f(\text{error}) = \begin{cases} 1.68\ \text{A} & \text{error} > 0 \\ -1.68\ \text{A} & \text{error} < 0 \end{cases} \tag{3.7}$$

From the definition of the relay controller we can obtain the relay amplitude h:

$$h = 1.68 \tag{3.8}$$

From the relay auto tuning method, the ultimate gain K_u is equal to the describing function $K = 4h/A\pi$. The ultimate period P_u and the oscillating amplitude A in the describing function K can be obtained from the characteristics of the oscillating response of the closed-loop relay-control system which uses the relay controller defined in function (3.7).

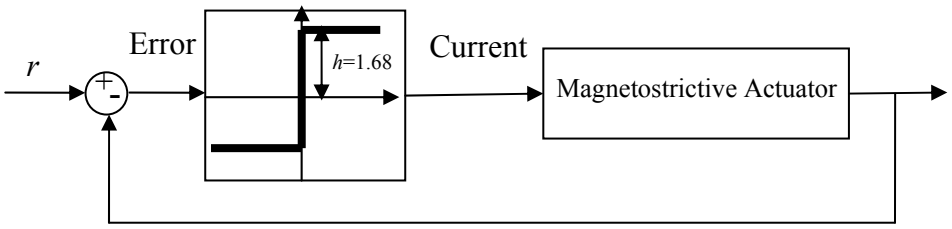

Fig. 3.18 Schematic diagram of the closed-loop system which uses the relay controller defined in function (3.7).

Experiment Result

The response of the closed-loop relay-control system which uses the relay controller defined in function (3.7) is shown in Fig. 3.19. As shown in Fig. 3.18, we can obtain a continuous oscillation with the amplitude A and period P as:

(3.9)

$$A = 0.032 \text{ mm}, P = 5.1 \text{ s}$$

After the oscillating amplitude A is known, the ultimate gain K_u can be found by calculating the describing function of the relay controller K as:

$$K_u = K = 4h/A\pi = 66.87 \tag{3.10}$$

Based on the auto relay tuning method, the ultimate period P_u is equal to the period P of the response of the closed-loop relay-control system. The ultimate period P_u is

$$P_u = P = 5.1\text{s} \tag{3.11}$$

After we obtain the ultimate gain K_u and the ultimate period P_u, the optimum gains of the PID controller $k_p(1+\frac{1}{T_I s}+T_D s)$ can be calculated. From Table 3.1, we can get k_p, T_I and T_D:

$$k_p = 0.6K_u = 40.12 \tag{3.12}$$

$$T_I = \frac{P_u}{2} = 2.55 \tag{3.13}$$

$$T_D = \frac{P_u}{8} = 0.6375 \tag{3.14}$$

Then, the PID controller we chose will be

$$D_{PID}(s) = k_P(1+\frac{1}{T_I s}+T_D s) = 40.12(1+1/2.55s+0.6375s) \tag{3.15}$$

The closed-loop step response of the position controller which included the PID controller will be discussed in Chapter IV.

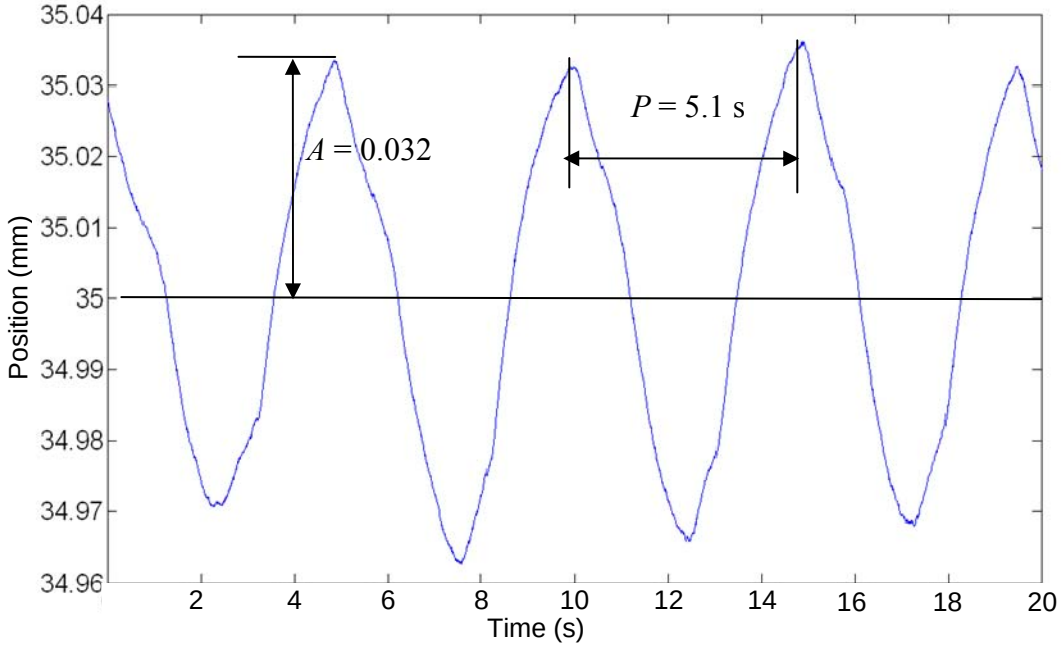

Fig. 3.19 Response of the closed-loop relay-control system using the relay controller defined in function (3.7).

3.3.2 Design of PID Controller by Root-Locus

With the relation between the current and the velocity, a dynamic model of the magnetostrictive actuator can be obtained approximately.

Dynamic Model of the Novel Linear Magnetostrictive Actuator

In this thesis, the underlying theory of the linear magnetostrictive motor shown in (2.2) presents the relation between velocity and peak magnetostrictive strain. If the linear magnetostrictive actuator is operated under no load condition, the mechanical strain resulting from the external load applied on the active material can be ignored and (2.1) can be simplified as

$$v = N f p \varepsilon_{\max} \tag{3.16}$$

Therefore, if the relation between the peak magnetostrictive strain and the current can be defined, the dynamic model between the current and the velocity can be found.

As mentioned before, the displacement of the active element of the linear magnetostrictive actuator is based on the magnetostrictive strain. Each time the magnetic field makes one travel through the entire active element, the active element will move forward by a distance which can be related to the magnetostrictive strain. Due to this characteristics, calculating how many cycles the magnetic field travels through the entire active element in a certain range allows us to find the magnetostrictive strain that occurs under a certain current. Moreover, if the relation between the magnetostrictive strain and the current is assumed to be approximately linear, the current can substitute the magnetostrictive strain in (3.16).

The local multi-phase operation frequency of the linear magnetostrictive actuator is 10 Hz, so the time it takes for the magnetic field to travel through the pitch of the actuator is 0.1 s. Fig 3.20 shows the current signal in one of the coils in the magnetostrictive actuator when the actuator is operated at a current of 1.68 A. That the current in the coil changes every 0.1 s proves that the period of the traveling magnetic field is 0.1 s. Fig. 3.21 shows that the position of the active element moves from 33 mm to 34 mm when the actuator is operated at a current of 1.68 A.

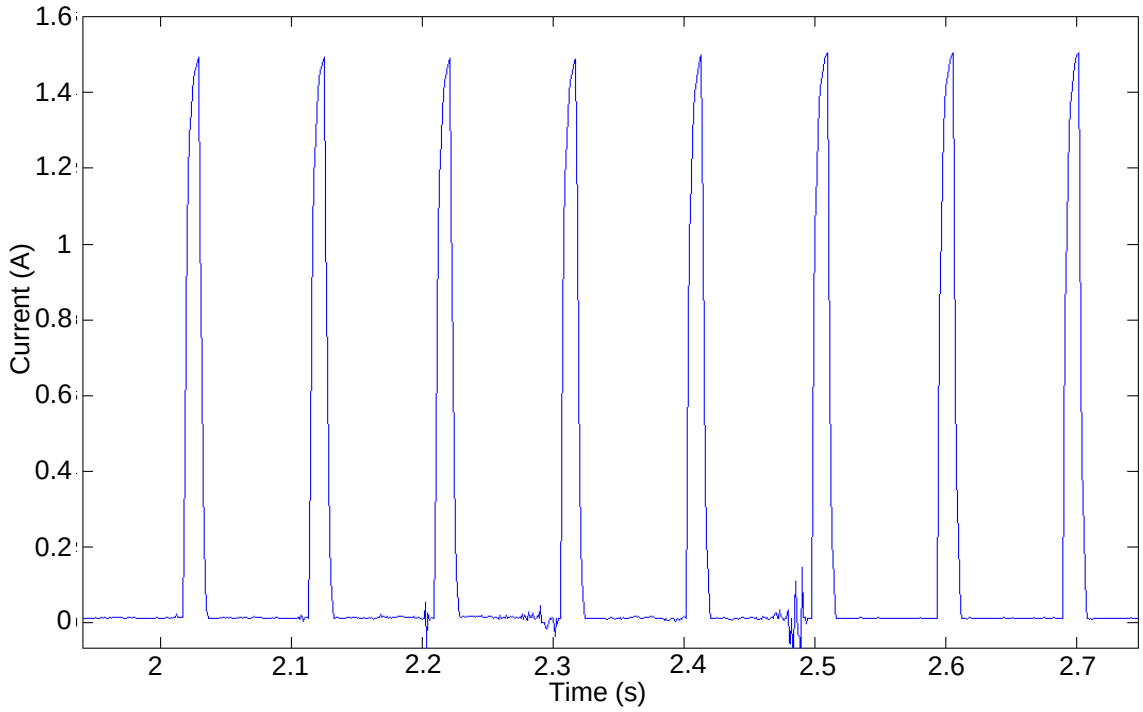

Fig. 3.20 Current signal in one of the coils in the magnetostrictive actuator when the actuator is operated at a current of 1.68 A.

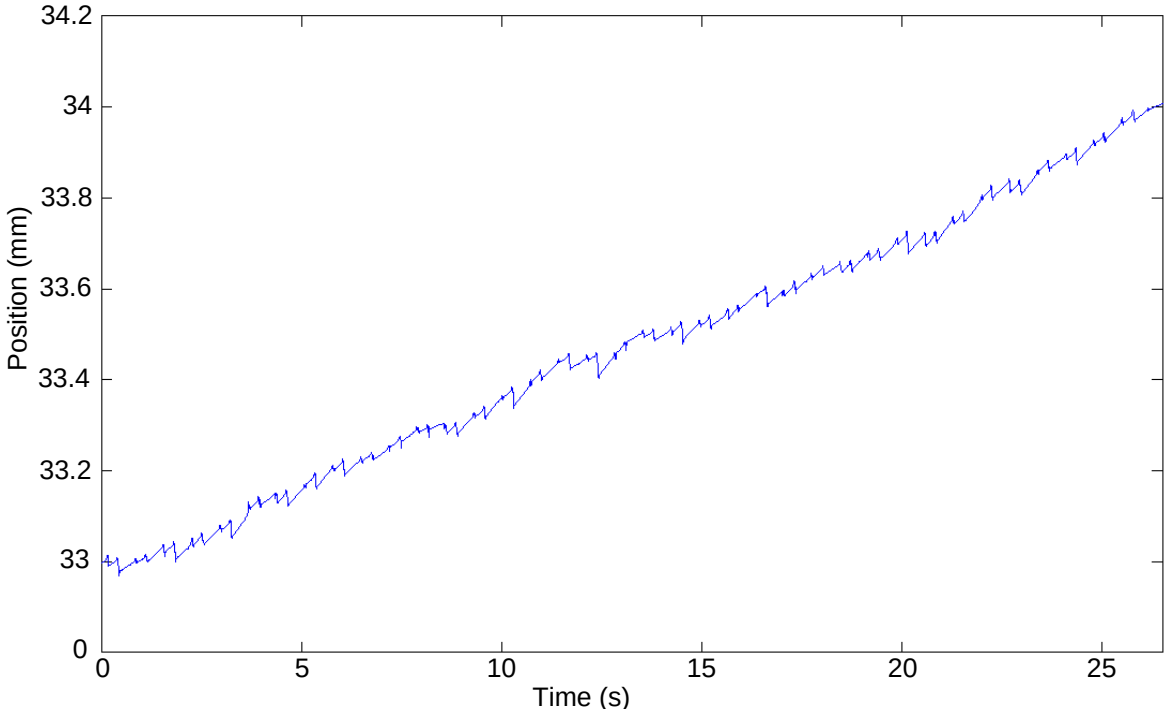

Fig. 3.21 Position of the active element moves from 33 mm to 34 mm when the actuator is operated at a current of 1.68 A.

The active element needs 26 s to move 1 mm. In other words, the active element will move 1 mm when the magnetic field travels through the entire active element 260 times. Therefore, the average expansion each cycle under the current of 1.68 A is

$$L_F - L_0 = \frac{1}{260} \text{ mm} = 0.0038 \text{ mm} \tag{3.17}$$

where L_F is the length after expansion and L_0 is the original length. The value of original length is approximately equal to the length of three coils which activate at the same time to generate the magnetic field to expand the active element. Therefore, the value of original length L_0 is

$$L_0 = 25 \text{ mm} \tag{3.18}$$

Then the magnetostrictive strain is

$$\varepsilon_{\max} = \frac{L_F}{L_0} - 1 = \frac{0.0038}{25} = 0.000152 \tag{3.19}$$

Then, as mentioned before, if the relation between the magnetostrictive strain and the current is assumed to be linear, the ratio between the magnetostrictive strain and the current can be found as

$$\text{Ratio} = \frac{\varepsilon_{max}}{I} = \frac{0.000152}{1.68} = 0.00009 \tag{3.20}$$

where $\varepsilon_{\max}$ is the magnetostrictive strain under the current of 1.86 A and I is the operating current of the magnetostrictive actuator. After substituting $\varepsilon_{\max}$ in (3.18) to (3.16), the dynamic model of the velocity and the current can be found as shown below

$$v = Nfp\,(0.00009I) \tag{3.21}$$

where N = number of phase (3)

f = local multi-phase operation frequency (10 Hz)

p = slot pitch (10.9 mm)

v = velocity (mm/s)

I = current

Substitute the parameters to (3.19) the dynamic model between velocity and current will be

$$v = 0.0294\, I \text{ mm/s} \tag{3.22}$$

After knowing the dynamic model between velocity and current, by the closed-loop position-control system shown in Fig. 3.9 and the transfer function (3.4) of the closed-loop current-control system the dynamic model of the magnetostrictive actuator can be modeled as

$$P(s) = \frac{v}{s} = \frac{1.7659K}{s+1.7659K}\frac{0.0294}{s}I(s) \tag{3.23}$$

where P is the position and $K = 10$.

Design of the PID Controller by Root-Locus

Equation (3.23) can be represented as the plant transfer function of the magnetostrictive actuator and can be used to design the PID controller. In this thesis, the root-locus is used to design the PID controller. The characteristic equation of the closed-loop position-control system is

$$1 + \frac{17.659}{s+17.659}\frac{0.0294}{s}\, C_{PID}(s) = 1 + \frac{17.659}{s+17.659}\frac{0.0294}{s}k_P\left(1 + \frac{k_I}{s} + k_D s\right) \tag{3.24}$$

If $k_P = K_R$, $k_I = T_I$ and $k_D = T_D$, equation (3.22) can be modified as

$$1 + \frac{17.659}{s+17.659}\frac{0.667}{s}K_R(1+ \frac{T_I}{s} + T_D s) \tag{3.25}$$

Fig. 3.22 shows the root-locus of $T_I = 1$, $T_D = 1$, Fig. 3.23 shows the root-locus of $T_I = 1$, $T_D = 0.1$ and Fig. 3.24 shows the root-locus of $T_I = 10$, $T_D = 0.1$. The loci of all the plots are in the left half-plane, (LHP) so the system will stable under these controllers.

The change of gain K_R on the root locus of the controller with the value of $T_I = 1$, $T_D = 0.1$ is smaller than the other two controllers. Therefore, Fig. 3.24 was used to design the PID controller for the closed-loop position-control system. For the design for PID controller, the goal of the performance is to make the closed-loop position-control system have a step response with the rise time t_r less than 18 s which is the time that the magnetostrictive actuator needs with the same distance. Due to the consideration, the natural frequency ω_n should be

$$\omega_n > \frac{1.8}{t_r} = \frac{1.8}{18} = 0.1 \text{ rad/s} \tag{3.26}$$

By evaluation the gain K_R in Fig. 3.24, when $K_R = 14.14$, the natural frequency is 0.664. Therefore, the rise time would less than 18 s. The PID controller which designed by root-locus is

$$k_P(1+ \frac{k_I}{s} + k_D s) = K_R(1+ \frac{T_I}{s} + T_D s) = 14.14\ (1 + \frac{1}{s} + 0.1s) \tag{3.27}$$

Fig. 3.25 shows the simulation step response of the closed-loop position-control system with the PID controller which designed by root-locus. It shows that the PID controller which designed by the root-locus in this section can make the linear magnetostrictive actuator stable.

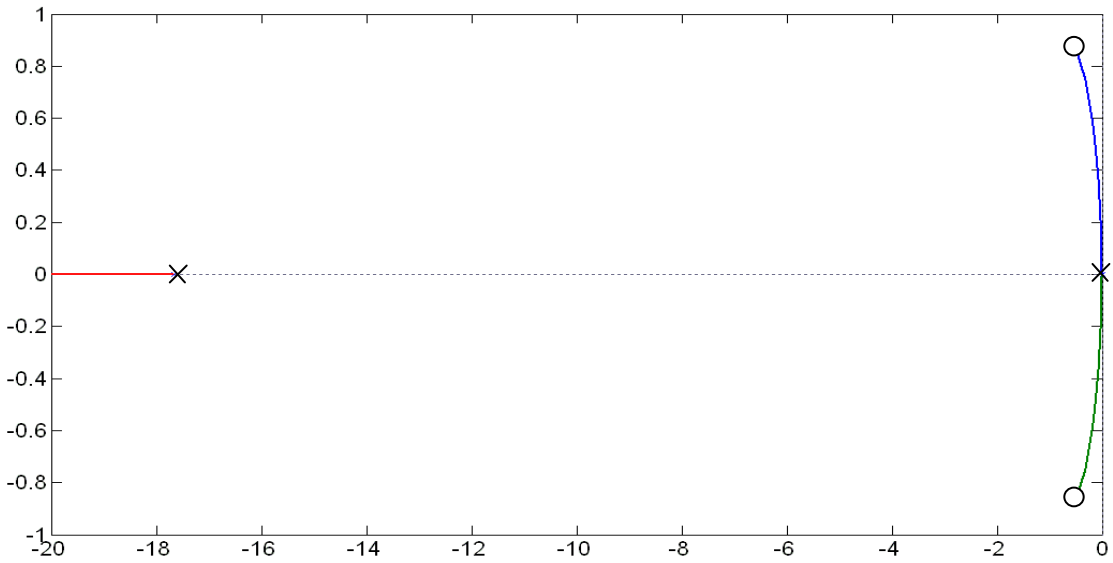

Fig. 3.22 Root-locus of $T_I = 1,\ T_D = 1$.

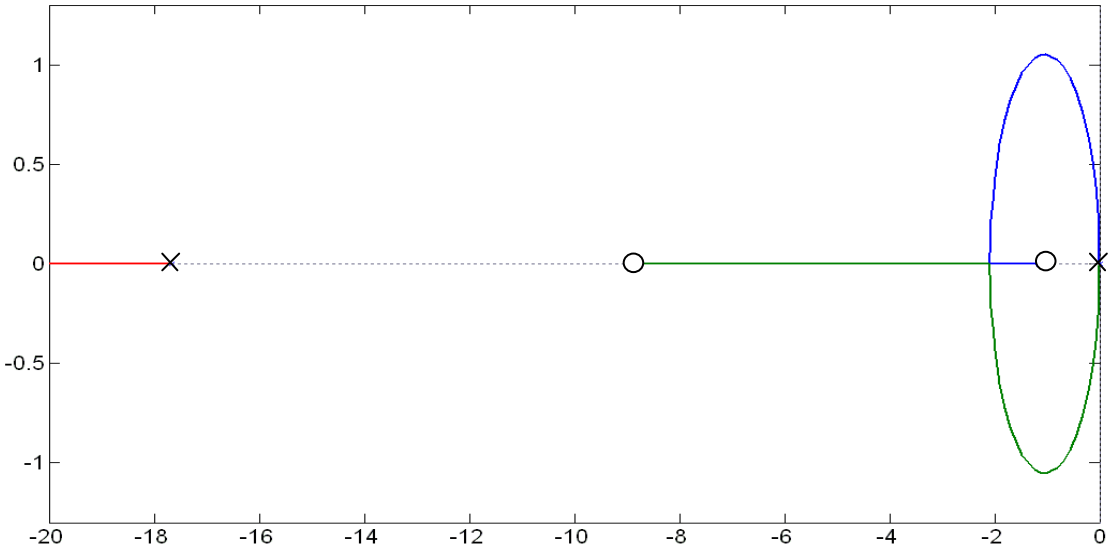

Fig. 3.23 Root-locus of $T_I = 1,\ T_D = 0.1$.

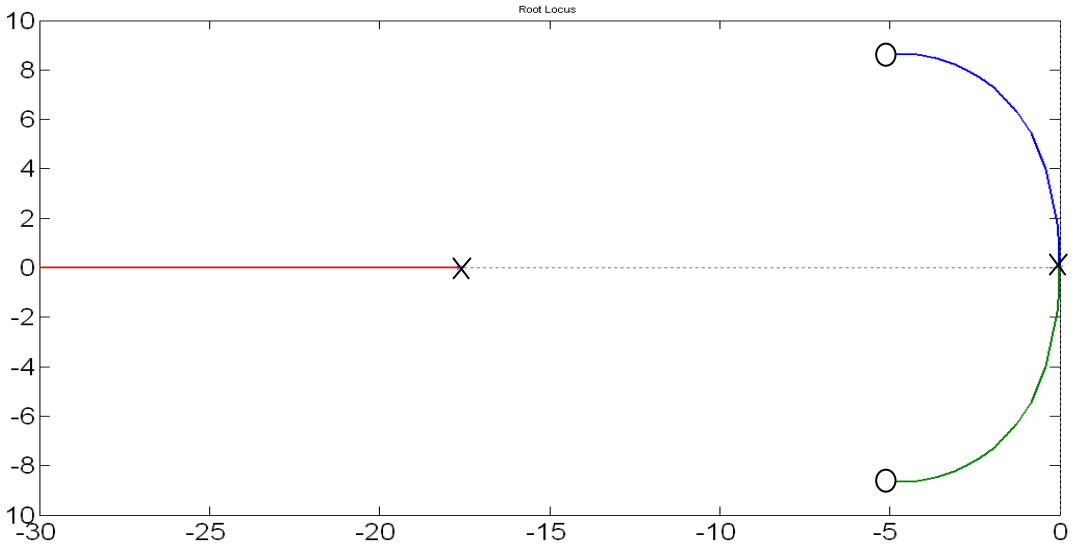

Fig. 3.24 Root-locus of $T_I = 10$, $T_D = 0.1$.

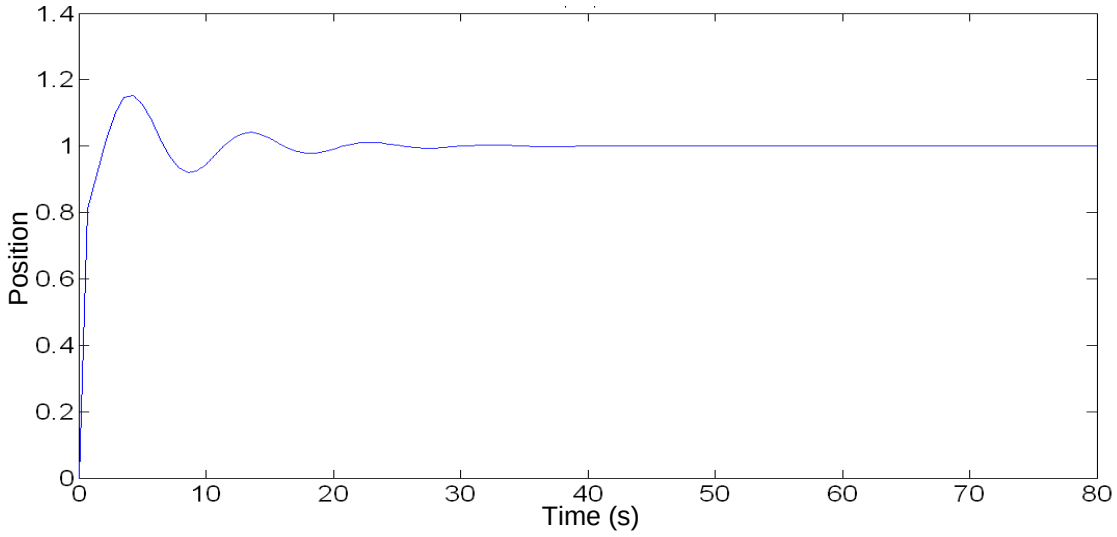

Fig. 3.25 Simulation of the step response of the closed-loop position-control system with the PID controller designed by root-locus.

3.4 Position Controller Design with Linear Variable-Velocity Controller

Because of the closed-loop current-control system, the closed-loop position-control system can use any kinds of position controller which control the

position by controlling the current. Therefore, the part of the PID controller in the position controller can be replaced by various controllers. In other words, the PID controller in Fig. 3.10 can be replaced. This section will present another controller which is different from the PID controller.

As with the position controller with the PID controller, since the current is controllable, the velocity of the active element can be controlled. Therefore, if we decrease the current, the velocity will decrease, too. The current-speed characterization curve is shown in Fig. 3.26. As shown in Fig. 3.26, the velocity will decrease to zero if the current is decreased to zero. Therefore, if a linear variable-velocity controller can make the current decrease to zero linearly with the error, the velocity will also decrease to zero linearly with the error.

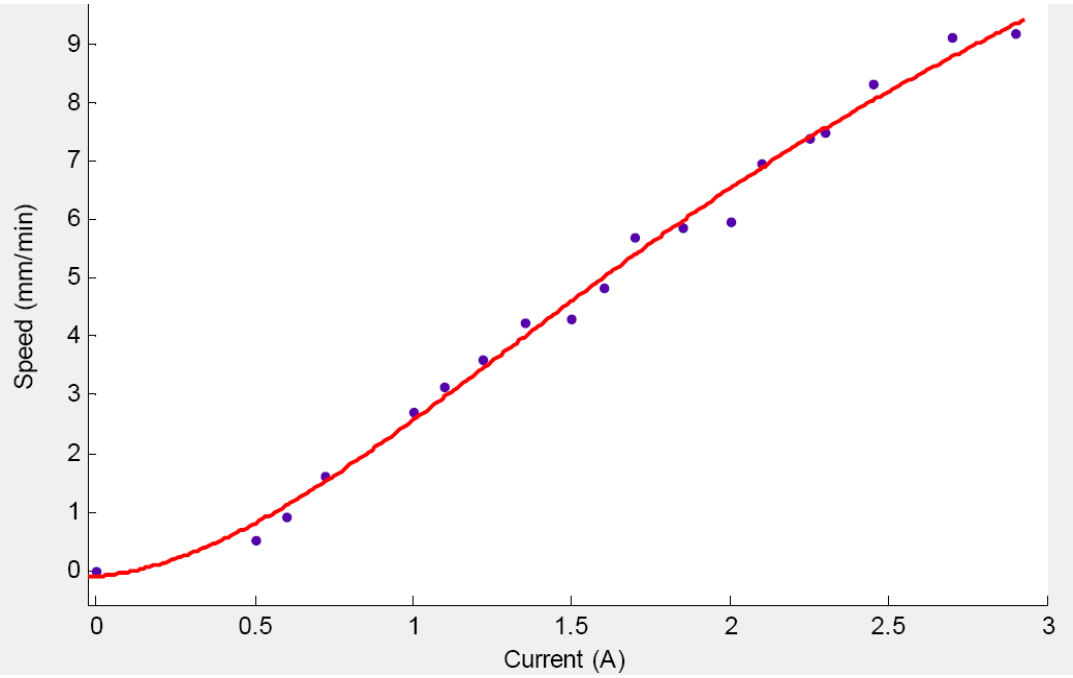

Fig. 3.26 Current-speed characterization curve [9].

In other words, unlike the relay-controller the velocity is variable within the dead-zone of relay controller. Because of this characteristic, the velocity of the active element would decrease linearly when it is near the desired position and the velocity would be zero when it reaches the desired position.

The schematic diagram of the linear variable-velocity controller is shown in Fig. 3.27, and it can be defined as:

$$\text{Current} = f(e) = \begin{cases} 1.68, & e > -20\ \mu\text{m} \\ \frac{1.86}{0.02} \times e, & -20\mu\text{m} < e < 0 \\ -\frac{1.86}{0.02} \times e, & 0 < e < 20\ \mu\text{m} \\ -1.68, & e > 20\ \mu\text{m} \end{cases} \tag{3.28}$$

where 1.86 A is the current that can make the active element move with its maximum speed when the actuator operates under 8 V and e is the position error. Under the definition, the current will change linearly with the error when the error is within ±20 μm and the current will remain at the maximum value when the error is not within ±20 μm.

The closed-loop position-control system with the linear variable-velocity controller is similar to the closed-loop position-control system with PID controller shown in Fig. 3.8, *E1* is the error of the position, *E2* is the error of the current, and *C* is the output of the position controller. The closed-loop step response of the linear variable-velocity controller will be presented in Chapter IV.

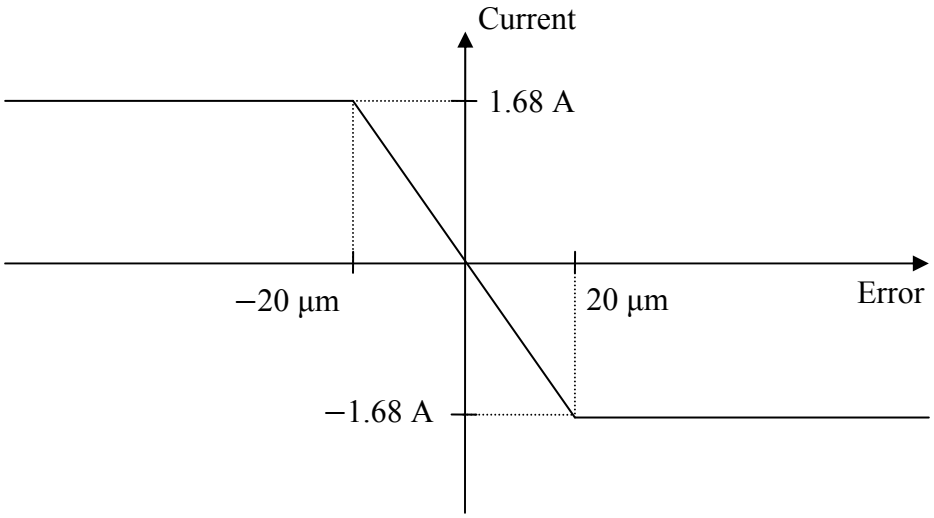

Fig. 3.27 Schematic diagram of a linear variable-velocity controller.

3.5 Position Controller Design with Sliding Mode Control

Sliding mode control (SMC) is a control method often used for the robust control of linear or nonlinear control systems. SMC has the advantage of simplifying the dynamic structure of the plant, and the response of the closed-loop control system will become insensitive to system uncertainties and disturbances. Moreover, by using SMC, the design of the control system can be relatively low cost compared with other system that has the same performance [27].

The concept of SMC is shown in Fig. 3.28. S stands for the sliding surface and X_i represents the state of control plant. The sliding surface S can be seen as the performance of a closed-loop control system and is called the sliding mode. If the system moving along with the desired trajectory, the sliding surface is [28]

$$S = 0 \tag{3.29}$$

And it shows that the system is in the perfect situation that the control plant is just on the ideal sliding surface.

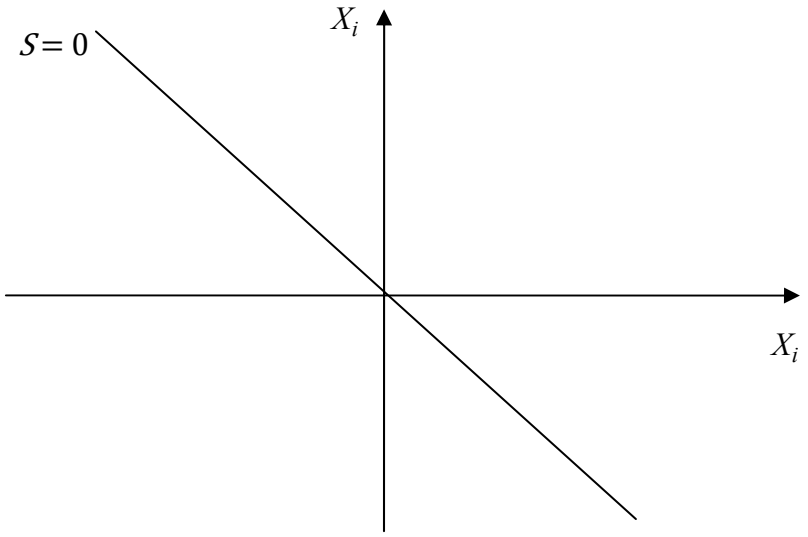

Fig. 3.28 The concept of sliding mode control.

However, in a real system, there must be a tracking error for the SMC. The tracking error shows the difference between desired state trajectory and the actual state trajectory. The SMC will force the S keep on the $S = 0$ and converge the tracking error to zero. For example, when the actual state trajectory moves beyond the desire surface, the sliding surface S falls off the surface $S = 0$. The SMC will calculate the new surface S again and returns it to the desired surface $S = 0$. If a plant of a control system is an n-th order system, the sliding mode S can be defined as [28]

$$S(x, t) = \left(\frac{d}{dt} + \lambda\right)^{n-1} \hat{x} \tag{3.30}$$

where $\hat{x} = x - x_d$, x_d is the set point and $\hat{x}$ is the error between x and x_d, and n is the order of the system.

Therefore, by (3.22), the state of the plant can be found as

$$\dot{x} = 0.0294\, I \tag{3.31}$$

and it is a first order system. Then, the sliding mode S can be modified as

$$S(x, t) = \hat{x} = x - x_d \tag{3.32}$$

Based on the theory of SMC, the system should force the sliding mode S move on the desired surface $S = 0$. Therefore, x can be assume equal to x_d at the perfect condition and because $S = 0$, $\dot{S} = 0$. $\dot{S}$ can be calculate from (3.28) and (3.29)

$$\dot{S}(x, t) = \dot{x} - \dot{x_d} = 0.667\, I - x_d = 0 \tag{3.33}$$

In the SMC, an equivalent control law Ueq is estimated to achieve the condition of $S = 0$ and $\dot{S} = 0$. The equivalent control law Ueq is

$$Ueq = \frac{\dot{x_d}}{0.667} = \frac{\dot{x}}{0.667}, \text{ because } x = x_d \tag{3.34}$$

Then,

$$U = Ueq + Ksgn(S) \tag{3.35}$$

U is called the sliding control mode of the SMC system and K is the switching gain to force the sliding mode S follow the desired surface $S = 0$. According to the results, the sliding mode control system is shown in Fig. 3.29. In the system, value of $Ksgn(S)$ is

$$E(t) \times -50 \tag{3.36}$$

where $E(t)$ is the position error. The reason the error times -50 is because when the error is less than 20 μm the sliding control mode which is the input of the controller if

the system only use $E(t)$ as the switching gain, the current will be too small to move the active element and cause large error. Therefore, by timing a constant -50, when the error is 20 μm, the sliding control mode can still have a value lager than 0.5 A. When the error is 10 μm, the sliding control mode can still have a value between 0.3~0.2 A. Due to the design, the SMC can have the accuracy less than 10 μm.

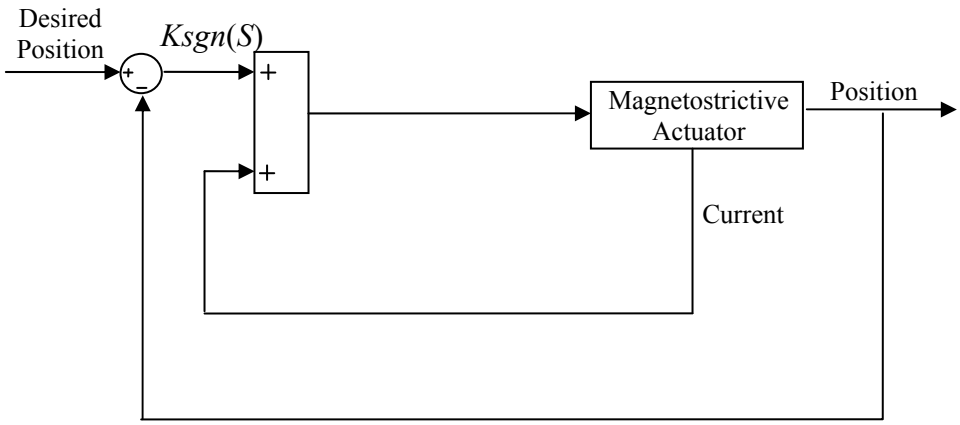

Fig 3.29 Sliding mode control system.

CHAPTER IV

EXPERIMENTAL RESULTS AND DISCUSSION

In this chapter, experimental results obtained after implementing the closed-loop control scheme described in Chapter III will be shown. The performances, such as the steady-state error and the step response, of various closed-loop position-control systems, including two position controllers which designed in this thesis and the relay controller which used in the previous research previous research which used the relay controller, will be discussed.

4.1 Closed-Loop Position Response with PID Controller

As mentioned in Chapter III, position control was achieved by designing the position controller and current controller. Based on the position error, the controller will switch between a PID controller and a constant value which is the maximum current. The rise time is mainly influenced by the value of maximum velocity when the actuator is operated under the maximum current. The accuracy is influenced by the PID controller when the error is within 20 μm.

For the controller of the closed-loop position-control system in this thesis, the PID controller was designed using two methods. The first is the relay auto-tuning method that designs the PID controller without a dynamic model. This method uses the response from a closed-loop relay-control system to find the optimum gains of the PID controller. The second method uses the root-locus to design the PID controller by analyzing the

dynamic model of the linear magnetostrictive actuator. The dynamic model is defined by simplifying the relation between the velocity and current. This model can be used only when the magnetostrictive actuator is operated in a no-load condition. The experiment results of the closed-loop position-control system with these two PID controllers will be presented in Sections 4.1.1 and 4.1.2.

4.1.1 PID Controller Tuning by Relay Auto-Tuning Method

Various step response experiments of the closed-loop position-control system with the PID controller which designed by relay auto-tuning method were performed for different commanded positions to move from 33 mm to 34 mm and from 34 mm to 34.5 mm. Fig. 4.1(a) shows the closed-loop 1-mm step position response from 33 mm to 34 mm. The rise time of the response is 26 s and the overshoot is 46 μm. Fig. 4.1(b) shows the closed-loop 0.5 mm step position response from 34 mm to 34.5 mm. The rise time is 18 s and the overshoot is 50 μm.

Fig. 4.2 shows the capability of the designing controller in tracking a sinusoidal reference input with amplitude of 0.5 mm and frequency of 0.04 rad/s. As shown in Fig. 4.2, in some range of time, it exhibited a time delay of 5 s. It is because the current does not always keep at the maximum current. Therefore, when the current is too small to lose the capability to move the active element, the delay will occur and the system needs more time to follow the change of sinusoidal position reference.

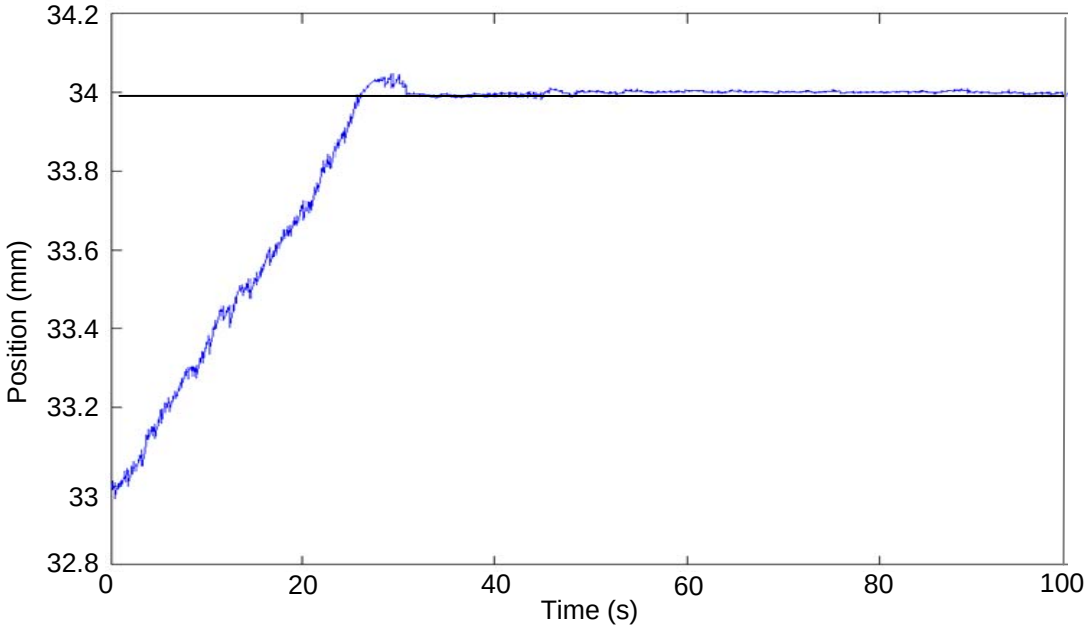

(a)

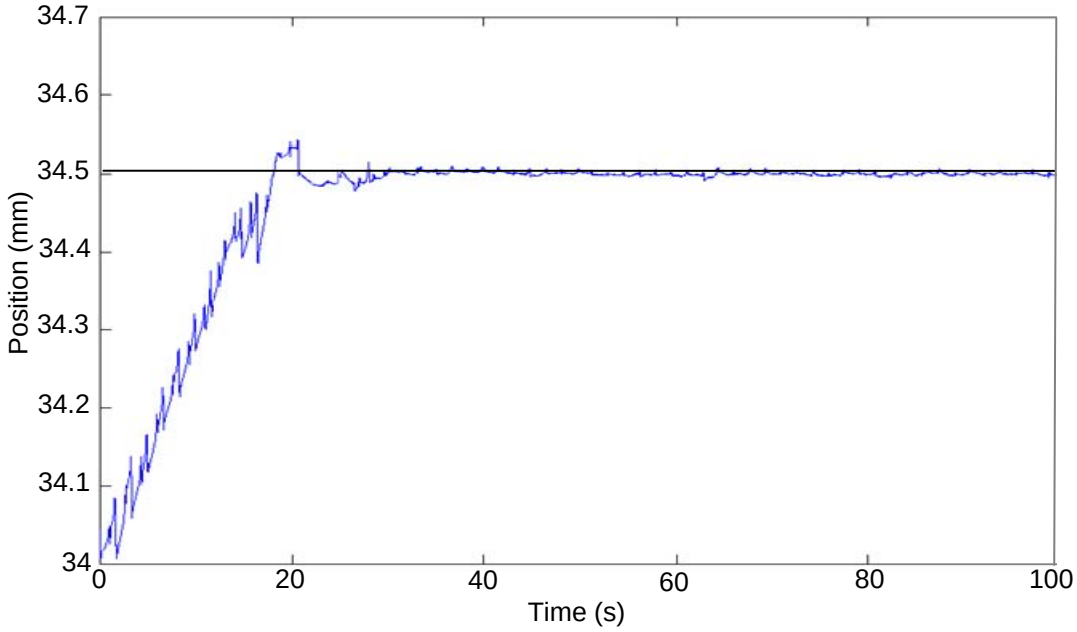

(b)

Fig. 4.1 (a) Closed-loop 1-mm step position response from 33 mm to 34 mm. (b) Closed-loop 0.5-mm step position response from 34 mm to 34.5 mm.

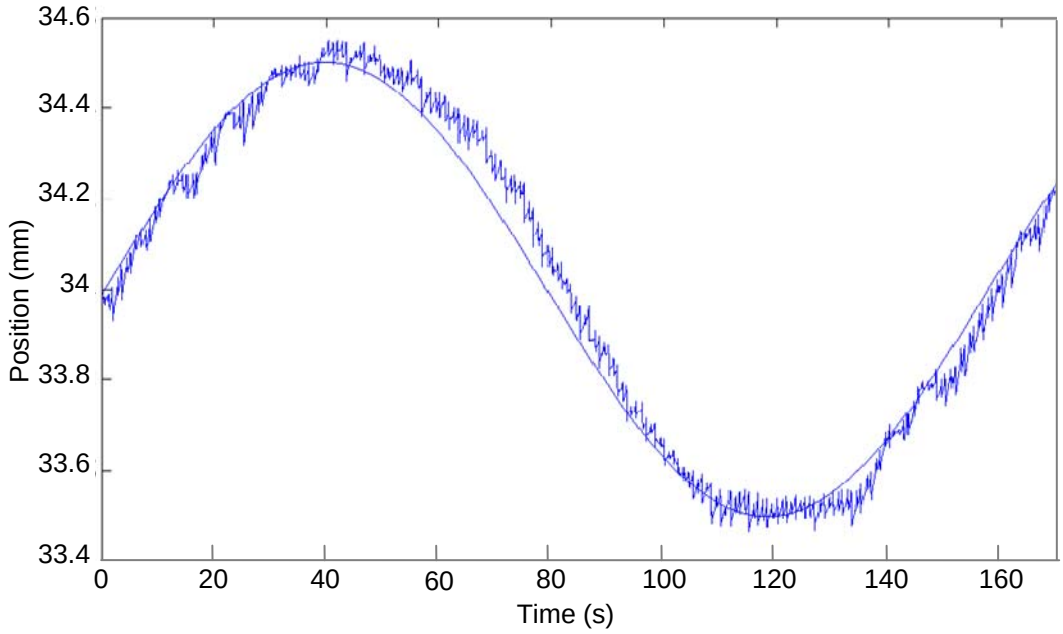

Fig.4.2 Closed-loop response to a sinusoidal reference input with an amplitude of 0.5 mm and frequency of 0.04 rad/s.

Steady-State Error

Fig. 4.3 shows the steady-state error of a closed-loop 0.5-mm step position response from 34 mm to 34.5 mm (Fig. 4.1(b)). As shown in Fig. 4.3, the peak-to-peak noise level was 5 μm. The presence of the noise limited the position resolution of the position control of the actuator. Some of the probable causes of the noise are as follows:

- The sensor for sensing the tip position was a laser distance instrument (model OADM 20I6460/S14F by Baumer Electric) with a resolution of 5~60 μm when incident on matte white ceramic. The sensor resolution may be one of the probable causes of this 10 μm peak-to-peak position noise. Fig. 4.4 shows the noise on matt white ceramic.
- Other contributors might be the A/D quantization noise, or the electrical noise.

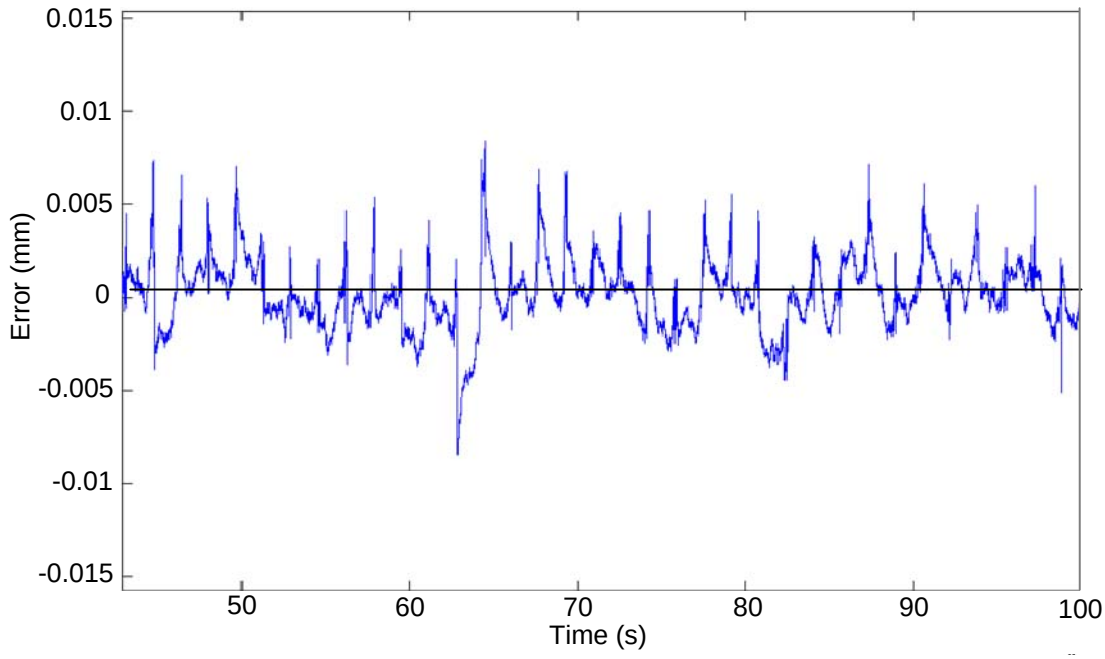

Fig. 4.3 Steady-state error of closed-loop 1-mm step position response from 34 mm to 34.5 mm.

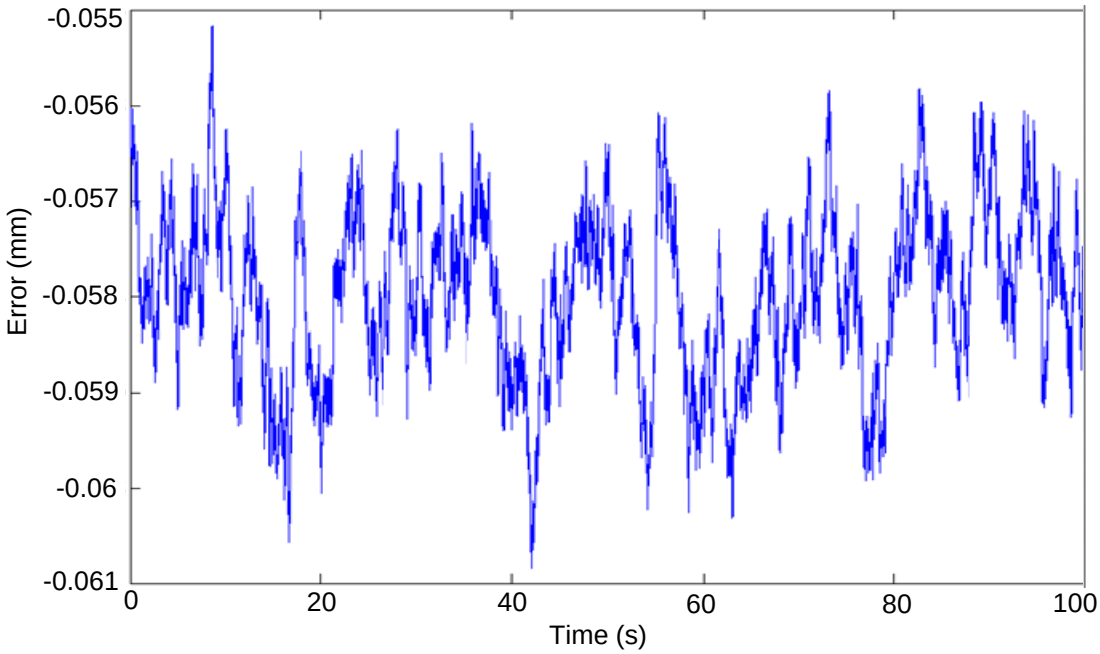

Fig. 4.4 Noise of the laser sensor on matt white ceramic.

4.1.2 PID Controller Designed by Root-Locus

The step response experiments of the closed-loop position-control system with the PID controller which was designed by the root-locus were performed by commanding the positions to move to 34.5 mm. Fig. 4.5 shows the closed-loop 0.5 mm step position response from 34 mm to 34.5 mm. The rise time of the response is 16 s and the overshoot is 30 μm. The rise time is almost the same with the response shown in Fig. 4.1(b). This is because, when the error is larger than 20 μm, the magnetostrictive actuator is operated on the maximum current and the PID controller has no influence on the responding time. There is a little different between Fig. 4.5 and the simulated step response shown in Fig. 3.22. This is because the dynamic model used to design the PID controller is obtained with a simplified relation between the current and the velocity.

Fig. 4.6 shows the capability of the designed controller to track a sinusoidal reference input with amplitude of 0.5 mm and frequency of 0.04 rad/s. As shown in Fig. 4.6, in some range of time, it also exhibited a time delay of 5 s like the response shown in Fig. 4.2. This is also because when the current is not large enough to move the active element, the system needs some time to follow the change of the reference.

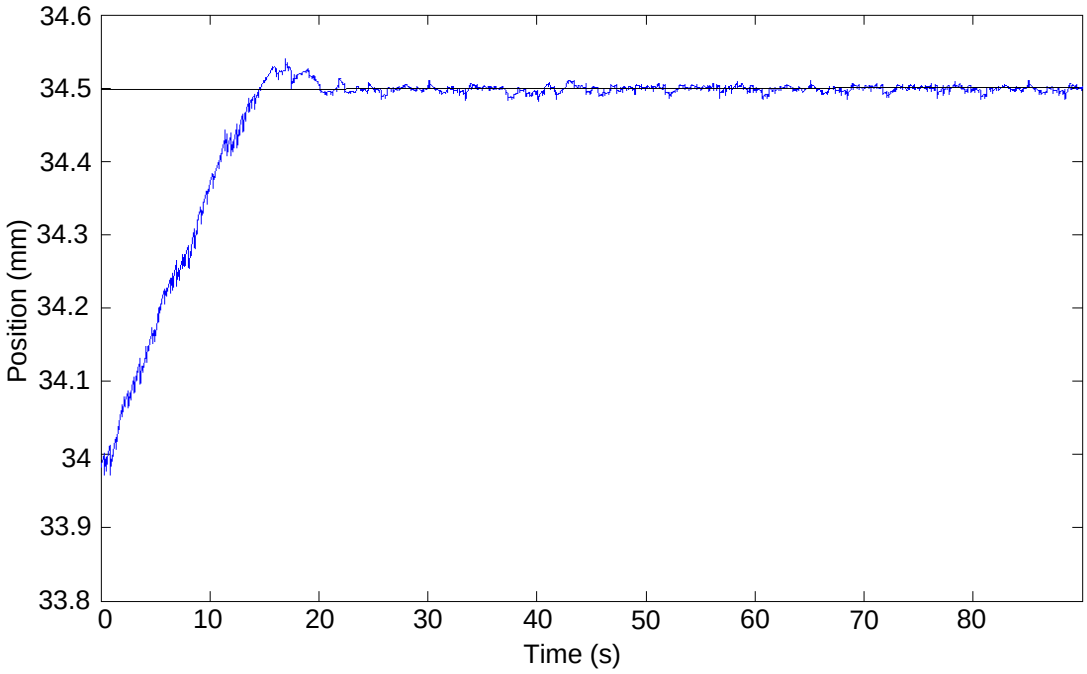

Fig. 4.5 Closed-loop 1-mm step position response from 34 mm to 34.5 mm.

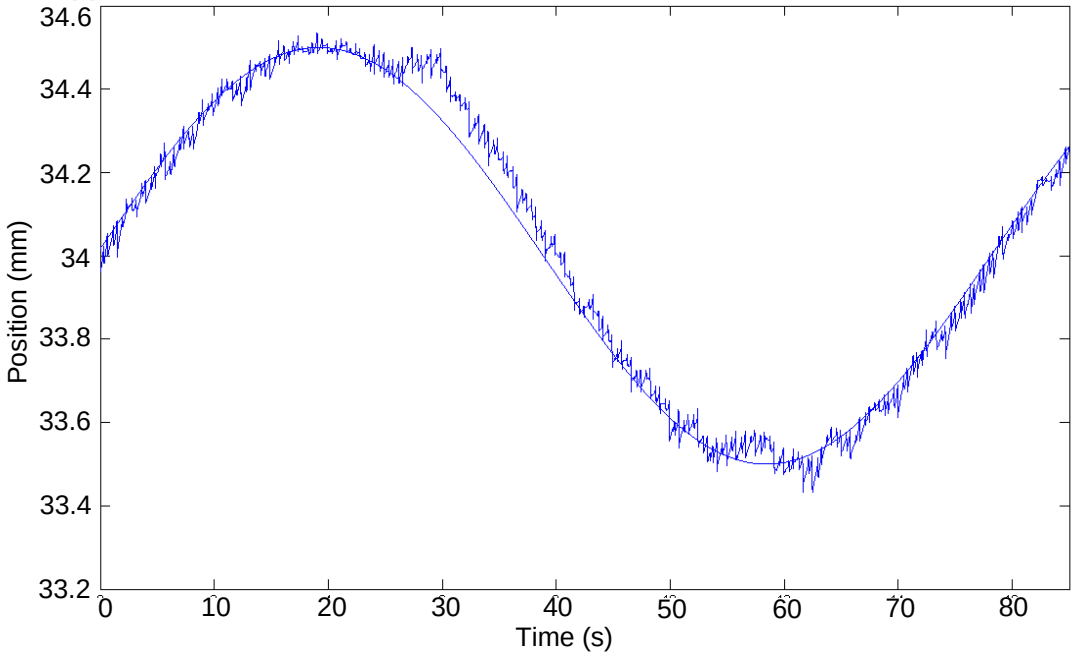

Fig. 4.6 Closed-loop response to a sinusoidal reference input with an amplitude of 0.5 mm and frequency of 0.04 rad/s.

Steady-State Error

Fig. 4.7 shows the steady-state error of a closed-loop 0.5-mm step position response from 34 mm to 34.5 mm (Fig. 4.1(b)). As shown in Fig. 4.7, the step response has an error of 3 μm with the 5 μm peak-to-peak noise. The noise occurs mainly because of the resolution of the laser sensor. The error is a little larger than the response of the position-control with the PID controller that was designed by the relay auto-tuning method. This difference may exist because of two possibilities. One possibility is the PID controller designed by root-locus is not an optimum PID controller. Another possibility is the PID controller is designed based on the dynamic model which simplifies the relation between the velocity and current so it would be different from the realistic dynamic model.

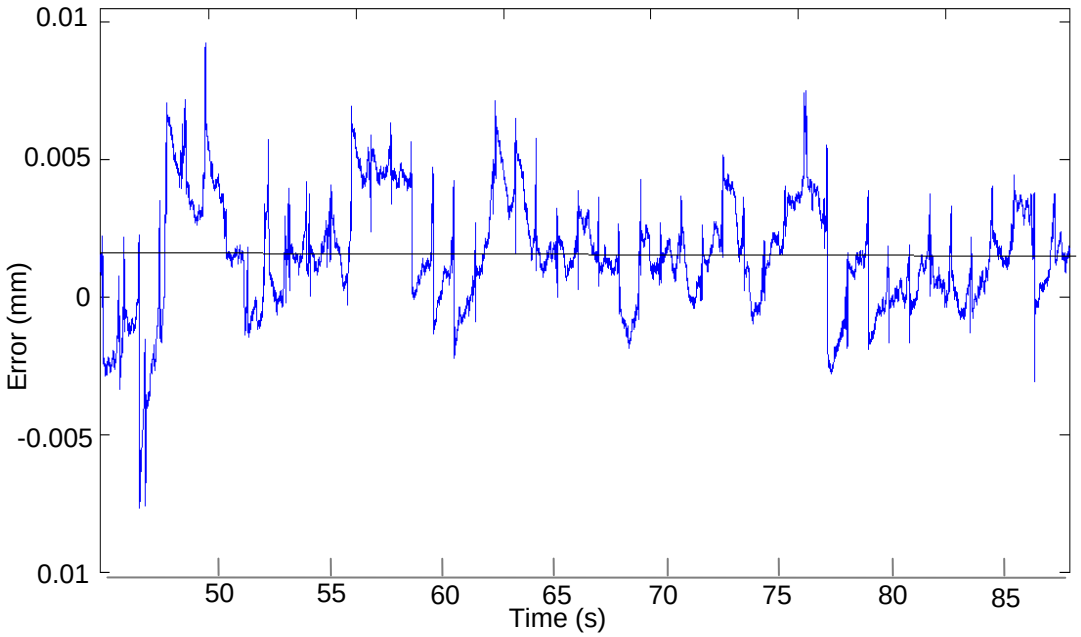

Fig. 4.7 Steady-state error of closed-loop 0.5-mm step position response from 34 mm to 34.5 mm.

4.2 Closed-Loop Position Response with Linear Variable-Velocity Controller

The Linear variable-velocity controller can make the velocity change until the active element reaches the desired position. Based on the error, the linear variable-velocity controller will make the velocity decrease to zero linearly when the error is within ±20 μm. The closed-loop position step response with linear variable-velocity controller is shown in Fig. 4.8. The rise time of the response is 18 sec and, unlike the step response of the position controller with PID controller, there is no overshoot.

Fig. 4.9 shows the capability of the designing controller in tracking a sinusoidal reference input with amplitude of 0.5 mm and frequency of 0.04 rad/s. As shown in Fig. 4.9, in some range of time, it exhibited a time delay of 3 s. Similar to the closed-loop position-control system with PID controller; it is also because the velocity does not always keep at the maximum velocity. Therefore, when the velocity is too slow, it need more time to follow the change of position reference.

4.2.1 Steady-State Error

The steady-state error can be seen from the steady-state of the step response from 33.5 mm to 34 mm with the linear variable-velocity controller and is shown in Fig. 4.10. The peak-to-peak noise level is 5 μm is mainly because of the noise of the laser sensor as mentioned in Section 4.1.1. Compared with Fig. 4.3, the steady-state error is larger than the position controller with PID controller. The characteristics of the linear variable-velocity controller accounts for the differences in the error. When the error is

close to zero, the current will be too slow to move the active element. Therefore, the active element will almost stop at the error of 5 μm.

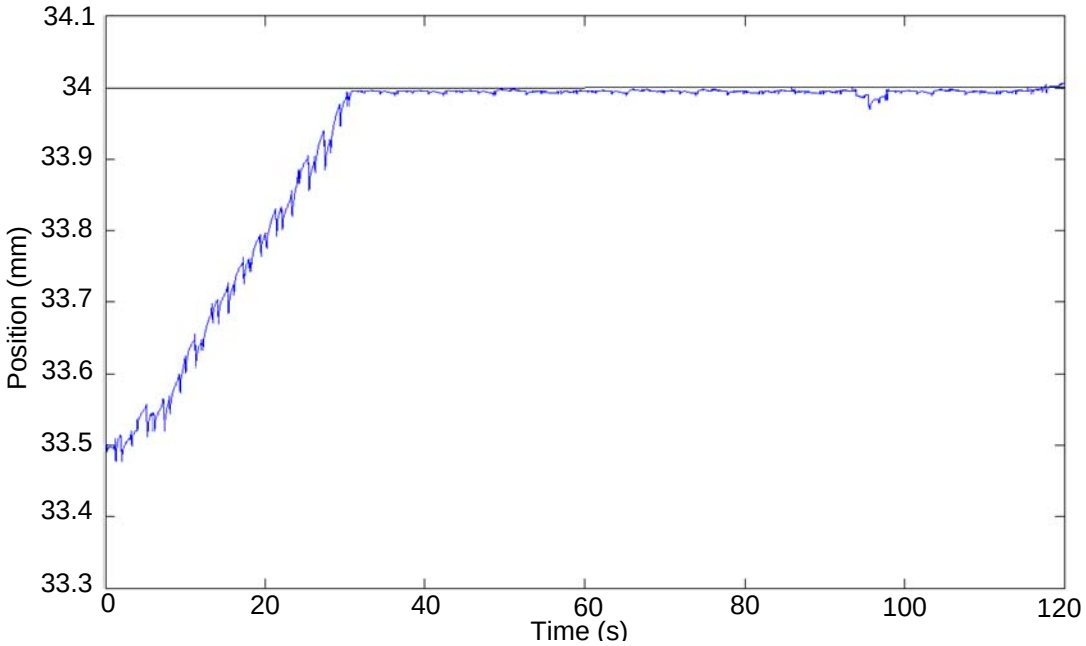

Fig. 4.8 Closed-loop position response with linear variable-velocity controller.

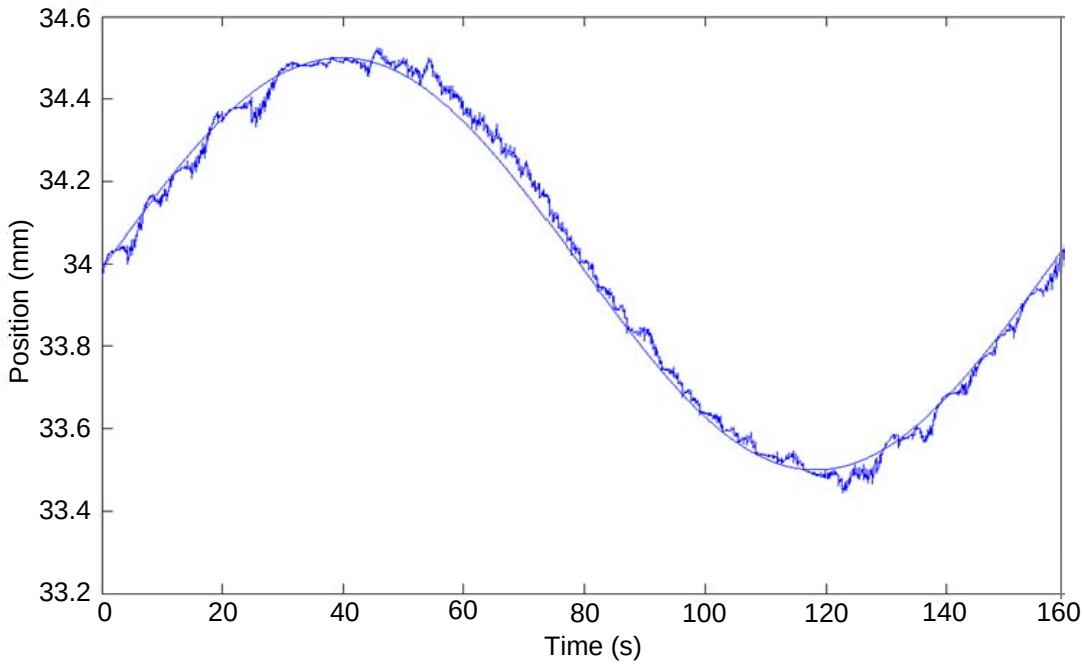

Fig. 4.9 Capability of the designing controller in tracking a sinusoidal reference input with amplitude of 0.5 mm and frequency of 0.04 rad/s.

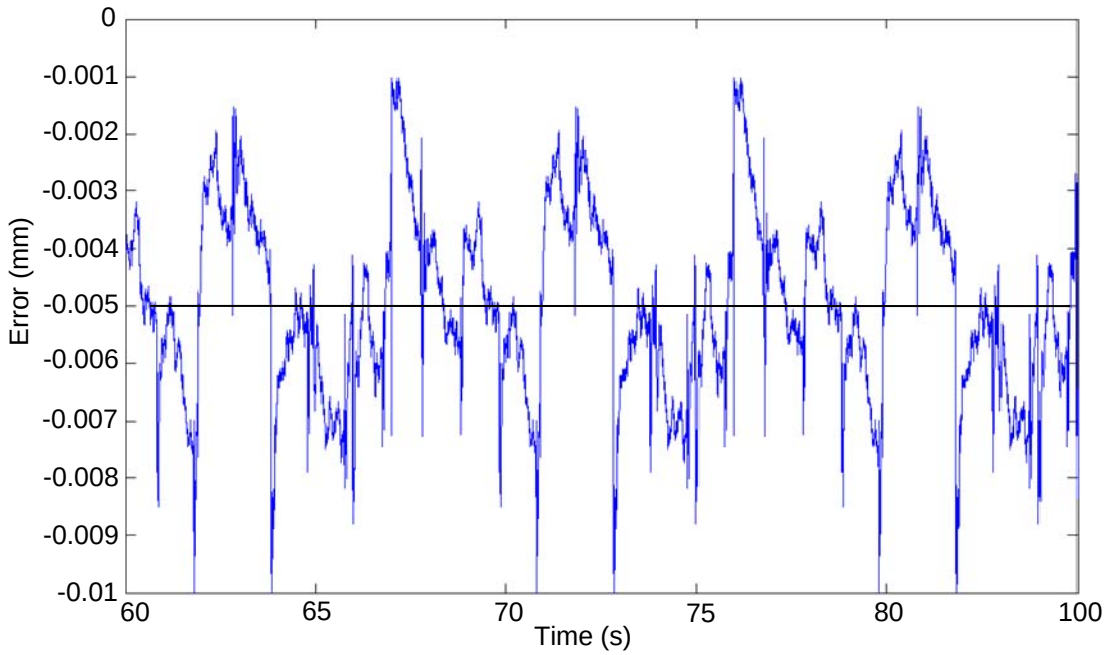

Fig. 4.10 Steady-state error of the closed-loop position response with linear variable-velocity controller.

4.3 Closed-Loop Position Response with Sliding Mode Control

The SMC is a control method that similar to the linear variable-velocity control system. The experiment result will be presented in this section. Fig. 4.11 shows the closed-loop step response from 34 mm to 35 mm. The responding time is 38 s and the overshoot is 15 μm. The rise time is higher than the response with the PIC controller because the magnetostrictive actuator does not operate at it maximum current with the SMC when the error is larger than 20 μm. Fig. 4.12 shows the response with a sinusoidal reference input. Similar to the response with other controllers, delay also occurs in the response and is also because the magnetostrictive actuator is not always operated under its maximum current.

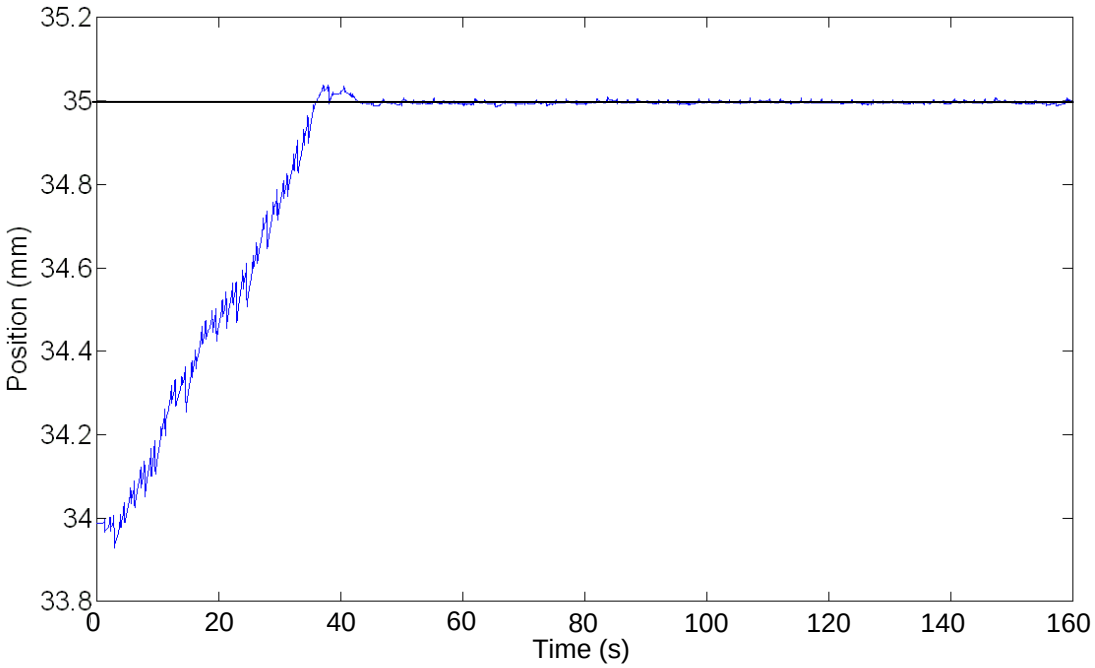

Fig. 4.11 Closed-loop position response with sliding mode control.

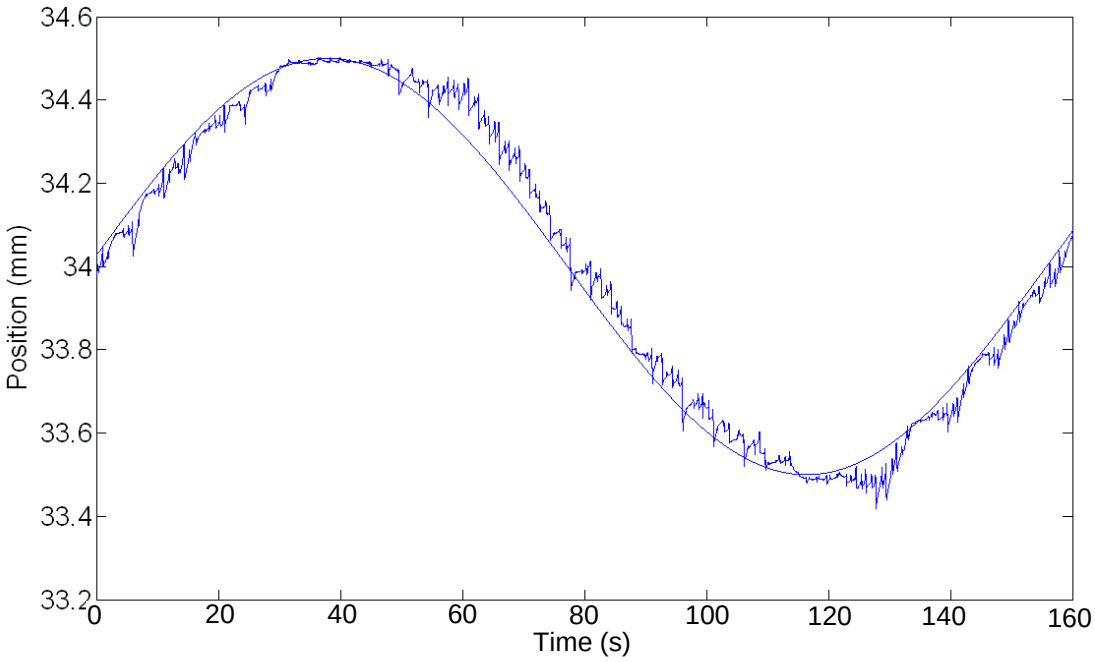

Fig. 4.12 Capability of the designing controller in tracking a sinusoidal reference input with amplitude of 0.5 mm and frequency of 0.04 rad/s.

4.3.1 Steady-State Error

The steady-state error can be seen from the steady-state of the step response from 34 mm to 35 mm with the SMC and is shown in Fig. 4.13. The error is about 3 μm with the condition of 5 μm peak-to-peak noise and this noise is mainly because of the noise of the resolution of the laser sensor as mentioned in Section 4.1.1. Compared with Fig. 4.10, the steady-state error is less than that with the linear variable-velocity controller. The reason the steady-stare error is different from the response of the position control with the linear variable-velocity controller is because the current controlled by SMC will not become too small to move the active element of the magnetostrictive actuator, unlike linear variable-velocity controller.

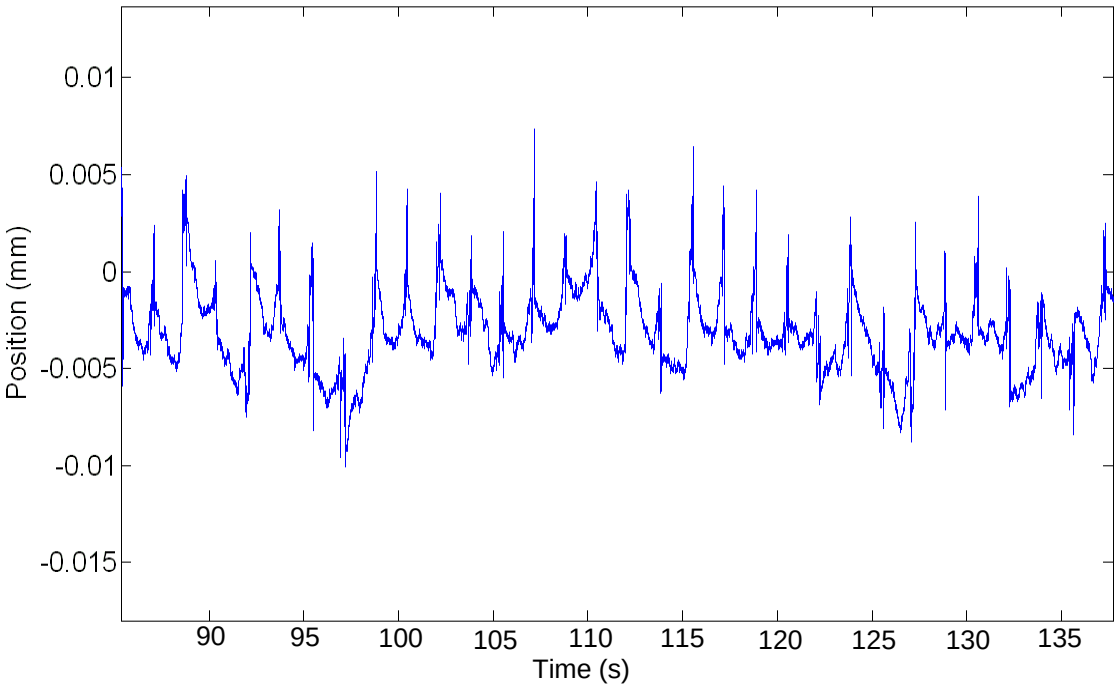

Fig. 4.13 Steady-state error of the closed-loop position response with sliding mode control.

4.4 Closed-Loop Position Response with Relay Controller

Improving the performance of the closed-loop control system which used a relay controller is one of the goals in this thesis. Fig. 4.14 shows the result of a 1-mm closed-loop step response with an excitation frequency at 10 Hz and a phase voltage of 8 V and the dead-zone threshold value of 20 μm. The steady-state error is about 20 μm [9].

When the error is within the dead-zone threshold values, the current in the coils will turn to zero immediately, and then the active element will stop moving and stop at the position near the dead-zone limit. Therefore, the dead-zone threshold could be one of the reasons that causes the 20 μm error and limits the accuracy of the linear magnetostrictive actuator. Form Figs. 4.1 and 4.9, the step response of the closed-loop position control with PID controller has the position-error within 5 μm which is much less than the relay-controller.

The reason the improved accuracy is because the velocity will keep changing when the error is within 20 μm, unlike the relay-controller, the velocity is zero. The active element will keep moving to the desired position rather than stop at the dead-zone limit. Similarly, the error of the position control system with linear variable-velocity controller which the error is within 10 μm is also less than the error of 20 μm by using the relay controller. The reason is also because the velocity will not decrease to zero immediately within the dead-zone of the relay controller. In the closed-loop response to a sinusoidal reference input as shown in Fig. 4.15, the response of the relay control is also has a delay with the sinusoidal reference, but it needs more time to follow the change of the input reference.

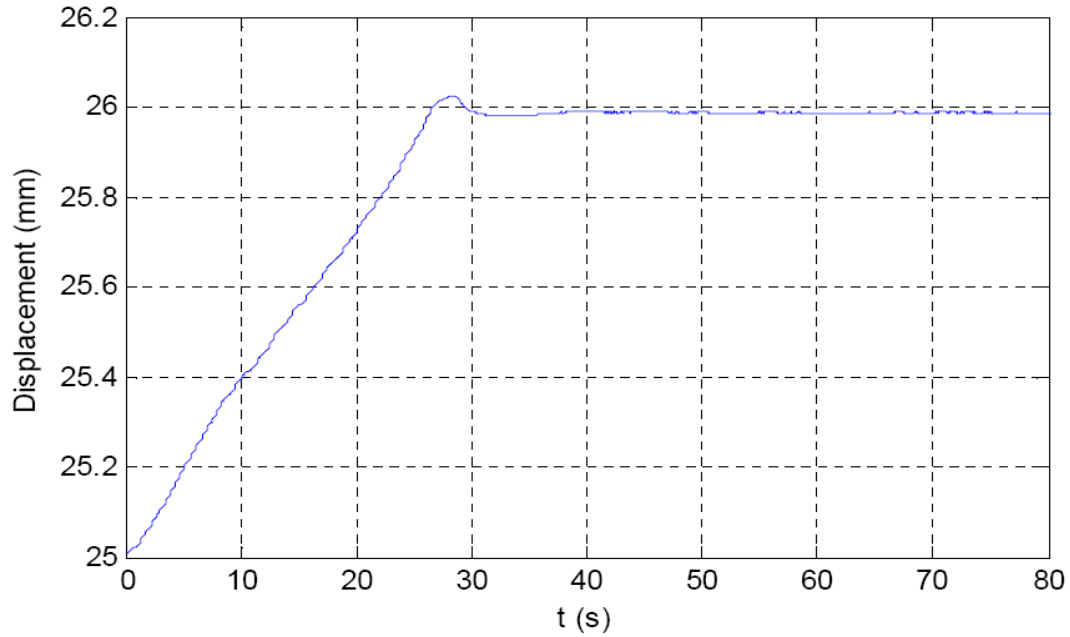

Fig. 4.14 1-mm closed-loop step response with an excitation frequency at 10 Hz and a phase voltage of 8 V and the dead-zone threshold values of ±0.02 mm [6].

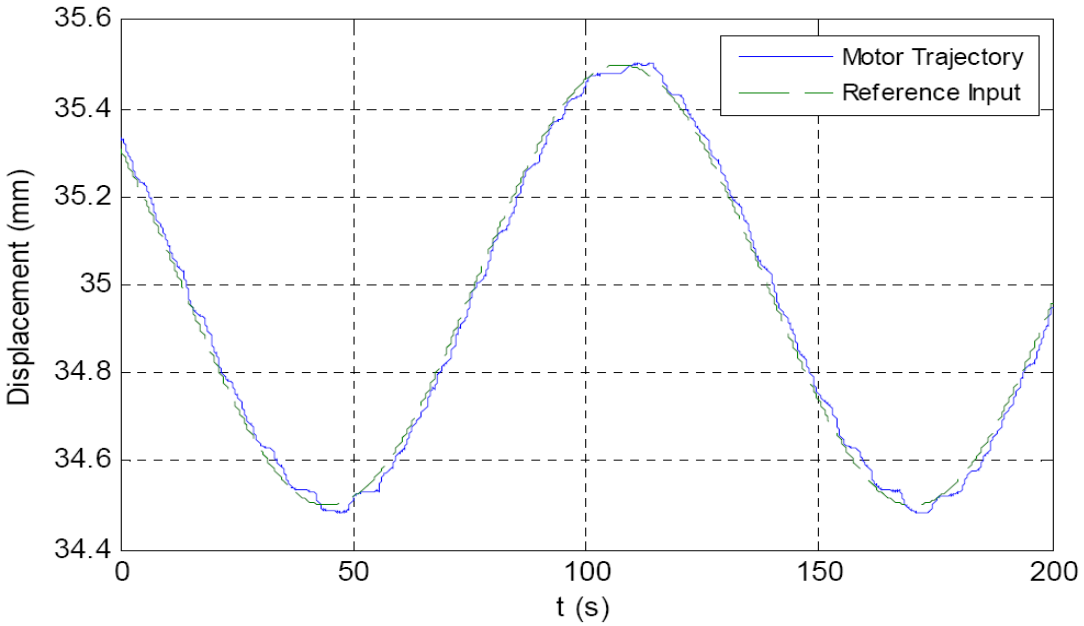

Fig. 4.15 Closed-loop response to a sinusoidal reference input with an amplitude of 0.5 mm and frequency of 0.05 rad/s [6].

The difference of the closed-loop response to a sinusoidal reference between different controllers is because the relay controller let the actuators move with its maximum speed when the error is larger than 20 μm, and the actuator will stop to move when the error is less than 20 μm so the relay-control system exhibited a larger response time. On the contrary, the velocity of the PID controller and the linear variable-velocity controller will change with the error and most of the time is not zero. Therefore, the response time to a sinusoidal reference is faster and the accuracy is higher than those with the relay control system.

CHAPTER V

CONCLUSIONS

In this chapter the achievements and contribution of this research are summarized and suggestions for future work are provided to improve the performance of the linear magnetostrictive actuator.

5.1 Conclusions

For the design of a closed-loop current-control system, a PWM amplifier has been added to the electronic model, and the experiment of using the PWM amplifier shows that the current in the coil of the electronic model can be controlled successfully by changing the duty ratio of the PWM signal. From the experiment, the relation between the duty ratio and the PWM signal has also been found and implemented in the design of the current controller in the closed-loop current-control system. Moreover, the peak-current-value calculator has been designed to feed back only the peak current value from the square wave of the current transducer. This successfully simplifies the design of the current controller and offers the flexibility to design a different position controller as long as it is based on changing the current. As shown in Fig. 3.7, the closed-loop current-control system can control the current with an error of ±10 mA, and the responding time is 1 s.

For the closed-loop position controller, after implementing the current-control system, two PID controllers, the linear variable-velocity controller, and the SMC

position control have been designed and discussed in this thesis. First, PID controllers were designed by the relay auto-tuning method and the root-locus were successfully implemented in the closed-loop position-control system. One PID controller was designed by the relay auto-tuning method based on the Ziegler-Nichols tuning methodology. This PID controller could be designed without knowing the dynamic model of the magnetostrictive actuator, because the relay auto-tuning method successfully finds the optimum gains of the PID controller. The step response of the PID controller shows that it has an accuracy of ±1 μm under the condition of a 5-μm peak-to-peak position noise. Another PID controller designed by the root-locus—has a step response with an accuracy of ±3~4 μm error under the condition of a 5-μm peak-to-peak position noise. Second, the linear variable-velocity controller was also implemented successfully to control the position of the magnetostrictive actuator. The step response of the controller has an accuracy of ±4 μm under the condition of 5 μm peak-to-peak position noise. Third, the SMC position-control system in this thesis controlled the position of the active element with an accuracy of ±3 μm under the condition of 5 μm peak-to-peak position noise.

A comparison of all the position-control systems in the thesis shows that the closed-loop position-control system with the PID controller designed by the relay auto-tuning method has higher accuracy than the other controllers. The accuracy of the closed-loop position-control system with the PID controller designed by the root-locus is not as good as that of the PID controller designed by the relay auto-tuning method because the root-locus method is designed from a simplified dynamic model. The

steady-state error shown in Fig. 3.25, which is the simulation of the step response, is zero, and this shows that the PID controller is working well with a simplified dynamic model. Therefore, the difference between the simplified dynamic model and the realistic model may cause the difference in performance.

The position control with the linear variable-velocity controller has the largest steady-state error of all the controllers in this thesis. The result is because the linear variable-velocity controller has the simplest working characteristics, in which the current changes with the error linearly. Due to the design, the active element will stop when the error is less than 4 μm, because the current is too small to move the active element when the error is less than 4 μm.

The SMC has an accuracy of within 3 μm, which is higher than the PID controller designed by the relay auto-tuning method and is less than the linear variable-velocity controller. The difference of the performances is because the SMC is also designed from the simplified dynamic model. Without using the realistic model, the performance will be different and cause the error of 3 μm.

The PID controller designed by the relay auto-tuning method has been designed without a dynamic model; therefore, it does not have the problem that the SMC and the PID controller designed by root-locus have. It also does not have the problem that the active element will just stop at one point. Therefore, the PID controller designed by the relay auto-tuning method has better performance than the other controllers in the thesis.

All the controllers have the similar 5-μm peak-to-peak position noise, and this is the limitation to control the position in the research no matter which controller is used as the controller of the position-control system.

Compared to the closed-loop relay-control system, the PID controller, linear variable-velocity controller, or SMC system offer improved accuracy. This result shows that the dead-zone value threshold of the relay controller in which the velocity is zero when the error is within the dead-zone threshold limits the accuracy of the controller. By controlling the current in the magnetostrictive actuator, the current can change with the error, and therefore, unlike the relay controller, the velocity can be controlled within the dead-zone threshold of the relay controller.

5.2 Suggestions for Future Work

Although the closed-loop current-control system has been successfully implemented as the inner loop of the closed-loop position-control system and two position-control systems have been designed, there are still some aspects of this actuator that remain unexplored. Based on that, the following recommendations for future work are suggested:

- The design of the closed-loop current-control system gives us the flexibility to design the position controller. Nevertheless, the main focus of this research was on the PID controller and linear variable-velocity controller. In the future, other kinds of controller can also be tried to reach the optimum operation of the actuator, as long as the controller is designed based on controlling the current in the

magnetostrictive actuator.

- In the design of the PID controller, the controller was tuned using the Ziegler-Nichols ultimate sensitivity method and the root-locus by analyzing the simplified dynamic model of the novel linear magnetostrictive actuator. In other words, in this thesis, the position controller is designed without the dynamic model or with a simplified dynamic model that is still different from the realistic model. Therefore, by defining the dynamic model of the novel linear magnetostrictive actuator more precisely, a better performance for the closed-loop position-control system could be designed.
- In the research, the resolution of the laser sensor limits the accuracy of the actuator because of the condition of 5 μm peak-to-peak position noise. Implementation of other kinds of sensors with higher resolution may eliminate the noise and improve the performance.

REFERENCES

[1] W.-C. Gan and N. C. Cheung, “Development and Control of a Low-Cost Linear Variable-Reluctance Motor for Precision Manufacturing Automation,” *IEEE Trans. Mechatronics*, vol. 8, no. 3, pp. 326−333, September 2003.

[2] H. Ishihara, F. Arai, and T. Fukuda, “Micro Mechatronics and Micro Actuators,” *IEEE Trans. Mechatronics*, vol. 1, no. 1, pp. 68−79, March 1996.

[3] W.-J. Kim and A. Sadighi, “Novel Low-Power Linear Magnetostrictive Actuator with Local Three-Phase Excitation,” *IEEE/ASME Tr. on Mechatronics*, vol. 15, no. 2, pp. 299−307, April 2010.

[4] J. A. Palmer and J. F. Mulling, T. Usher, E. Grant, J. W. Eischen, A. I. Kingon, and P. D. Franzon,” The Design and Characterization of a Novel Piezoelectric Transducer-Based Linear Motor,” *IEEE Trans. Mechatronics*, vol. 9, no. 2, pp. 392−398, June 2004.

[5] F. Claeyssen, N. Lhermet, and T. Maillard, “Magnetostrictive Actuators Compared to Piezoelectric Actuators” in *Proc. SPIE Conf. Smart Structures in Engineering and Technology*, vol. 4763, March 2003, pp. 194−200.

[6] F. Claeyssen, N Lhermet, and G. Grosso, “Giant Magnetostrictive Alloy Actuators,” *J. Applied Electromagnetic in Materials*, vol. 5, pp.67−73, July 1994.

[7] S. Karunanidhi and M. Singaperumal, “Design, Analysis and Simulation of Magnetostrictive Actuator and its Application to High Dynamic Servo Valve,” *Sensors and Actuators A: Physical,* vol. 157, no. 2, pp. 185−197, February 2010.

[8] F. Claeyssen, N. Lhermet, R. L. Letty, and P. Bouchilloux, “Acuators, Transducers and Motors Based on Giant Magnetostrictive Materials,” *J. Alloys and Compounds*, vol. 258, pp. 61−73, August 1997.

[9] A. Sadighi, *Development of a Novel Linear Magnetostrictive Actuator*, PhD Dissertation: Texas A&M University, August 2010.

[10] L. Kiesewetter, “The Application of Terfenol in Linear Motors,” in *Proc. 2nd Int. Conf. Giant Magnetostrictive Alloys*, 1988, ch. 7, pp. 15.

[11] W. -J. Kim, J. H. Goldie, M. J. Gerver, J. E. Kiley, and J. R. Swenbeck, “Extended-Range Linear Magnetostrictive Motor with Double-Sided Three-Phase Stators,” *IEEE Trans. Industry Applications*, vol. 38, no. 3, pp. 651–659, June 2002.

[12] D. Kendall and A. R. Piercy, “The Frequency Dependence of Eddy Current Losses in Terfenol-D,” *J. Applied Physics*, vol. 73, pp. 6174–6176, May 1993.

[13] J. M. Nealis and R. C. Smith, “Robust Control of a Magnetostrictive Actuator," CRSC Technical Report CRSC-TR03-05; *Proceedings of the SPIE, Smart Structures and Materials* 2003, vol. 5049, pp. 221–232, March 2003.

[14] T. Zhang, C. Jiang, H. Zhang and H. Xu “Giant Magnetostrictive Actuators for Active Vibration Control,” *Smart Materials and Structures,* vol. 12, no. 3, pp. 473–478, April 2004

[15] W. S. Oares and R. C. Smith “Optimal Tracking Using Magnetostrictive Actuators Operating in Nonlinear and Hysteretic Regimes,” *J. Dyn. Sys., Meas., Control* , vol. 131, no. 3, pp. 31–41, May 2009

[16] E. Monaco, F. Franco, and L. Lecce ”Experimental and Numerical Activities on

Damage Detection Using Magnetostrictive Actuators and Statistical Analysis," *Journal of Intelligent Material Systems and Structures*, vol. 11, no. 7, pp. 567–578, July 2000.

[17] E. Monace and F. Franco, L. Lecce "Structural Damage Identification Using Magnetostrictive Actuators," in *Proc. Smart Structures and Materials 1999: Smart Structures and Integrated Systems,* June 1999, vol. 3668, pp. 295–404.

[18] J. Goldie, M. J. Gerver, J. Kiley, and J. R. Swenbeck, "Observations and Theory of Terfenol-D Inchworm Motors," in *Proc. SPIE 5th Annu. Int. Symp. Smart Structures and Materials*, March 1998, vol. 3329, pp.780–785.

[19] F. Claeyssen, R. Le Letty, N. Lhermet, R. Bossut, and B. Hamonic, "Analysis of Magnetostrictive Inchworm Motors Using Finite Element Modeling," i*n Proc. Elsevier Conference Magnetoelastic Effects and Applications*, Holland, June 1993, pp. 161–167.

[20] M.E. H. Benbouzid, G. Reyne, and G. Meunier, "Finite Element Modeling of Magnetostrictive Devices: Investigations for The Design of The Magnetic Circuit," *IEEE Trans. Magnetics*, vol. 31, no 3, pp.1813–1816, May 1995.

[21] D. G. Alciatore and M. B. Histand, *Introduction to Mechatronics and Measurement System*. 3 rd., Mc-Graw Hill, 2007.

[22] Baumer Inc., [Online]. Available: http://www.dspaceinc.com

[23] G. Engdahl, *Handbook of Giant Magnetostrictive Materials*. CA: pp. 1813-1816, May 1995.

[24] G. F. Franklin, J. D. Powell and E. N. Abbas, *Feedback control of Dynamic systems*. Pearson Prentice hall, 2002.

[25] D. Xue, Y. Chen and D. P. Atherton, *Linear Feedback Control*. Society for Industrial and Applied Mathematics, 2008.

[26] A. Flores, *Relay Feedback Auto Tuning of PID Controller*, PhD Dissertation: Universidad Iberoamericana, October 2007.

[27] A. Flores, *Modeling and Control of a Magnetostrictive System for High Precision Actuation at a Particular Frequency,* MS Thesis: North Carolina State University.

[28] A. Edwards and S. K. Spurgeon, *Theory and Application* of *Sliding Mode Control*. Taylor and Francis Inc., 1998.

APPEXDIX A

SIMULINK ® BLOCK DIAGRAMS

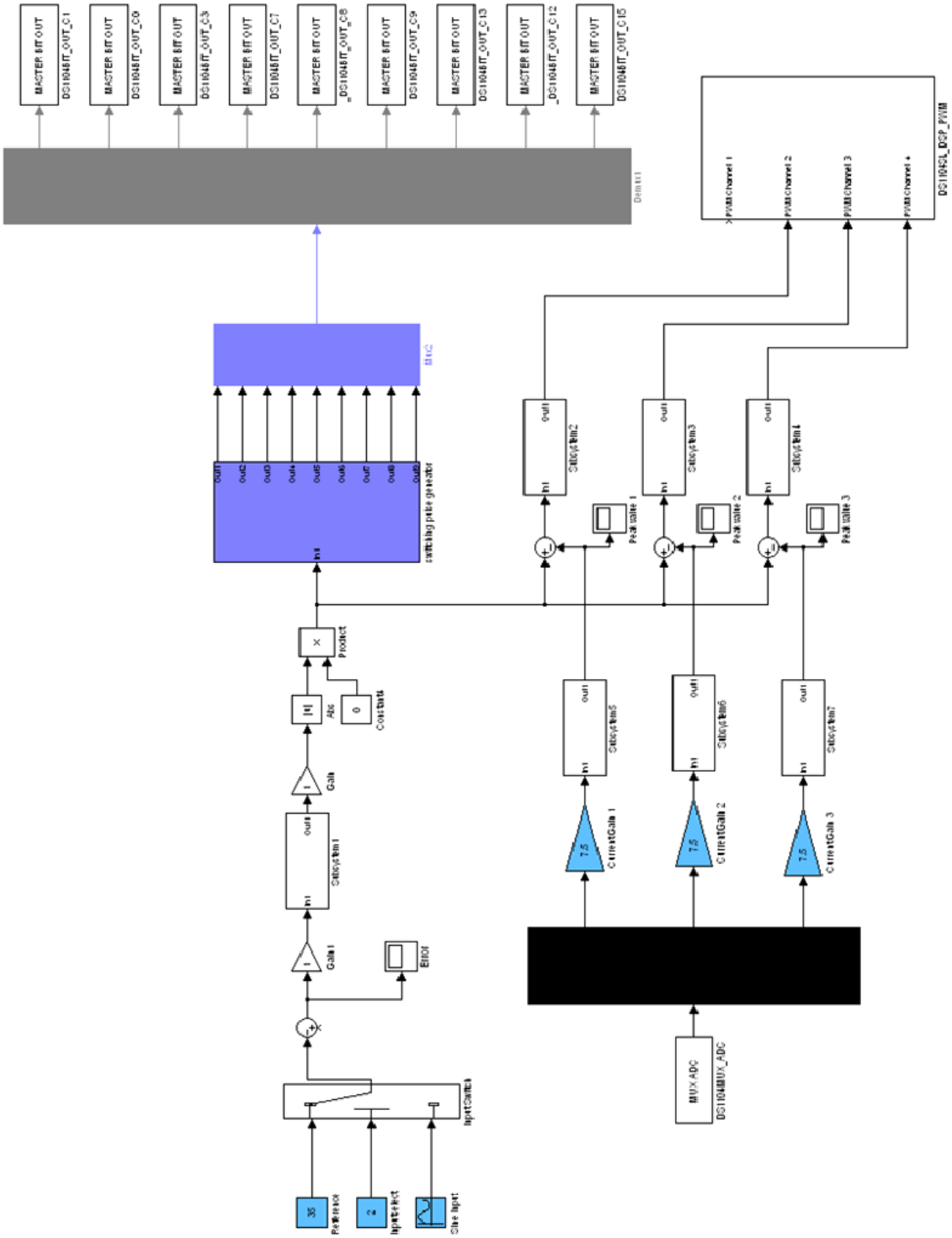

Fig. A.1. Simulink block diagram for real-time position control with PID, linear variable-velocity controller and sliding-mode controller.

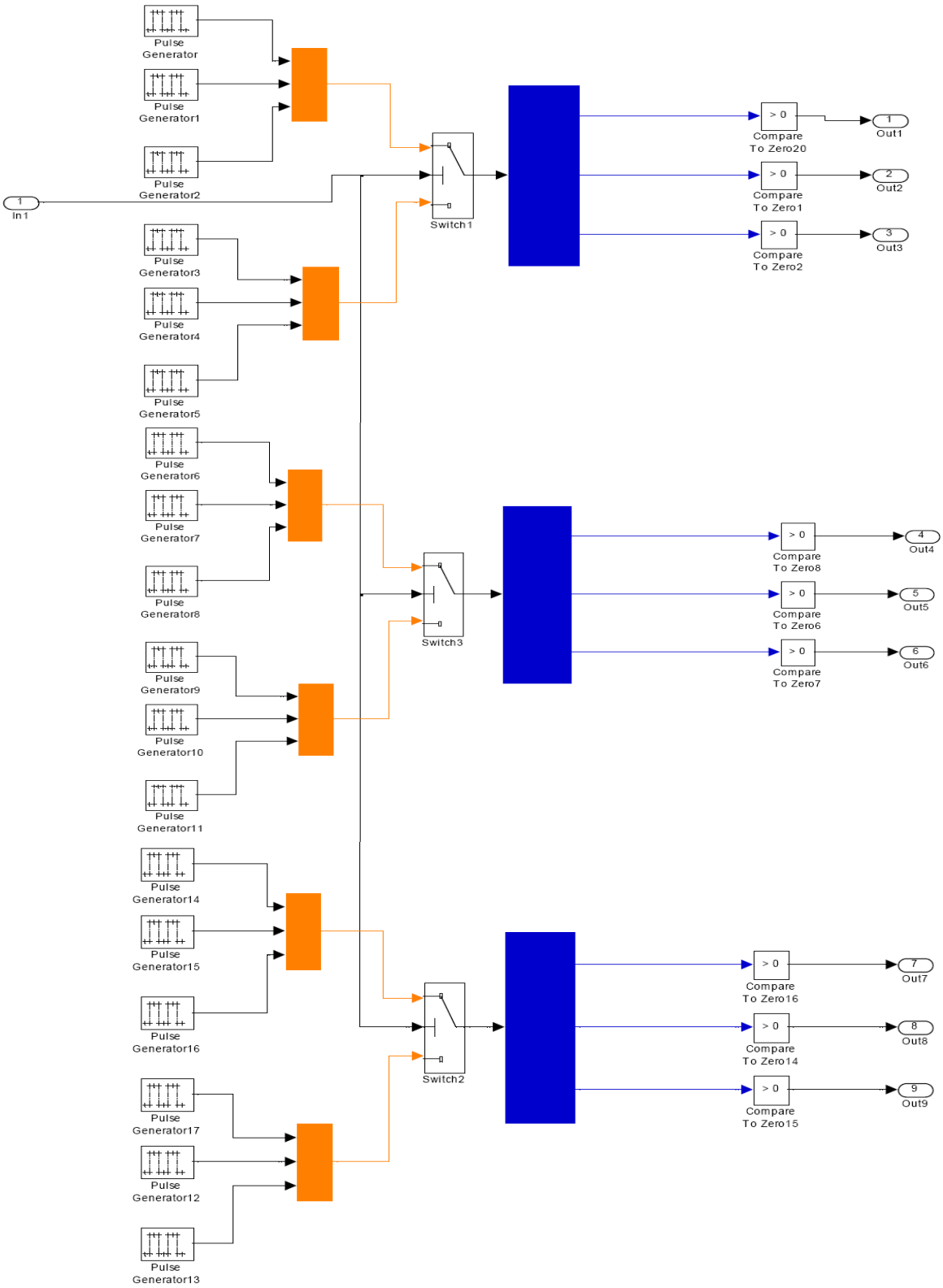

Fig. A. 2. Simulink block diagram for switching pulse generator.

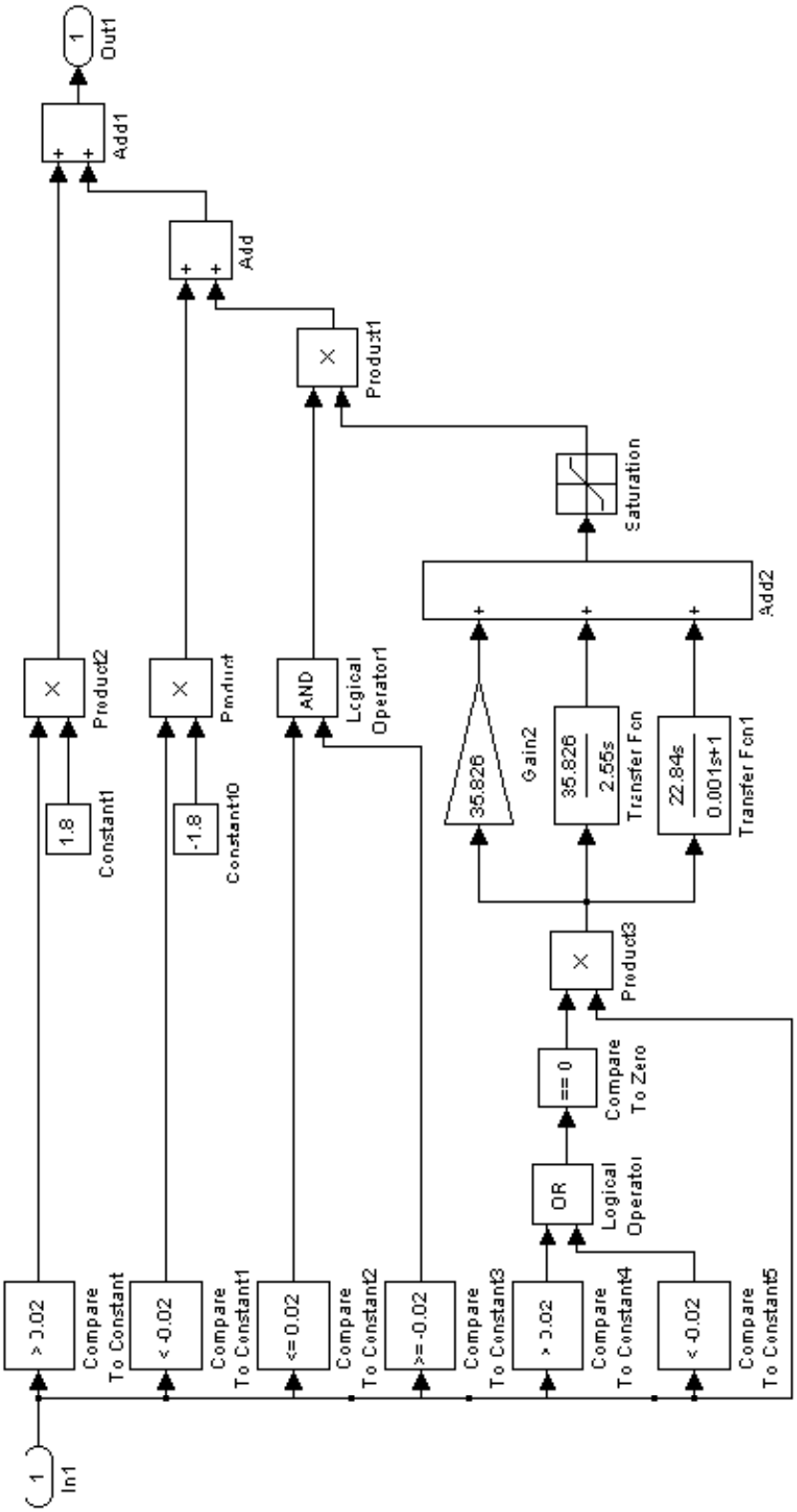

Fig.A.3 Simulink block diagram for subsystem 1 in real-time position control with PID controller which designed by relay-auto tuning method.

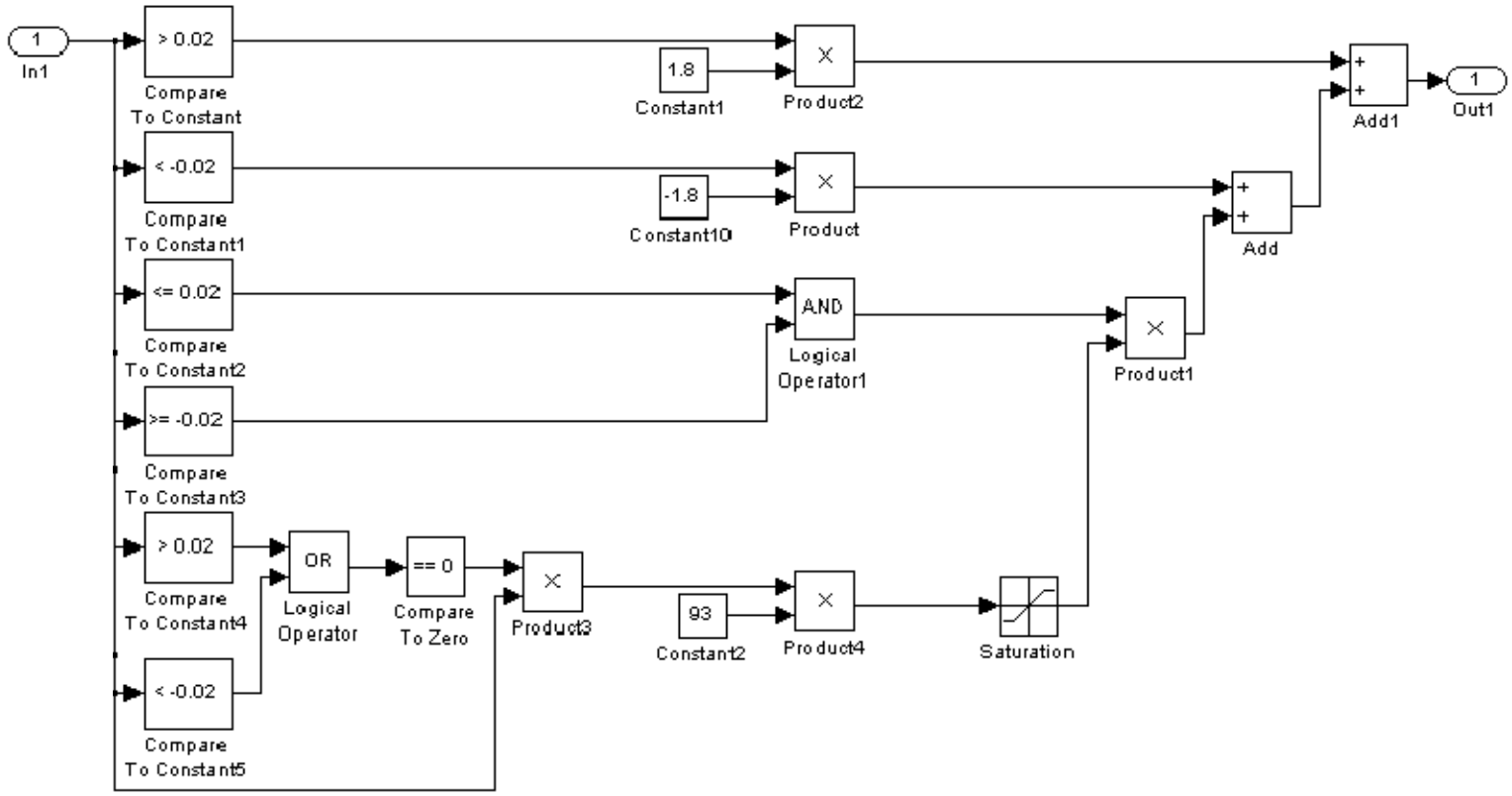

Fig.A.4 Simulink block diagram for subsystem 1 in real-time position control with linear variable-velocity controller.

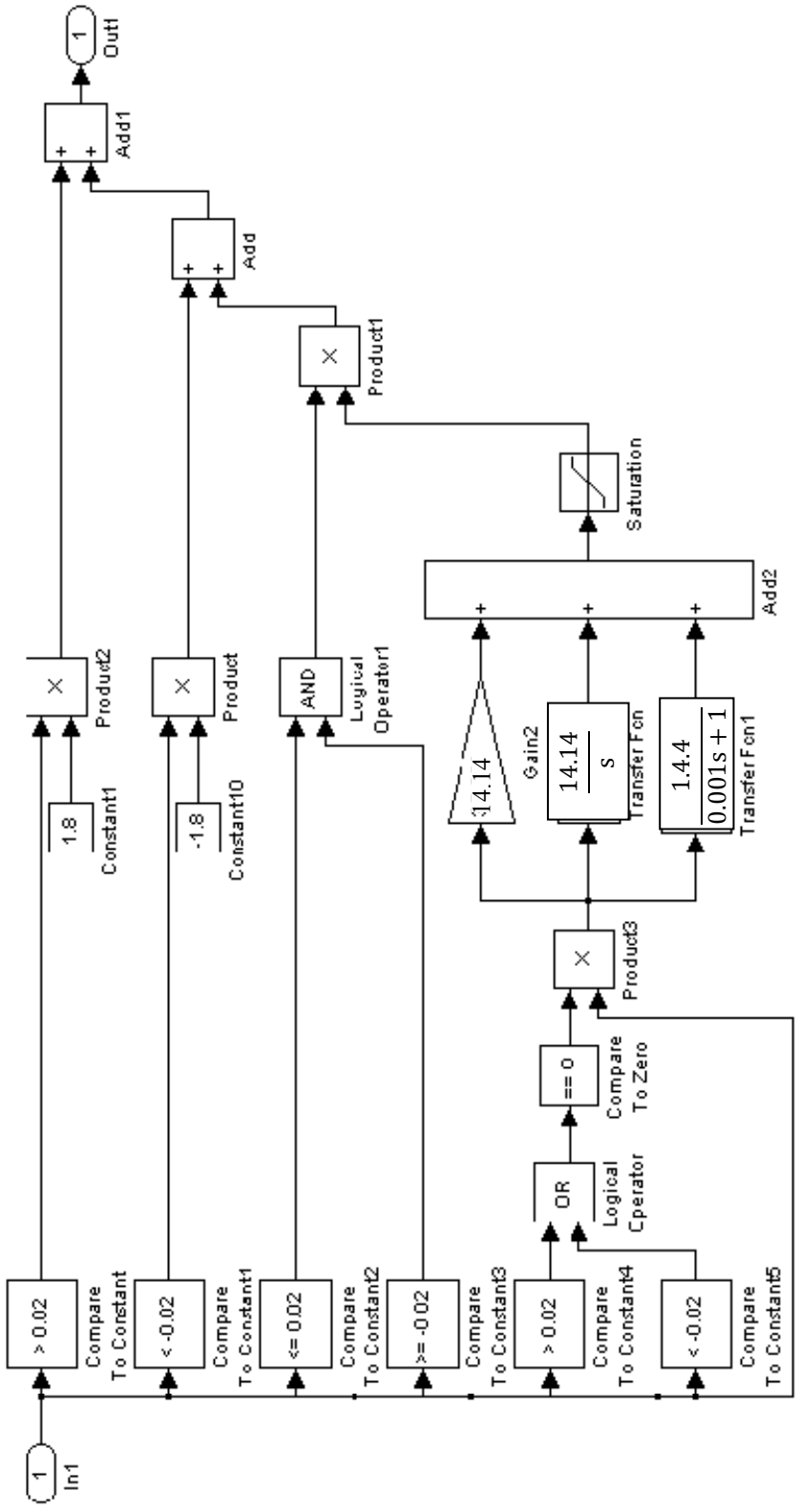

Fig.A.5 Simulink block diagram for subsystem 1 in real-time position control with PID controller which designed by root-locus.

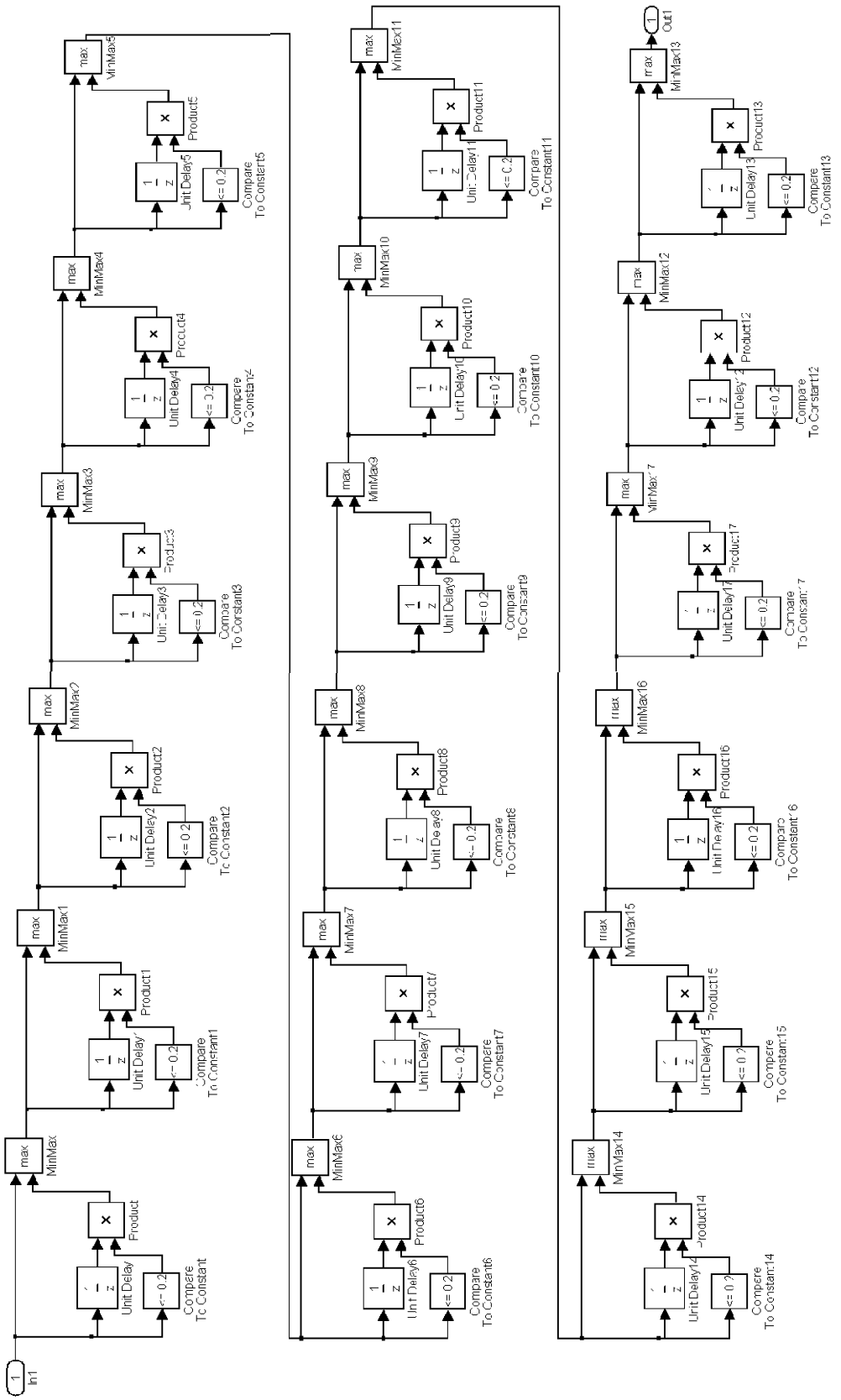

Fig. A.6. Simulink block diagram for subsystem 5, subsystem 6 and subsystem 7 in real-time position control.

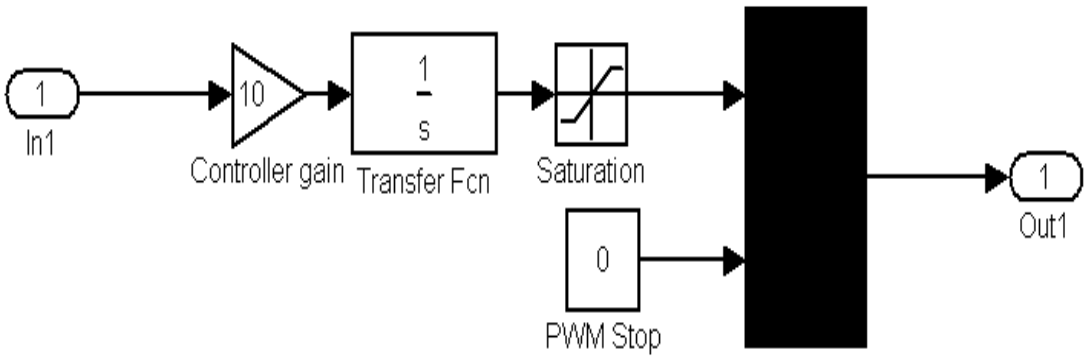

Fig. A.7. Simulink block diagram for subsystem 2, subsystem 3 and subsystem 4 in real-time position control.

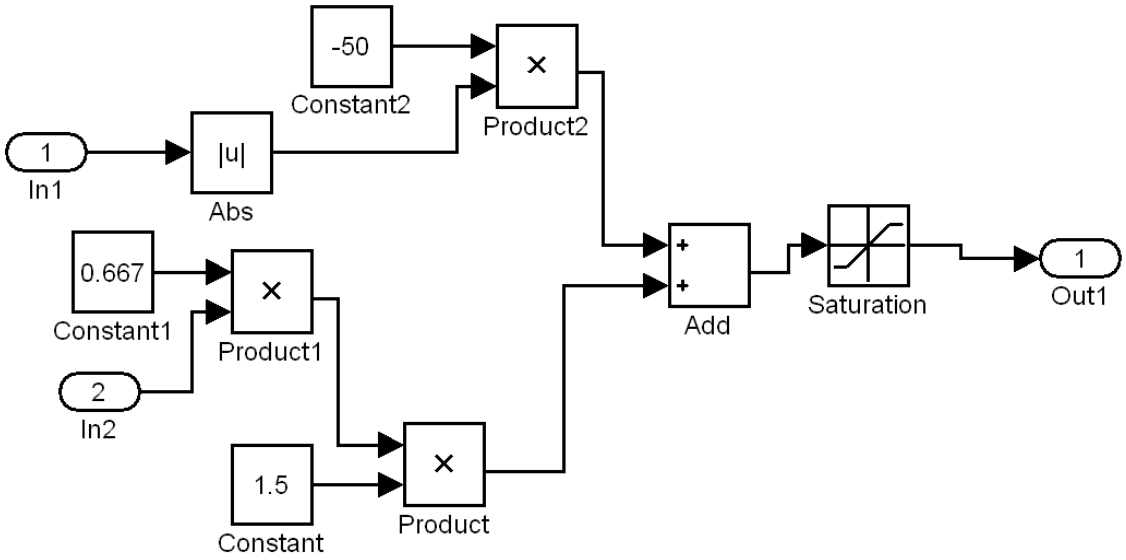

Fig. A.8. Simulink block diagram for subsystem 1 in real-time position-control system in Fig. A.1.

VITA

Chien-Fan Chen was born in Taoyuan, Taiwan. He received his Bachelor of Science degree in Mechanical Engineering from the National Taiwan University in 2007. He entered Texas A&M University in September 2008 and received his M.S. degree in mechanical engineering.

Name: Chien-Fan Chen

Address: No. 16, Lane 8, Singlong St., Bade City, Taoyuan County, 33443 TAIWAN

Email Address: B92502111@ntu.edu.tw

Education: B.S., Mechanical Engineering, National Taiwan University, 2007.

M.S., Mechanical Engineering, Texas A&M University, 2010.